USGS
science for a changing world

U.S. DEPARTMENT OF THE INTERIOR
U.S. GEOLOGICAL SURVEY

PRELIMINARY SCIENTIFIC RESULTS OF THE CREEDE CALDERA CONTINENTAL SCIENTIFIC DRILLING PROGRAM

P.M. Bethke, Editor

Open-File Report 94-260-G

2001

STABLE ISOTOPE GEOCHEMISTRY OF THE CREEDE FORMATION AND IMPLICATIONS FOR THE ORIGIN OF FLUIDS RESPONSIBLE FOR HYDROTHERMAL VEIN MINERALS IN THE CREEDE MINING DISTRICT

By

Robert O. Rye
U.S. Geological Survey, Denver, CO
Philip M. Bethke
U.S. Geological Survey, Reston, VA
David B. Finkelstein[1]
University of Illinois, Urbana, IL

Present address:
[1] Dept. of Geological Sciences, Indiana University, Bloomington, IN 47405

INTRODUCTION

In the Overview Chapter of this report, Bethke, et al. (Chapter A this Open-file Report) presented a conceptual model for the hydrothermal system that deposited the epithermal silver and base-metal ores of the Creede mining district first proposed by Bethke and Rye (1979) and extended by Rye, et al. (1988). The hypothesis proposes that the ore fluids were ultimately derived from evaporated lake water, circulated deeply, rose in the northern part of the district, and mixed with overlying meteoric waters along the top of most of the vein system. The ore fluids also mixed with lake water and/or pore fluids along the southern margin of the district. This model was based largely on the interpretation of five stable isotope data sets: 1) hydrogen and oxygen isotope data on the inclusion fluids in main stage and late stage ore and gangue minerals, 2) sulfur isotope data on the main stage barites in the veins, 3) hydrogen and oxygen isotope data on fluids responsible for pre-ore rhodochrosites, 4) carbon and oxygen isotope data on the pre-ore vein rhodochrosites and earlier wallrock calcite, 5) hydrogen and oxygen isotope data on clay mineral alteration overlying the mineralized veins. The conceptual model, modified to emphasize the isotopic constraints, is shown in Figure 1. This hypothesis has been incorporated in, and found to be consistent with, other detailed studies of the Creede ore deposits (Barton, et al., 1977, Wetlaufer, 1977, Plumlee, 1989, Foley, et al., 1989, Foley, 1990, Hayba, 1993). However, it was not until core samples from the Creede Caldera Moat Drilling Program were available that the hypothesis could be adequately tested by direct observation of pertinent aspects of the Creede Formation itself. This chapter presents the initial results of a carbon, hydrogen, oxygen, and sulfur isotope study of sedimentary and/or diagenetic pyrite and calcite, of diagenetic silicates, and of veinlet calcite in the Creede Formation. It is complemented by finer-scale SHRIMP microprobe studies of vein and stratiform pyrite (McKibben et al., 1993; McKibben and Eldridge, 1994) and laser microprobe studies of veinlet and stratiform pyrite and conventional carbon, oxygen isotope studies of veinlet calcite (Ilchik and Rumble, 1993, 1994), all from core samples. Stable isotope data on calcite and silica from outcrops of travertine mounds that interfinger with the lacustrine facies of the Creede Formation along the margin of the Creede caldera are also presented. The travertines contain important information on the history of Lake Creede and extend the stratigraphic range of samples on the Creede Formation at least 500 feet above the level of the drill cores.

One of the important aspects of stable isotope geochemical studies is that the data on minerals can be interpreted in terms of the composition and history of the fluids that produced them. In order to evaluate the involvement of lake or pore waters in the Creede hydrothermal system it is necessary to compare the history of three fluids: 1) lake water, 2) diagenetic fluids in the sediments, and 3) ore-forming fluids in veins. If lake waters or Creede Formation pore fluids were indeed involved in the ore-forming process, the data for all of these fluids must fit into a consistent evolutionary model. The previous studies at Creede have established the history of the ore fluids. The present study deals with the history of the lake waters and Creede Formation pore fluids and their possible relationship to the origin of the ore deposits. Four different stages of lake history, referred to as *initial, early, transitional,* and *late* stages, are distinguished on the basis of isotope data on the lacustrine carbonates in the Creede Formation

and an *end* stage is distinguished by data on the pre-ore rhodochrosites in the veins.

SULFUR ISOTOPE GEOCHEMISTRY

Stable isotope systematics of sulfur-bearing vein minerals from the Creede mining district.

The main stage sulfides in the veins at Creede are characterized by a narrow range of $\delta^{34}S$ values (-2±2‰) typical of volcanic or magmatic sulfur in a Tertiary volcanic environment; the vein barites, however, show a very large range of $\delta^{34}S$ values from about 4 to 44‰ (Rye et al., 1988). The aqueous sulfate and sulfide species in the hydrothermal fluids were not in isotopic equilibrium and each sulfur specie was derived from different sources with profoundly different histories. The isotope data on the barites at Creede are so unusual for a hydrothermal deposit in a Tertiary volcanic environment that we have long known that some factor was present at Creede that normally does not exist in such hydrothermal systems.

The sulfur and oxygen isotope data on hydrothermal barites are summarized in Figure 2 (Rye et al., 1988). The isotopic composition of the barites varies from north to south in the district with values from the northern mineralized areas being lower in both $\delta^{34}S$ and $\delta^{18}O$. The data fall in a triangle that can best be interpreted as a mixture of three components. The lower apex ($\delta^{18}O$ = 2‰; $\delta^{34}S$ = 1‰) is interpreted as deep sulfate from the hydrothermal system. The right apex ($\delta^{18}O$ = 20‰; $\delta^{34}S$ = 35‰) is a critical one; the combination of large sulfur and oxygen values *require* that the sulfate went through a bacteriogenic reducing cycle in a sedimentary environment, interpreted to be the Creede Formation. The top apex ($\delta^{18}O$ = 8‰; $\delta^{34}S$ = 48‰) has even larger sulfur but lower oxygen values. Rye et al. (1988) interpreted the top apex to represent sulfate that had evolved by bacteriogenic reduction but had undergone further isotopic evolution by oxygen isotope exchange with ore fluids and thermochemical reduction of sulfate in the presence of organic matter. This further evolution occurred as lake water or Creede Formation pore fluids mixed with deeply circulating ore solutions in the southern part of the district.

Bacteriogenic reduction of sulfate in a sedimentary environment produces diagenetic pyrite if iron is available. Therefore, the formation of diagenetic pyrite in the Creede Formation is a *requirement* of the hypothesis that the hydrothermal sulfate underwent a bacteriogenic cycle in the Lake Creede sediments. The search for such pyrite was one of the principal objectives of the drilling program. Drilling was critical to such a search because Creede Formation rocks exposed at the surface have been oxidized and any diagenetic pyrite removed by weathering.

Description of pyrite occurrences in the Creede Formation

Pyrite is the only sulfide so far identified in Creede Formation rocks. Pyrite occurs in minor amounts throughout the Creede Formation; the entire section of Creede Formation from CCM-1 averaged approximately 1% pyrite by weight, based on total sulfur analyses of composite samples by Michelle Tuttle (oral communication, 1993). Pyrite is ubiquitous in all lithologies, but coarse-grained facies tend to have higher concentrations of pyrite than do fine-grained facies.

Pyrite is least abundant in the air-fall tuff sections. By far the most common occurrence is as disseminated grains ranging in size from <1 to >50mμ. Very fine grains often occur in clouds in the matrix between phenocrysts and shards, and clots or aggregates of sub- to euhedral or anhedral grains (rarely framboids) are common. Among the larger grains (>10mμ), sub-hedral to euhedral grains are by far most common followed by anhedral grains and framboids. Pyrite also commonly occurs along phenocryst feldspar and, occasionally, shard grain boundaries. Replacement of titano-magnetite is common and pyrite is also seen to partially replace hornblende and biotite, although biotite is remarkably fresh in most samples of Creede Formation. Typically, high concentrations of pyrite represent stratiform replacements of matrix and, occasionally, shards and phenocrysts. However, in some cases pyrite-rich beds may represent direct sedimentary accumulations. Pyrite also occurs in veinlets in both the Snowshoe Mountain Tuff that underlies the Creede Formation and in the Creede Formation itself. The occurrence of pyrite in veins and the common replacement textures indicate that pyrite was mobile during and after diagenesis, but the overall textural features and distribution are those expected for diagenetic pyrite in anoxic sediments (c.f. Love and Amstutz, 1966, Tuttle, 1991). The abundance and modes of occurrence of pyrite in the Creede Formation cores are consistent with a bacteriogenic origin for some of the hydrothermal sulfate. More compelling evidence of such an origin is the sulfur isotopic composition of the pyrite, presented below.

$\delta^{34}S$ of sedimentary pyrite in the Creede Formation

Figure 3 shows the sulfur isotope data obtained by conventional analyses of bulk samples of various types of sedimentary pyrite, of sulfur in organic matter, and of pyrite from veinlets in Snowshoe Mountain Tuff from the deeper levels of CCM-2. The $\delta^{34}S$ values of the sedimentary sulfides range from about -20 to 36 ‰. The large range of $\delta^{34}S$ values of the Creede Formation pyrite is typical of diagenetic pyrite derived from the bacteriogenic reduction of sulfate (c.f. Goldhaber and Kaplan, 1974, Tuttle and Goldhaber, 1991). $\delta^{34}S$ values for bulk samples of vein pyrite and sulfur in organic matter fall within the range of disseminated and stratiform pyrite consistent with formation as part of the same diagenetic process.

Initial $\delta^{34}S$ of sulfate Lake Creede

Presumably the sulfate in the lake was derived largely from the leaching of the volcanic ash that was erupted from ring fracture volcanoes many times during the deposition of the Creede Formation. During eruptions of ash much of the sulfur in the magma-fluid system was probably present as SO_2 which was subsequently oxidized to leachable sulfate as at El Chichon, (Rye, et al., 1984; Varekamp et al., 1984) and Pinatubo (McKibben and Eldridge, 1993). The $\delta^{34}S$ of the volcanic sulfate is not known at this time but almost certainly was between 1 and 5‰ as indicated in Figure 3. The actual value(s) will not be known until we obtain sulfur isotope data on the ring fracture volcanics (Fisher Quartz Latite) and possibly on sulfate in authigenic and detrital apatite in the sediments.

Sulfur isotope geochemistry of lake-pore fluids and fractionation factors

The sulfur isotope geochemistry of the lake-pore fluid system can be complicated and to fully define it we need extensive data on isotopic compositions of pyrite as a function of pyrite textures and concentrations, chemical composition of sediments, and their organic content. We also need to know if bacteriogenic reduction and pyrite formation was limited by the amount of iron, sulfur, or organic matter. The first sulfides produced during bacteriogenic reduction of sulfate would have lower $\delta^{34}S$ values than the starting sulfate by an amount dependent on the sulfur isotope fractionation factor. As reduction of sulfate proceeds, the later sulfides would have successively larger $\delta^{34}S$ values. Knowledge of net and instantaneous fractionation factors during sulfate reduction is critical. Typically, the fractionation factor is a function of the rate of sulfate reduction, which in turn depends upon environmental conditions such as the amount of organic material and temperature. Under optimal conditions conducive to rapid rates of reduction, fractionations can be as small as 20 permil; under extreme conditions conducive to slow rates of reduction, fractionations can be much larger and approach equilibrium values. As reduction proceeds, the fractionation factor may change in response to changing environmental conditions. The lowest $\delta^{34}S$ values in Figure 3 are about -20 ‰ which would indicate a net fractionation of about 20-25 permil assuming a $\delta^{34}S$ of 1 to 5 ‰ for the initial volcanic sulfate. The large range of $\delta^{34}S$ values produced by small net fractionations is typical of sedimentary pyrite formed in lacustrine environments. Such sulfur isotope systematics probably reflect abundant sulfate supply during the life of the system and enough organic matter to favor small sulfur isotope fractionations during initial reduction of sulfate. According to Leventhal (1994) the initial organic content of the Creede Formation sediments was not sufficient to account for the amount of pyrite present. However, due to renewal from volcanic sources sulfate was probably abundant and organic matter was probably removed extensively by rapid reduction of sulfate. Also, as shown later, some of the Creede Formation sediments were flushed by meteoric water during diagenesis, a process that probably removed additional organic matter from the sediments.

Stratigraphic variations in $\delta^{34}S$ of pyrite in Creede Formation

The sulfate concentration of lakes is usually low because they rarely have large sources of sulfate in their drainage systems. In the volcanic environment at Creede, however, the sulfate concentration of the lake was probably renewed after each eruption of volcanic ash and then gradually depleted as sulfate reduction occurred. This renewal in the sulfate concentration of the lake after each eruption may be reflected in the $\delta^{34}S$ values of diagenetic pyrite.

Figure 4 shows the $\delta^{34}S$ values of pyrite samples that occur immediately above and below various tuff units and their stratigraphic relationship to the CCM-2 section. The $\delta^{34}S$ values of pyrite which straddle the top and bottom of sediment intervals separated by tuffs are connected by tie lines. The $\delta^{34}S$ values of pyrite just above the tuff units are lower than those below the units. Presumably, right after an eruption the sulfate concentration of the lake was high and the sulfate prior to reduction had a $\delta^{34}S$ close to that of the volcanic sulfur. Just before an eruption however, the lake (or upper several meters of sediments) was likely depleted in sulfate and the residual sulfate enriched in ^{34}S by bacteriogenic reduction. This approach to tracing the evolution of $\delta^{34}S$ of sulfate

in the lake is probably greatly oversimplified because much of the reduction of sulfate likely occurred well into the sediments where the pore fluids were isolated from the lake and able to move both horizontally and vertically through the sediments, blurring the record. Nevertheless, the initial results are encouraging and a number of additional intervals between tuff units should be studied in detail.

Temporal variations in $\delta^{34}S$ values of pyrite in Creede Formation

Diagenesis is a complicated process and different textures of diagenetic pyrite in the sediments may reflect different environmental conditions of deposition. One of the easiest ways to study the sulfur isotope geochemistry of sediments is to determine if $\delta^{34}S$ values of pyrite vary as a function of pyrite morphology; sulfur isotope studies of sedimentary pyrite should be tied to detailed petrographic studies. For example, sample 2R150A 6.8/6.8 in Table 1 contains a stratiform layer of disseminated framboidal pyrite and another layer that is largely later overgrown euhedral pyrite. The $\delta^{34}S$ values of these two types of pyrite are 16.9 and 17.0‰, respectively. For this sample there was no evolution in the sulfur isotopic composition of pore fluids between early and later diagenesis, but such detailed, petrographically-based studies should be done on many more samples. Significant temporal ^{34}S enrichments have been noted in some of the diagenetic sulfides and very large and reoccurring enrichments have been observed in the pyrite veinlets (McKibben et al., 1993; Ilchik and Rumble, 1993; 1994) as discussed below.

$\delta^{34}S$ values of sulfur in organic matter

The $\delta^{34}S$ values of the three samples of sulfur in organic matter reported by Leventhal et al. (1994) are also shown in Figure 3. The values range from about 0 to 17‰ and are in the range of values for diagenetic pyrites. The data are consistent with other diagenetic systems where the $\delta^{34}S$ of sulfur in organic matter typically is typically 10 to 20 permil larger than that of diagenetic pyrite (Goldhaber and Kaplan, 1974).

Average $\delta^{34}S$ values of vein pyrite in the Creede Formation and underlying Snowshoe Mountain Tuff.

The $\delta^{34}S$ variations in veinlets have been the principal focus of study by SHRIMP microprobe (McKibben et al. 1993, McKibben and Eldridge, 1994) and laser based microsampling (Rumble and Ilchik, 1993; 1994). Both studies showed extreme and recurring variations in the $\delta^{34}S$ values across some of the veinlets. These variations are best explained by extreme bacteriogenic reduction of limited sulfate reservoirs at or near the site of pyrite deposition. Most likely, some of the reduction of sulfate occurred under conditions which favored slow rates of reduction (such as elevated temperature or limited supply of organic matter) which in turn favored large sulfur isotope fractionations.

Our data on the veinlets (Figure 3) were obtained by drilling across the veinlets and analyzing the samples by conventional means. $\delta^{34}S$ values range from about -4 to 18‰. These data can be compared to those obtained by microbeam analyses where values range from about -20 to 150‰ over just a few millimeters across a veinlet (McKibben et al., 1993). The average $\delta^{34}S$ values for individual veinlets in Figure 3 are well within the range of diagenetic pyrites and

indicate that the extreme values obtained by microbeam analyses represent only a very small fraction of the total pyrite in the veinlets. It is unlikely that these pyrite veinlets have any connection to the hydrothermal ore deposits. They probably formed earlier as part of the diagenetic processes in the deeper parts of the Creede Formation, perhaps as suggested by Ilchik and Rumble (1994) shortly after caldera resurgence.

Summary Interpretation of pyrite $\delta^{34}S$ data

The sulfur isotope geochemistry of the Creede Formation has been studied only superficially and with the limited objectives. The topic remains a fertile subject for future research. The large range of $\delta^{34}S$ values on both authigenic pyrite in the Creede Formation and vein pyrite in the underlying Snowshoe Mountain Tuff are best interpreted to have resulted from the bacteriogenic reduction of sulfate during diagenesis. However formed, the isotopically heavy authigenic pyrites require formation of isotopically heavy sulfate in the Creede Formation pore fluids and likely in the overlying lake waters. Sulfate concentration of the lake waters was probably high, especially after volcanic episodes. Bacteriogenic reduction of the aqueous sulfate probably led to depletion of organic matter in the sediments. All current sulfur isotope data on the Creede Formation pyrites are consistent with that part of the model of the Creede hydrothermal system that proposes that the deeply circulating ore fluids mixed with pore fluids or lake waters in the southern part of the district leading to the highly unusual $\delta^{34}S$ and $\delta^{18}O$ values of the hydrothermal barites.

Ilchik and Rumble (1994) have proposed that most Creede Formation and veinlet pyrite was derived from the oxidation of fumarolic H_2S. Leventhal (1994) also proposed that epigenetic or diagenetic H_2S was added to the system. Sediment-hosted botryoidal pyrite and marcasite occurring near travertines in veinlets with organic rich calcite and sparry calcite have been encountered in diamond drill holes along the postulated southern extension of the southern Amethyst vein system into the Creede caldera moat (Plumlee, 1989). One sample of these minerals is coated by amethystine quartz suggesting that the sulfides may be pre-ore and part of the travertine formation cycle. Although it is likely, that fumarolic H_2S was introduced into the moat, much of the sulfur isotope systematics of the Creede Formation were clearly controlled primarily by bacteriogenic reduction of sulfate.

HYDROGEN AND OXYGEN ISOTOPE GEOCHEMISTRY

δD_{H2O} and $\delta^{18}O_{H2O}$ of hydrothermal ore fluids

Figure 5 summarizes the δD_{H2O} and $\delta^{18}O_{H2O}$ values obtained from analyzes of inclusion fluids in the main- and late-stage vein minerals from the Creede mining district (Rye et al., 1988). These data, which are direct determinations of the isotopic composition of the hydrothermal fluids, fall on a well defined trend extending off the meteoric water line. When the temperature and salinity data on fluid inclusions (Hayba, 1986, 1993) are considered as well, it is clear that the hydrothermal fluids were mixtures of two components as shown by the arrow in Figure 5. One component was a primary ore fluid with a salinity of about 13 wt. % NaCl equivalent and δD and $\delta^{18}O$ of at least -3 ‰ and -50‰, respectively. The other component was a nearly fresh meteoric water with a δD of about -110‰ and a $\delta^{18}O$ of about -15‰, respectively. These fluids mixed as shown in Figure

1. The isotopic compositions of the Creede ore fluids are extraordinary for a hydrothermal system in a Tertiary volcanic environment. They were derived neither from magmatic or exchanged meteoric water but were most likely derived ultimately from water that had undergone extensive evaporation in Lake Creede prior to recharge into the hydrothermal system (Bethke and Rye, 1979; Rye et al., 1988).

The occurrence of rhodochrosite as the first mineral in the paragenetic sequence in the hydrothermal veins at Creede is also extraordinary as this mineral is almost always late in the paragenesis of epithermal systems. Figure 6 shows the estimated isotopic composition of fluids responsible for the precipitation of pre-ore rhodochrosites in the Bulldog Mountain and the southern portion of the Amethyst vein system (Rye et al., 1988). These compositions are based the measured δD_{H2O} of inclusion fluids and the $\delta^{18}O_{H2O}$ values calculated from temperature estimates and ^{18}O mineral data. The large horizontal bars reflect the uncertainty in the temperatures due to lack of suitable fluid inclusion material. Fluid inclusions are abundant in the rhodochrosites, but the grain size, and therefore the inclusion size, is small and no inclusions with optics sufficiently good for thermometric studies have yet been found. The average temperature of 190°C is based on the observation that at one locality rhodochrosite alternates with hydrothermal barite and quartz whose temperatures of deposition can be reasonably inferred. The rhodochrosite fluids show a considerable range of isotopic composition over a well defined trend as shown on Figure 6. The data also show a less well defined trend from north to south in the vein system; southern fluids tend to have larger $\delta^{18}O$ and lower δD values. The simplest interpretation of the data is that during pre-ore rhodochrosite deposition the hydrothermal fluids mixed not with meteoric water but with highly evaporated lake water having an exceptionally high $\delta^{18}O$ in the southern part of the district. The origin of the isotopic composition of such a water is discussed in a later section.

The difference in $\delta^{18}O_{H2O}$ and δD_{H2O} between the pre-ore rhodochrosite and main-stage ore fluids has important implications for the isotopic evolution of the lake when viewed in the context of the model in Figure 1 for the Creede hydrothermal system. In this model water from the lake or pore fluids that was recharged into the hydrothermal system at the southern end of the district eventually came back and mixed with meteoric water and/or later lake or pore fluid water. The compositions of ore and pre-ore fluids summarized in solid and shaded rectangles in Figure 1 indicates that water recharged into the hydrothermal system was isotopically different than lake or shallow pore fluid water at the time of ore deposition. This difference may mean that the lake evolved rapidly during the time of ore deposition or that the hydrothermal system was recharged by water from an older lake or from deep pore fluids in the Creede Formation. Many questions remain about the timing of recharge into the hydrothermal system. The important question, then, is would the isotopic evolution implied in Figure 6 be reasonable for water in ancient Lake Creede?

δD_{H2O} and $\delta^{18}O_{H2O}$ of hydrothermal clay minerals

The δD and $\delta^{18}O$ data of illites from alteration zones in the northern Amethyst, the OH and southern Amethyst veins are shown in Figure 7. The δD and $\delta^{18}O$ values of the illites define a linear trend with increasing $\delta^{18}O$ and

decreasing δD values toward the southern parts of the district. This is a remarkably systematic data set which indicates that all of the clay alteration in the district was related to the evolution of a single hydrothermal system. The temperatures of alteration are not known but can be inferred from the temperature structure of main stage mineralization as the alteration is believed to be due to degassing of main-stage hydrothermal fluids. The nature of the illite-water isotope fractionations is such that the trend of the data must reflect both a decrease in the alteration temperature and increase in the $\delta^{18}O_{H2O}$ of the fluids from north to south in the district. The temperature decrease is supported by an increase in the expandable layer content of the illites from north to south in the district (Horton, 1983, 1985, Vergo, 1984). Calculated fluid compositions using presumed temperatures are shown in Figure 7. The temperature of formation for the northern Amethyst illites is assumed to be 200°C. The temperature of formation for the southern Amethyst illites is assumed to be 150°C. The fluid compositions can be interpreted as the result of mixing of hydrothermal and ^{18}O enriched lake water (as for the rhodochrosite fluids in Figure 6) in the southern part of the district with the addition of an overlying meteoric ground water component.

$\delta^{18}O_{H2O}$ and $\delta^{13}C_{CO2}$ of hydrothermal ore fluids

The $\delta^{13}C$ and $\delta^{18}O$ values of the pre-ore rhodochrosites in the Bulldog Mountain vein system in the southern part of the district are introduced in Figure 8 because they show trends that compliment those shown for δD_{H2O}–$\delta^{18}O_{H2O}$ data on the rhodochrosite fluids in Figure 6. They also introduce an important reference point for the interpretation of lacustrine carbonate isotope data discussed later. Although the spatial variations are not entirely systematic along the vein system, the isotopically heaviest carbonates tend to occur in the south and the lightest in the north. As for the δD_{H2O}–$\delta^{18}O_{H2O}$ data discussed above, the simplest interpretation is that the trend in the $\delta^{13}C$-$\delta^{18}O$ data represents the mixing of hydrothermal fluids and isotopically heavy lake or pore fluids in the southern part of the district. The calculated $\delta^{13}C_{CO2}$ and $\delta^{18}O_{H2O}$ values for the fluids are shown by the hachured area in Figure 8. The $\delta^{13}C$ values of CO_2 in the fluids at the southern end are consistent with those of an alkaline lake whose aqueous carbon was derived from the atmosphere and/or volcanic sources. The lower $\delta^{13}C$ values of CO_2 in the fluids at the northern end require a organic component for the aqueous carbon, a conclusion that is supported by previous gas chemistry studies of inclusion fluids in the rhodochrosites in which the fluids for the more northerly rhodochrosites show a greater amount of gas derived from thermal decomposition of organic matter (Landis and Rye, 1988).

The fields shown in Figure 8 outlining the composition of ore and pre-ore fluids are an important reference in later figures for comparison of hydrothermal and lake water compositions. The high $\delta^{18}O_{H2O}$ and $\delta^{13}C_{CO2}$ rhodochrosite fluid compositions define the *end* stage composition of the lake. Another important reference shown by the solid circle in Figure 8 are reasonable $\delta^{18}O$ values for meteoric water and $\delta^{13}C$ values atmospheric and/or volcanic CO_2 at the time of ore deposition. The $\delta^{13}C$ of neither is known precisely but an average value of -7‰ is reasonable for both. As suggested later, most of the CO_2 in Lake Creede was probably derived from volcanic sources. These limiting fluid

compositions will help us bracket depositional temperatures and calculate fluid compositions for sedimentary and diagenetic carbonates.

The δD-$\delta^{18}O$ of Late Oligocene and present day meteoric water

The fluid inclusion data on late-stage vein minerals establishes the approximate δD-$\delta^{18}O$ of the meteoric water component of the ore fluids and, by extension, of the water (δD = -100 to -115‰) that flowed into Lake Creede during the Late Oligocene. The δD and $\delta^{18}O$ values of pore fluids recovered from CCM-1 core (Conca, 1994 are -120 and -15‰, respectively. Thus, the isotopic composition of Late Oligocene meteoric water during ore deposition at Creede was about the same as that observed for meteoric water today in the area, implying a similar climate. As noted later, the δD of fluids for kaolinite in megabreccia beneath the Creede Formation was about -125‰ while fluid inclusion in calcite veinlets in the underlying Snowshoe Mountain Tuff have δD = -122 to -128‰. Both minerals are believed to have formed before the time of ore deposition. Inclusion fluids in travertines that interfinger with lacustrine sediments along the margins of the caldera, and which will later be shown to have formed from fluids which had a major meteoric water component, have δD values of -105 to -128‰. Taylor (1974) calculated δD values of -110 to -130‰ for meteoric water (corresponding to $\delta^{18}O$ values of about -15 to -17‰) in the western San Juans from studies of hydrothermal alteration in 33-25 my old intrusive and volcanic rocks. All evidence indicates that the δD of meteoric water in the Creede area during deposition of the Creede Formation lay within these values.

The possible evolution of δD-$\delta^{18}O$ and salinity of lake water

During evaporation the δD-$\delta^{18}O$ values of dilute meteoric water will change along an approximate 5:1 slope depending on environmental factors such as average wind speed and humidity and can reach extreme isotope enrichments as shown by the solid line in Figure 9. However, during the isotopic and chemical evolution of closed basin lakes δD-$\delta^{18}O$ values do not increase monotonically with increasing salinity. As salinity increases an appreciable amount of water is tied up in hydration spheres around cations, and isotope exchange between the hydration water, the unbound water, water molecules leaving the liquid-air interface, and atmospheric water vapor apparently causes a change of slope and a hook in the δD-$\delta^{18}O$ trajectory (Sofer and Gat, 1975, Holser, 1979; Knauth and Beeunas, 1986). The $\delta^{18}O$ of sea water, for example, increases about 10 permil before hooking back. The relationship between the isotopic composition of evaporated water and salinity is complicated and highly dependent on starting salinity and environmental conditions; at present it cannot be modeled for ancient Lake Creede. Furthermore closed basin lakes, like Mono Lake, CA discussed below, may alternate between periods of stagnation and periods where they overturn and these events can have a great effect on the isotopic and chemical evolution of the lake. A *summary* path for the isotopic evolution of lake water that is consistent with the isotopic composition of ambient meteoric water, the ore fluids, and end stage lake water (as indicated by the pre-ore rhodochrosite fluids) is shown by the dashed line in Figure 9, but many such paths as well as two-stage paths can be drawn. In order to predict the isotopic

composition of Lake Creede after evaporation to a salinity of 13%, it is useful to look at a possible modern analog.

Mono Lake, a possible modern analog

Mono Lake, California is an evaporative, alkaline lake in a dominantly Tertiary volcanic terrain, although the Mono Basin is bounded on the east by the metasedimentary and intrusive rocks of the Sierra Nevada. Mono Lake is a remnant of Pleistocene Lake Russell which had a surface area five times that of the present lake and a lake level about 200 meters higher (Russell, 1889; Lajoie, 1968). Stine (1990) has traced the lake level fluctuations of Mono Lake for the past 3,800 years and shown them to be as large as 40 meters over that period, and that for the past 1,000 years they have been quite regular with transgressive-regressive cycles with a period of about 200 years. Since 1940 much of the Mono lake water supply has been diverted by the Los Angeles Department of Water and Power causing a steady decline in lake level until 1982, since which time it has more or less stabilized. The lake is recharged by snow melt from the nearby Sierra Nevada mountains in a geographic setting similar to that at Creede. The climate at Mono Lake is similar to that at Creede today and probably to that at Creede during the time of ore deposition, but average precipitation is only about one half that in the Creede area. Furthermore, Mono Lake currently has a salinity of about 10% (Bischoff et al., 1993), similar to the predicted values for ancient Lake Creede, has tufa or travertine mounds with ikaite pseudomorphs at the lake margins, and contains no evaporite minerals in the sediments or aquatic life with hard parts. Although abundant diatoms are found in the Mono Lake sediments they have been found only in the travertine mounds that intertongue with the Creede Formation and not in the lake sediments. As shown in Table 2 the isotopic composition and salinity of water in present-day Mono Lake is similar to that of the Creede ore fluids. Mono Lake currently has a salinity of 10%, a δD of -60‰, and a $\delta^{18}O$ of -2.7‰. The isotopic composition of meteoric water flowing into Mono Lake is also similar to that postulated for the ancient Creede area. The Mono Lake data indicate that Lake Creede water could reasonably have evolved to the salinity and isotopic composition observed in the ore fluids. Even if such were the case, an important question is whether the lake water actually reached such isotopic compositions and salinity during the time represented by the portion of the Creede Formation that is still preserved. Approximately one half of the stratigraphic thickness of the Creede Formation has been removed by erosion. The ore fluids may have been derived from a later lake whose history was recorded in sediments which have been eroded.

The δD-$\delta^{18}O$ evolution of Lake Creede water

That Lake Creede waters likely did evolve along a trajectory such as shown in Figure 9 is suggested by the δD and $\delta^{18}O$ values determined for a calcite pseudomorph, presumed after ikaite ($CaCO_3 \cdot 6H_2O$), collected from outcrops of flaggy, sandy siltstone about 750 m north of the CCM-2 drill hole in a section of mixed lacustrine and deltaic sediments. These samples are approximately 150 feet stratigraphically above the collar of CCM-2. The pseudomorphs are represented by casts filled with brownish calcite "pearls" ranging from approximately 0.2 to 2.0 mm diameter. A photograph of pseudomorphs from this locality is pictured in Figure 3 in Larsen (1994). Calcite pseudomorphs after

ikaite (referred to as "rice grains") are common in the lacustrine siltstones of the Creede Formation and will be described later. Most rice grains are 1-2 cm in long dimension, but those described above are exceptionally large, up to at least 10 cm in length. The δD of the water in which the rice grains grew can be determined directly from analyses of water in inclusion fluids. The $\delta^{18}O$ of the water can be determined indirectly from calculations based on the $\delta^{18}O$ of the rice grains and the fact that the primary ikaite precipitated at about 2°C (Larsen, 1994). δD values of the inclusion fluids are -64‰. The $\delta^{18}O$ values for 6 individual "pearls" range from 34 to 36‰ and give an average calculated $\delta^{18}O$ value of 3‰ for the water in which they grew. The isotopic composition of the water plots long the summary δD–$\delta^{18}O$ trajectory in Figure 9, far from a typical (e.g., 5:1) evaporation curve for dilute water, indicating that the pearls grew in a highly evaporated, saline water. The location of the sample in a mixed deltaic-lacustrine section suggests that the ikaite grew either in lake water or in an evaporating pond. In the first case, the δD-$\delta^{18}O$ values indicate that the lake had undergone a high degree of evaporation and attained a significant salinity by the time approximately half the Creede Formation was deposited. In the latter case, the data indicate that Lake Creede waters would have attained such a degree of evaporation and salinity during, or just preceding, the end stage of lake evolution. We prefer the first alternative because it is consistent with our interpretation of the $\delta^{13}C$-$\delta^{18}O$ data on lacustrine carbonates developed in a later section. Painstaking sampling and analysis of stratigraphically lower and higher rice grains may resolve the issue. Whatever the stage of lake evolution represented by the fluids in these rice grains, it is clear that they had a substantially different isotopic composition than did the main stage Creede ore fluids.

The isotopic composition of pore fluids

Lake water was trapped in the tuffaceous sediments during sedimentation and reacted with the glass in the tuff to form alumino-silicate minerals (mainly clinoptilolite and clays) and silica (see Finkelstein et al., 1994 and Larsen and Crossey, 1994) for a complete discussion of the diagenetic mineralogy). Because of the nature of the isotope fractionations between fresh volcanic glass and water, water in the pore fluids of volcanic sediments will tend to be enriched in deuterium and depleted in ^{18}O during the formation of hydrous minerals and zeolites (Savin and Epstein, 1970a; Muelenbachs, 1972). However, noticeable depletion of pore fluid water in ^{18}O occurs only under very low water/rock conditions in the sediments. Under such conditions (with assumptions about clinoptilolite-water isotope fractionation factors and data on the isotopic composition of the tuffs) the water in the pore fluids could have had $\delta^{18}O$ values as low as approximately -20‰. It is unlikely that the water/rock ratio was low enough to produce such extreme values because the volcanic glass probably began to react with the water laid tuffs before compaction resulted in low water/rock ratios in the pore fluid-sediment system. However, as shown later, primary pore fluids in portions of the Creede Formation during diagenesis were replaced by meteoric or lake water. These displaced pore fluids may have been recharged into the hydrothermal system and their isotopic composition may have been modified by exchange with Creede Formation sediments.

δD and $\delta^{18}O$ of authigenic silicate minerals in Creede Formation

Table 3 summarizes isotope data for smectite (after removal of interlayer water) in the CCM-2 drill core and the data for smectite and K-feldspar from the zeolitized tuff in CCM-1. Also shown in Table 3 is the data for interstitial kaolinite in collapse breccia underlying the Creede Formation from CCM-1. This kaolinite is paragenetically earlier than coexisting calcite whose fluid inclusions have filling temperatures averaging 165±2°C. The data on smectite are preliminary because a significant amount of SO_2 evolved from the samples during thermal decomposition for δD analyses. The smectites are very fine grained (<0.2 μm) and the SO_2 is likely derived from structural sulfate or included sulfate which has eluded detection by x-ray diffraction techniques. Recent studies indicate that the samples contain up to 0.1 wt percent SO_4. Until the affects of the SO_2 on the data is determined interpretations based on the isotopic composition of smectites are tentative.

Although their relative paragenesis is not known, smectite and K-feldspar and likely the veinlet kaolinite formed during diagenesis of the Creede Formation. The δD and $\delta^{18}O_{H2O}$ of the fluids in equilibrium with smectite and K-feldspar at the temperatures indicated by the geothermal gradient from studies of silicate mineralogy (Finkelstein et al., 1994) are shown in Table 3. Also shown are the δD and $\delta^{18}O_{H2O}$ of fluid in equilibrium with kaolinite at the temperatures indicated by filling measurements in fluid inclusions in coexisting calcite (N. Foley, oral communication). It is apparent from Table 3 that the smectites and kaolinites at CCM-1 equilibrated with fluids of greatly different $\delta^{18}O_{H2O}$ values than the K feldspars. The fluids in equilibrium with the smectite and kaolinite have an average $\delta^{18}O_{H2O}$ of -7.5‰; fluids in equilibrium with K feldspar have a $\delta^{18}O_{H2O}$ of -13‰. As shown later the $\delta^{18}O_{H2O}$ values for smectite fluids are similar to those that were in equilibrium with veinlet calcite fluids (Table 9 and Figure 34). The $\delta^{18}O_{H2O}$ of these fluids may have been buffered by equilibration with zeolitized tuffs in the Creede Formation. It is also apparent that the smectites at CCM-2 equilibrated with fluids having larger $\delta^{18}O_{H2O}$ than at CCM-1. Calculated $\delta^{18}O_{H2O}$ for fluids in equilibrium with most smectites at CCM-2 range from about -2 to 2 ‰. As shown later, the larger fluid $\delta^{18}O_{H2O}$ values are consistent with those calculated for late lake water from the composition of lacustrine carbonates while the lower values are consistent with those of the ore fluids.

The δD_{H2O} of the veinlet kaolinite fluids is about -125‰ and these fluids were clearly predominantly meteoric water. The δD_{H2O} of the smectite fluids in Table 3 are only approximate because of uncertainty in the hydrogen isotope water-smectite fractionations but the fluids were almost certainly enriched in deuterium over the minerals with values ranging from about -80 to -110‰. Interpretation of the δD data on the smectites is difficult due to their susceptibility to post depositional hydrogen isotope exchange. Nevertheless, δD values as large as -84‰ for the smectites indicate exchange with deuterium enriched pore fluids. Such fluid compositions may reflect anything between exchange with evaporated lake water during diagenesis to exchange with recent meteoric water.

The isotopic composition of diagenetic fluids appears to have been variable in both time and space. It is clear that some diagenetic minerals such as K-feldspar and veinlet kaolinite formed from isotopically light meteoric water. Other

diagenetic minerals such as smectite may have equilibrated with evaporated lake water or fluids buffered isotopically by equilibration with tuffs.

Summary interpretation of δD-$\delta^{18}O$ data

The δD of meteoric water that was the source of water for Lake Creede can be constrained to have been between and -110 and -130‰ with corresponding $\delta^{18}O$ values between -15 and -17‰. The δD and $\delta^{18}O$ values of ground water from the CCM-1 drill hole are -120 and -15‰, respectively. These values imply that the general climate in the Creede area during the Oligocene was similar to that of the present. Water of this composition could easily have evaporated to the salinity and isotopic composition characteristic of the ore fluids in the mining district such as has occurred at Mono Lake which lies in a geographic and climatic setting in California similar to that of ancient Lake Creede. This possibility is supported by direct measurement of Lake Creede water compositions (δD = -64‰, $\delta^{18}O$ = 3‰) from analyses of water in inclusion fluids and the $\delta^{18}O$ of host calcite in rice grains collected from Creede Formation outcrop about 150 feet stratigraphically above the collar of the CCM-2 drill core. These data indicate that the water in Lake Creede evaporated on a δD-$\delta^{18}O$ trajectory consistent with significant salinity. The lake water or pore fluids may have also passed through isotope compositions consistent with those in the hydrothermal system. The isotopic composition of diagenetic fluids during silicate diagenesis varied in time and space. At times during silicate diagenesis portions of the Creede Formation was open to exchange with meteoric water fluids resulting in low $\delta^{18}O$ values of silicates. At other times the Creede Formation may have been closed to external fluids and the $\delta^{18}O_{H2O}$ of the fluids was governed by exchange with sediments under low water/rock conditions. Although the measured δD-$\delta^{18}O$ values of either Lake Creede or Creede Formation pore water do not directly match those of the main stage hydrothermal ore fluids, the implied isotopic evolution of the lake is consistent with derivation of the hydrothermal fluids from either lake water or pore fluids.

CARBON AND OXYGEN ISOTOPE GEOCHEMISTRY

The occurrence, chemistry and stable isotope geochemistry of carbonate minerals in the Creede Formation (and their relation to those in the veins and adjacent wallrock of the Creede mining district) play a critical role in the interpretation of the evolution of Lake Creede and the possible involvement of its water in the Creede hydrothermal system. Carbonates occur as lacustrine limestone lamellae, as introduced cements and concretions, and as calcite pseudomorphs after ikaite (rice grains) in the Creede Formation. Calcite also occurs as numerous travertine mounds along the margins of the Creede Formation (Figure 10) often with calcite pseudomorphs after ikaite and late vug fillings of sparry calcite, and as veinlets in the Creede Formation and underlying caldera-filling Snowshoe Mountain Tuff. The location of lacustrine and travertine carbonate samples analyzed for this study are shown on Figure 10. Calcite also occurs in openings in the wallrocks hosting the veins in the Creede mining district where it is occasionally seen to be replaced by pre-ore rhodochrosite.

The presence of abundant lacustrine carbonates in the Creede Formation and travertine mounds along the margins of the Creede Formation indicate that the

lake was normally saturated with respect to $CaCO_3$. Where did the Ca and aqueous carbon come from and how did calcite precipitate? The tuffs units in the Creede Formation have very little Ca and the Creede Formation as a whole is enriched in Ca relative to the tuffs (Larsen, 1994). This indicates that most Ca in the lake was probably derived from volcanic sources via thermal springs such as shown later to have produced the travertines. Sources of aqueous carbon in the lake include terrestrial organic matter contributed to the lake during spring runoff, organic matter in the lake, volcanic and atmospheric CO_2. The sources of aqueous carbon can be determined from $\delta^{13}C$ data on the carbonates. The $\delta^{13}C$ values of organic matter in the sediments average about -23‰ (Leventhal, et al., 1994). A reasonable average $\delta^{13}C$ value for both volcanic and atmospheric CO_2 is about -7‰. Analogous to present day Mono Lake, most of the aqueous carbon in Lake Creede was probably from volcanic sources (Bischoff et al., 1993). The pH of the lake, especially in the early stages, was probably not high enough for most of the -7‰ CO_2 to have been from atmospheric sources. Precipitation of carbonate in the lake and travertine mounds may have resulted from mixing of Ca and CO_2 rich waters, loss of CO_2 during organic productivity, cooling and/or a pH shift where thermal water mixed with lower temperature alkaline lake water whose pH was controlled by the decomposition of volcanic glass.

Description of lacustrine carbonate occurrences in the Creede Formation

Lacustrine carbonates occur in the Creede Formation as micritic and pelletal lamellae, as rice-grain shaped calcite pseudomorphs and as disseminated micrite grains or clusters of grains. Stratigraphic sections of CCM-1 and CCM-2 showing the distribution of the different lacustrine carbonate occurrences are shown in Figure 10. In Figure 10 the two columns have been indexed to the H tuff (of Larsen and Nelson, 1994) to facilitate comparison. Carbonate lamellae are abundant in the sedimentary siltstones to depths of approximately 1560 feet in the CCM-2 core and 935 feet in the CCM-1 core. Although abundant, the lamellae are not evenly distributed in the cores; there are two hiatuses in the deposition of carbonate lamellae as indicated by light shading in Figure 10. The lamellae range in thickness from less than 0.1 mm to over 2 cm, and consist of either micrite of uniform grain size ranging from 5 to 20 μm (typically 10±3μm) or accumulations of elongated pellets approximately up to 0.1 by 1.0 mm. Often, both occur in the same lamella, typically with the pellets forming the base. We interpret the pellets as brine shrimp fecal pellets as found at Great Salt Lake, Utah (Eardly, 1938) and Lake Urmia, Iran (Kelts and Shahrahi, 1986), on the advice of Richard Forester who has examined several typical specimens at our request (personal communication, 1994). The nature of the carbonate lamellae changes with depth in each of the holes. With depth, the pellets tend to lose their identity and show up as darkened areas or "ghosts" in micrite layers or to become fragmented. The size of the pellets decreases with depth, and within the pellets, the size of the individual grains increases. These changes with depth may be the result of varying degrees of recrystallization as discussed below. Micrite layers become a larger portion of the lamellae with depth, in part because of the loss of identity of the pellets. Near the bottom of the holes the lamellae tend to become thinner (some are only one or two micrite grains thick) and more discontinuous, and zones of individual micrite grains or clusters of grains become the dominant occurrence of lacustrine carbonate.

In addition to the carbonate lamellae and disseminated grains, calcite occurs as rice grains to depths of 580 feet in the CCM-1 core and 804 feet in the CCM-2 core. Rice grains become increasingly rare in the deeper parts of each hole (Figure 10). They are represented in surface exposures as molds, sometimes partially filled with "pearls" of calcite. The rice grains appear to have grown displacively in the tuffaceous muds on the lake bottom, and range in length from 1 to 10 cm, those around 1 cm being by far the most common. These rice grains were originally interpreted as pseudomorphs after gaylussite ($Na_2CaCO_3)_2{\cdot}5H_20$) by Bodine et al., (1988), but Larsen (1991, 1994) has interpreted them as pseudomorphs after ikaite similar to those associated with the travertine mounds discussed in the later section on travertines. The distinction between the two proposed precursor minerals is an important one because each provides different environmental constraints. Gaylussite forms stably at normal surface temperatures (e.g. 0-25°C) and is an indicator of moderate salinity (Bischoff, et al. 1991 Bischoff et al., 1993) whereas ikaite forms metastably at temperatures near 0°C independent of salinity but only when calcite precipitation is inhibited - for example in the presence of orthophosphate (Bischoff, et al. 1993; Larsen, 1994). There are no known unambiguous criteria by which to distinguish between the two precursor minerals; the most indicative is the bipyramidal shape of the rice grains which appears more like the morphology of ikaite (Larsen, 1994). We concur in the interpretation of Larsen, but recognize the possibility that some of the stratal rice grains may be pseudomorphs after gaylussite, gypsum aragonite or some other hydrous carbonate phase. Unequivocal ikaite formation was common in the travertine facies of the Creede Formation.

The possible effects of recrystallization on isotope composition of lacustrine carbonates

Both micrites and pelletal limestone appear to have undergone varying degrees of recrystallization, and in some samples the space between pellets has been filled by clinoptilolite or clear, monocrystalline calcite, presumably of diagenetic origin. Microfabric determinations were made on isotopically analyzed samples from CCM-1 and CCM-2. SEM analyses of lamellae etched with dilute acid indicate that aragonite was the dominant precursor to low-Mg calcite. There is an increase in the degree of recrystallization with depth at CCM-2 . Perhaps all of the lacustrine carbonates, including rice grains, have at least partially recrystallized. Stable isotope compositions of carbonates can be changed during recrystallization only to the degree that the carbonate can exchange with an external reservoir of fluid. The affect of recrystallization on the isotope compositions of lacustrine carbonates from the Creede Formation has not been completely evaluated and is a project for further study. Carbonates that undergo recrystallization in systems closed to fluids will preserve their primary isotope signatures. Only those carbonates that undergo recrystallization in systems open to fluids will undergo changes in isotopic composition. As discussed below our study shows that the Creede Formation was open to meteoric water fluids during at least a part of diagenesis at CCM-1 and it is apparent that isotope exchange occurred between these fluids and the lacustrine carbonates. It is not apparent, however, that CCM-2 was open to such fluids nor

is it apparent that isotope exchange occurred between lacustrine carbonates and any diagenetic fluids at CCM-2.

$\delta^{13}C$ and $\delta^{18}O$ of lacustrine carbonates

General characteristics of the stable isotope systematics for lacustrine carbonates

Figure 11 summarizes the $\delta^{13}C$ and $\delta^{18}O$ data for all types of lacustrine carbonates from both drill core and outcrop. The data are summarized and samples described in Tables 4-6. The $\delta^{13}C$ - $\delta^{18}O$ data set for Lake Creede is extraordinary and, to the best of our knowledge, differs from that reported for any other lake, ancient or modern. It therefore commands special interest. The following points can be made about these data: 1) The range of both $\delta^{13}C$ and $\delta^{18}O$ for the entire data set is very large. This large range of values requires that precipitation of lacustrine carbonates involved fluids having a range of temperature and carbon and oxygen isotopic composition. 2) The data fall into two groups. One group *($\delta^{13}C$ and $\delta^{18}O$ covariant)* has $\delta^{13}C$ values from 4 to -9‰ and $\delta^{18}O$ values from 7 to 27‰ and a well defined negative covariance between $\delta^{13}C$ and $\delta^{18}O$. The other group *($\delta^{18}O$ invariant)* has uniform $\delta^{18}O$ at 35±2‰ and $\delta^{13}C$ from about 6 to -9‰. The stable isotope systematics between the groups are so different that they require fundamental changes in the lake and its environment and/or in mechanisms of carbonate deposition. 3) The negative covariance of isotope data for carbonates in the *covariant group* is opposite from that normally reported for lake sediments, and requires that they precipitated from mixtures of fluids of different temperature and $\delta^{18}O$ values. 4) The narrow range of $\delta^{18}O$ for carbonates in the *^{18}O invariant group* requires that they precipitated from fluids with a narrow range of both temperature and isotopic composition. 5) The $\delta^{18}O$ values of sedimentary carbonates at CCM-1 are as much as 5 permil lower than those at CCM-2 and from outcrop, while the corresponding _ ^{13}C values are as much as 2 permil lower. This difference requires either 1) that CCM-1 carbonates precipitated from fluids which had higher temperatures and/or lower $\delta^{18}O_{H2O}$ values, or 2) that CCM-1 carbonates underwent partial isotopic exchange with later diagenetic fluids, such as those that overprinted much of the silicate mineralogy (Finkelstein, et al., 1994; Larsen and Crossey, 1994). We prefer the latter interpretation.

Figures 12-14 show the $\delta^{13}C$ and $\delta^{18}O$ data set by occurrence type (pellets, micrites, rice grains) for CCM-1, CCM-2 and outcrop samples, respectively. The following points can be made about the data in these figures. 1) The ranges of $\delta^{13}C$ and $\delta^{18}O$ values for micrites and pellets are similar. At CCM-2, where the data set is most complete, micrites and pellets have data points in both the *^{18}O invariant* and *covariant* data groups. This indicates that depositional mechanisms for micritic and pelletal carbonate were similar and implies that the pellets were derived from shrimp that ingested micrite crystallites. 2) Most rice grains occur in the *^{18}O invariant* data set where they have the lowest $\delta^{13}C$ values of the three types of carbonates. The few rice grains that do occur in the *covariant* data set also have the largest $\delta^{18}O$ and lowest $\delta^{13}C$ values in that set. The low $\delta^{13}C$ in the rice grains reflects that fact that the ikaite precipitated in mud where the isotopic composition of aqueous carbon was influenced by decaying organic matter. 3) The narrow range of $\delta^{18}O$ values for all carbonates in the *^{18}O invariant* group including rice grains indicates that they precipitated from water enriched in ^{18}O relative to local meteoric water and at low temperatures (≤4°C). 4) The $\delta^{13}C$

values in the micrites and pellets are very large for lacustrine carbonates and indicate methanogenesis in water or sediments, extreme modification of dissolved organic matter in the lake by photosynthesis, or igneous or atmospheric CO_2 sources of aqueous carbon in the lake. The first two possibilities are not likely because the *maximum* $\delta^{13}C$ values in all of the data sets are those expected for volcanic or atmospheric CO_2 sources for aqueous carbon.

Stable isotope systematics for lacustrine carbonates from CCM-2

In Figure 15 the $\delta^{13}C$ and $\delta^{18}O$ values of micritic carbonates sampled from individual thin sections are indicated by their depth of occurrence at CCM-2. In Figure 16 the $\delta^{13}C$ and $\delta^{18}O$ values of all three types of carbonate occurrences, including the micrites, at CCM-2 are shown for various depth ranges. The salient features of the $\delta^{13}C$ and $\delta^{18}O$ systematics for sedimentary carbonates at CCM-2 are as follows: 1) At the deepest levels, below 1300 feet, both the $\delta^{13}C$ and $\delta^{18}O$ values of micrites from individual thin sections tend to fall in clusters with narrow ranges (~ ±2‰). The average $\delta^{13}C$ and $\delta^{18}O$ values for these clusters show a wide range, and an overall inverse $\delta^{13}C$ and $\delta^{18}O$ covariance (with the exception of the sample from 1344 feet). 2) At intermediate depths, between 700 and 1300 feet, the $\delta^{13}C$ and $\delta^{18}O$ values of micrites and pellets from *individual* thin sections also show an inverse covariance wherein the range of values for samples in individual thin sections is ≤ 15‰ for $\delta^{18}O$ and ≤ 4‰ for $\delta^{13}C$. The data set as a whole also shows an inverse $\delta^{13}C$ and $\delta^{18}O$ covariance, but the trajectory for the overall data set is steeper than those for individual thin sections. 3) At shallow depths, above about 700 feet, rice grains appear and $\delta^{18}O$ values for all lacustrine carbonates become invariant in spite of a significant range of $\delta^{13}C$ values. 4) As indicated by the variation of isotopic composition of pellets and one micrite sample over the range of approximately 550-750 feet (Table 5; Figure 16), the change in the stable isotope systematics from one group to another does not occur abruptly but oscillates over a stratigraphic interval of at least 200 feet. Similar oscillations may have occurred for individual samples in the covariant group whose isotopic systematics change around 1300 feet. The internal aspects of these data for individual samples suggests that the stable isotope systematics are largely determined by primary precipitation from lake water and not to exchange with external fluids during diagenesis. The different stable isotope systematics for lacustrine carbonates at deep, intermediate, and shallow levels at the footages listed above at CCM-2 define the *initial, early, transitional* and *late* stages of lake history.

Stable isotope systematics for lacustrine carbonates from CCM-1

Figure 17 shows the $\delta^{13}C$ and $\delta^{18}O$ values of micritic and rice grain carbonates sampled from individual thin sections in relation to their depth of occurrence at CCM-1. Figure 18 shows the same for pelletal limestones from CCM-1. The overall stable isotope systematics at CCM-1 for lacustrine carbonates are very similar to those for the deeper levels of CCM-2, which is not surprising considering the stratigraphic correlations between the two sites by Larsen and Nelson (1994) (see Figure 11). The $\delta^{13}C$ and $\delta^{18}O$ values of micrites and pellets from individual thin sections in CCM-1 tend to fall in clusters or show an inverse covariance as in CCM-2. However, in spite of the general similarities of isotope systematics the $\delta^{18}O$ values for micrites and pellets in a

early and intermediate carbonates in CCM-1 are as much as 5‰ lower than in CCM-2, consistent with isotope exchange during diagenesis at CCM-1.

$\delta^{13}C_{CO2}$ and $\delta^{18}O_{H2O}$ of lacustrine carbonate fluids

Figure 19 shows the calculated fields of $\delta^{13}C_{CO2}$ and $\delta^{18}O_{H2O}$ values of the initial (asterisks), early and transitional (solid symbols), and late lake (open symbols) fluids in equilibrium with the lacustrine carbonates from at CCM-2. Temperatures assumed in the calculations were 25°C for the samples with the lowest $\delta^{18}O$ in *covariant* group and 2°C for samples with the largest $\delta^{18}O$ in the covariant and for all samples in the *$\delta^{18}O$ invariant* group. The 25°C temperature gives the best fit for the limiting $\delta^{18}O$ value for meteoric water. The 2°C temperature is required by the presence of rice grains in the sample group. The fractionation factors used are based on the equation of O'Neil, et al. (1969) for ^{18}O and Bottinga (1969) for ^{13}C. The dashed lines in the figure show the fractionations at 25°C and 2°C for specific samples which limit the data field. The largest fluid $\delta^{13}C$ values for both groups of fluids are typical of an evaporative lake whose aqueous carbon was derived from atmospheric or volcanic CO_2. The lowest fluid $\delta^{13}C$ values are typical of carbon from organic sources. The lowest $\delta^{18}O_{H2O}$ values are typical of local meteoric water. The largest $\delta^{18}O_{H2O}$ values indicate that the lake, especially the late (*invariant*) lake, was highly evaporated. The $\delta^{18}O_{H2O}$ of the early and transitional (*covariant*) lake appears to have reached values of at least -8 to -4‰ while the average value of the late *^{18}O invariant* lake was about 2‰.

Figure 20 shows the isotopic composition of calculated fluids for lacustrine carbonates from CCM-1. As shown by the upper dashed line, the limiting $\delta^{18}O$ and $\delta^{13}C$ values for meteoric water require a temperature of at least 40°C for equilibrium between the lowest $\delta^{18}O$ samples and meteoric water. The $\delta^{18}O_{H2O}$ of the fluids for the few rice grains in CCM-1 are also lower than those observed for rice grains in CCM-2. The difference in $\delta^{18}O$ values between the CCM-1 and CCM-2 carbonates reflect either 1) higher initial temperature of deposition and/or lower $\delta^{18}O_{H2O}$ of water at CCM-1. However, a temperature of 40°C, nearly 15°C higher than that at CCM-2, is clearly too high for primary carbonate deposition and there is no evidence that the $\delta^{18}O$ of meteoric water was ever lower than -17 permil in the late Oligocene at Creede; 2) alteration of primary isotope compositions by exchange with external fluids during diagenesis at CCM-1. This possibility is consistent with the observations by Larsen and Crossey (1994) and Finkelstein et al. (1994) that silicate sediments at CCM-1 have a greater hydrothermal overprint and lower $\delta^{18}O$ values (Table 3) and probably had an initially higher geothermal gradient than the sediments at CCM-2. This possibility is also supported by a greater degree of introduced carbonate in the sediments at CCM-1 than at CCM-2. As discussed below this possibility is also supported by stable isotope data from CCM-1 on a large ikaite pseudomorph that presumably was rafted from a near shore travertine mound. Data on this pseudomorph (CCM-1R066 0.70 in Table 4), which likely retained primary compositions obtained during precipitation from evaporated lake water, can be compared with those on micrites near the same stratigraphic level and which appear to have undergone post depositional isotope exchange.

Models of carbonate precipitation mechanisms

As previously mentioned Lake Creede is believed to have been a saline closed basin lake containing brine shrimp much like Mono Lake, CA. To the extent that this is true, carbonate precipitation mechanisms at Mono Lake and other such lakes provide a framework for preliminary interpretations of the isotope data on the lacustrine carbonates of the Creede Formation. Generalizations here regarding carbonate deposition at Mono Lake are based on the summary report of the Mono Basin Ecosystem Study Committee of the National Research Council (1987) and similar saline lakes (Gat, 1980). Lacustrine carbonate deposition is related to the organic productivity of the lake and occurs in the spring and summer as photosynthetic algae remove CO_2 from the water. We can infer that the isotopic compositions of the carbonates (presumably micrites) resulting from this algal activity will reflect the temperature and isotopic composition of water at the productive zone of the lake. As brine shrimp graze on the algal organic matter they also ingest fine carbonate grains that become fixed in their fecal pellets. Thus we can infer that fecal pellets and micrites will be isotopically indistinguishable. Because of the relatively large size of the pellets they will tend to form the bottom of carbonate lamellae that are related to single algal blooms while slower settling carbonate grains form the micritic top. During spring run-off when the lake is most productive evaporated lakes typically have a shallow surface layer of unevaporated low ^{18}O meteoric water which is warmed by solar radiation (Talbot, 1991). The water in the productive zone can thus have a range of isotopic compositions depending the factors which control the level of productivity in the lake and on its position relative to the chemocline. As is typical of saline lakes (Gat 1980), the deep saline water is isolated from the rest of the lake during periods in which it is meromictic (stratified) and the $\delta^{18}O$ of the deeper portion of lake may be expected become invariant until the lake begins to overturn again. Stratification occurred a Mono Lake following run off of exceptionally heavy snowfall in 1983. In addition to water from spring run off, Mono Lake also receives meteoric water containing both dissolved Ca and CO_2 from near shore springs which upon mixing with saline lake water produce tufa mounds at the lake margins (Bischoff et al., 1993). The aqueous carbon at Mono Lake is largely derived from volcanic sources; the lake is not alkaline enough for the aqueous carbon to be dominated by atmospheric CO_2.

The isotope data on carbonates from the *^{18}O invariant* group in the upper part of CCM-2 require low temperature and a large and constant $\delta^{18}O$ of lake water. These data preclude mixing as a depositional mechanism and suggest that carbonate deposition occurred in a stratified lake in which most of the productivity of the lake was in stratified water below the interface between meteoric and saline water (chemocline). In contrast, the isotope data on the carbonates from the *covariant group* in the lower part of the section at CCM-2 are best explained by deposition in mixtures of meteoric water containing volcanic (or atmospheric) CO_2 with cool evaporated lake water containing CO_2 derived through the oxidation of organic carbon. Dilute meteoric water may have been added to the lake from springs and/or from spring run off and CO_2 may have been added from volcanic sources. Isotopic mixing could have been affected by overturning in the lake and/or by variations in the level of carbonate precipitation in a gradational interface, perhaps related to the location of abundant organic activity in the upper levels of the lake conditioned by depth of penetration of light required for photosynthesis.

$\delta^{13}C$ and $\delta^{18}O$ of lacustrine carbonates over time

The $\delta^{18}O$ and $\delta^{13}C$ values of lacustrine carbonates at CCM-2 are plotted versus stratigraphic position in Figure 21. A similar plot for $\delta^{18}O$ values at CCM-1 is shown in Figure 22. The stratigraphic axis at CCM-2 may represent as much as 600,000 years of sedimentation. The following salient features of the data (indicated by the trend lines on Figure 22) at CCM-2 and their interpretation can be made. 1) The lowest $\delta^{18}O$ values are constant until about 700 feet and then show a steady increase up section. These data indicate a fairly constant $\delta^{18}O$ for meteoric water in the early and transitional lake at lower levels and a decreasing involvement of meteoric water in carbonate precipitation for the lake at higher levels. 2) The largest $\delta^{18}O$ values increase with stratigraphic level until they become constant at about 700 feet. These data are interpreted to indicate a gradual increase in salinity and carbonate deposition from mixed waters until the lake became stratified at higher levels, after which carbonate deposition was largely from saline waters. 3) The lowest $\delta^{13}C$ values increase at higher stratigraphic levels. These data indicate an increasing role of atmospheric and/or volcanic CO_2 in the aqueous carbon of the lake relative to that from the oxidation of organic matter. 4) The highest $\delta^{13}C$ values also increase at higher stratigraphic levels, also possibly indicating an increasing role of atmospheric and/or volcanic CO_2 in the aqueous carbon of the lake as the lake became stratified and/or became more alkaline.

The $\delta^{18}O$ of lacustrine carbonates at CCM-1 are plotted versus stratigraphic position in Figure 22. The section at CCM-1 is less well characterized and the lowest part of the section has not been analyzed. The isotopic systematics at CCM-1 are noticeably different than those at CCM-2 as indicated by the trend line in Figure 22: 1) The lowest $\delta^{18}O$ values are not constant and are lower than the lowest $\delta^{18}O$ values at CCM-2. 2) The largest $\delta^{18}O$ values are lower than the largest values at a comparable stratigraphic level at CCM-2. 3) The largest $\delta^{18}O$ values for lacustrine carbonates are lower than the largest values for a large ikaite pseudomorph at 580 feet whereas the $\delta^{18}O$ values for this pseudomorph are similar to those for the largest $\delta^{18}O$ values at comparable stratigraphic level at CCM-2 . This pseudomorph was probably rafted from a travertine mound near the paleo-shore. As will be discussed, studies of these ikaite pseudomorphs have shown that they originally precipitated in unmixed lake water and we may expect them to be extremely resistant to post depositional isotope exchange. The above observations suggest that the lacustrine carbonates at CCM-1 underwent post depositional exchange with meteoric water during diagenesis but that such exchange probably did not occur at CCM-2.

Factors controlling evolution of the Lake

The $\delta^{13}C$ and $\delta^{18}O$ data suggest that the interplay of environmental factors (e.g. climate, hydrologic balance) affecting carbonate deposition underwent fundamental changes twice during the time interval represented by the CCM-2 core, and that the conditions between changes remained relatively constant for long periods of time. The nature of the interplay between environmental factors and carbonate precipitation at each of the three stages of the lake evolution, and the factors causing them to change are not yet fully understood and are a subject of future study. It seems very likely that as the lake evolved the $\delta^{18}O$ of the

evaporated lake water gradually increased, that carbonate deposition involved increasingly less mixing with meteoric water, and that the lake eventually became stratified and remained *^{18}O invariant* for as much as 500,000 years, although more data are required to document the constancy of the $\delta^{18}O$ values over such a long time period. An intriguing possibility is that this evolution was related to a climate change that occurred in the late Oligocene during a major expansion of the Antarctica ice sheet (Hay, 1988). However, the evolution may have been related simply to a gradual increase in salinity coupled with gradual changes in physiography which changed the hydrologic balance or thermal structure in the lake. The range of $\delta^{13}C$ values in the *^{18}O invariant* group carbonates reflects various mixtures of carbon from organic matter and atmospheric or volcanic CO_2 in the stratified portion of the lake. If the lake was stratified for long periods of time, as appears to have been the case, the major source of aqueous carbon was most likely volcanic rather than atmospheric CO_2 as the stratified portion of the lake would have been isolated from the atmosphere.

Lake Creede and ore deposition

Now let us consider whether the ultimate source of the ore fluids could have been the lake that was contemporaneous with the preserved part of the Creede Formation. At this stage of our discussion we will assume that the ore fluids were derived directly from the lake rather than from pore fluids and that the isotopic composition of the lake water was not altered by exchange with wallrock during recharge into the hydrothermal system. These assumptions may have to be modified in the future. The $\delta^{18}O_{H2O}$ and $\delta^{13}C_{CO2}$ of the hydrothermal fluids responsible for pre-ore rhodochrosite and ore deposition as discussed earlier are shown in Figure 22 for comparison with those of the Lake Creede fluids. The $\delta^{18}O_{H2O}$ values for the hydrothermal and lake fluids do not match in such a way as to identify specific lake fluids involved in ore deposition. The $\delta^{18}O_{H2O}$ values of the *initial* and *early* lake appear too low to have been the source of the ore fluids while those of the *late* lake are too large. However, mixtures of early and late lake fluids as well as mixtures of meteoric water with various stages of lake water could account for the $\delta^{18}O_{H2O}$ of the hydrothermal fluids. It is also possible that the ore fluids could have been derived from the late lake pore fluids. In any event, the lake had not reached the extreme $\delta^{18}O_{H2O}$ values characteristic of the fluids during rhodochrosite deposition. Thus, even though the lake from which the preserved portion of the Creede Formation was deposited may have had sufficient salinity and isotopic composition it is possible that water from *that* period of lake history was not the source of the ore fluids. That the ore deposits may have formed from fluids derived from a later, more evolved version of Lake Creede than represented by our drill core samples is not surprising. The upper one half to two thirds of the Creede Formation has been eroded. Our study has shown that the lake underwent considerable evolution and although the late lake water appeared to have been isotopically constant for a long time we would expect that the lake continued to evolve (especially when it eventually became more shallow) until the time of ore deposition, which may have occurred as much as 1 my after the deposition of the oldest preserved Creede Formation (Lanphere, 1994). There is no evidence to indicate whether or not the lake existed during ore deposition.

$\delta^{13}C$ and $\delta^{18}O$ of diagenetic carbonates

Calcite cements are common in both cores, particularly in the coarser layers, and calcareous concretions occur throughout the section; both are interpreted as diagenetic products. The $\delta^{13}C$ and $\delta^{18}O$ values of diagenetic carbonates from CCM-1, CCM-2, and outcrop are summarized in Figure 24 along with calculated fluid compositions for end member samples of the data set (connected by tie lines). The calculated temperatures associated with tie lines in Figure 24 are, in turn, constrained by the end member $\delta^{18}O_{H2O}$ and $\delta^{13}C_{CO2}$ values of the data set. The important features of the data are: 1) Both $\delta^{18}O$ and $\delta^{13}C$ values for the entire data set show a large range indicating that diagenesis involved fluids with a large range of isotopic compositions and temperatures consistent with the isotope data on the diagenetic silicates shown earlier. 2) The lowest $\delta^{18}O$ and $\delta^{13}C$ values for the diagenetic carbonates at CCM-2 are lower than the $\delta^{13}C$ and $\delta^{18}O$ values for lacustrine carbonates. 3) Insofar as the data are representative of the range of stable isotope compositions for diagenetic carbonates for each hole, the data range at CCM-1 extends to lower $\delta^{18}O$ values than that for CCM-2, consistent with a similar difference noted above for isotopic compositions of lacustrine carbonates and for diagenetic smectites at the two sites.

It is clear that some diagenesis at CCM-1 involved the exchange with meteoric water at elevated temperatures as samples having the lowest $\delta^{18}O$ values at CCM-1 must have precipitated from unexchanged meteoric water at about 80°C. This temperature is consistent with those inferred for diagenesis from the silicate mineralogy of the Creede Formation (Finkelstein et al., 1994). As previously discussed, the involvement of meteoric water during diagenesis at CCM-1 is also consistent with the origin of diagenetic K feldspar in the tuffaceous sediments of the Creede Formation. As will be discussed, it is also consistent with the large heated meteoric water component in the travertine fluids along the margin of the caldera. Diagenesis at CCM-2 appears to have occurred at lower temperatures and involved isotopically heavier water such as lake water as shown by constrained calculated fluid compositions in Figure 24. The low $\delta^{13}C$ values for many diagenetic carbonates reflect the contribution of organic sources to the aqueous carbon of diagenetic fluids.

Summary interpretation of $\delta^{13}C$ and $\delta^{18}O$ data for lacustrine and diagenetic carbonates

The stable isotope data on lacustrine carbonates place important constraints on the evolution of the lake and on the relationship of the lake to ore deposition. The inverse correlation for $\delta^{13}C$ and $\delta^{18}O$ values for lacustrine carbonates in the deeper part of the Creede Formation is the opposite of that normally observed in either open or closed basin lakes (Talbot, 1991). We believe that this trend reflects carbonate precipitation from mixtures of warm dilute meteoric water containing volcanic and/or atmospheric CO_2 and cool saline water containing CO_2 derived from the oxidation of organic carbon. Mixing may have involved the introduction of spring water or may have been facilitated by overturning in the lake or by changes in the relative positions of the productive zone and the chemocline. The narrow range of large $\delta^{18}O$ values and the abundance of rice grains in the upper part of the CCM-2 core indicates that all later carbonates precipitated below the mixing interface at low temperatures from ^{18}O enriched

waters with an average $\delta^{18}O$ of about 2‰. This condition was likely caused by a prolonged period of stratification of the lake after it had developed significant salinity. The cause of the shift in conditions of carbonate deposition may reflect a gradual increase in salinity or changes in the hydrologic balance of the lake as a result of changes in climate or physiography.

Although the carbonate isotope data alone cannot be used to indicate water salinity, much evidence indicates the late lake had significant salinity, although high salinities are not reflected in the diagenetic silicate mineralogy or the compositions of the carbonates (Finkelstein et al, 1994; Larsen and Crossey, 1994). This evidence includes: 1) the isotopic compositions of the lake water measured directly from rice grains and contained inclusion fluids that are consistent with water that evaporated on a hooked δD-$\delta^{18}O$ trajectory typical of saline water, and 2) the presence of brine shrimp which tolerate salinities above 10%, 3) a long period of invariance of $\delta^{18}O_{H2O}$ consistent with a stratified saline lake, and 4) a gradual increase up section in both the maximum and minimum $\delta^{18}O$ values for the lacustrine carbonates. Although a specific period of lake history can not the identified the carbonate isotope data are consistent with either the lake or Creede Formation pore fluids as the source of the hydrothermal fluids.

The stable isotope data on diagenetic carbonates along with data presented earlier on diagenetic silicates indicate that the nature of diagenetic fluids varied in time and space in the Creede Formation. It also appears, on the basis of preliminary data, that carbonate diagenesis at CCM-1 involved greater amounts of meteoric water and higher temperatures than at CCM-2. Diagenesis at CCM-2 involved isotopically heavier fluids such as lake water. Diagenetic fluids at both localities acquired aqueous carbon from the hydrolysis of organic matter and thus probably removed organic matter from the sediments.

Description of travertines

Travertine mounds occur along both the inner and outer margins of the Creede Formation (Figure 25) where they interfinger with sediments of the Creede Formation and appear to have mostly formed sub-aqueously similar to the tufa mounds of Mono Lake, CA and Pyramid Lake, NV. Calcite occurs as massive to banded travertine and in elongated square-sided pyramidal structures up to one meter in length similar to the thinolites associated with the tufa mounds of Mono and Pyramid lakes. Larsen (1991,1994) first recognized these structures at Creede and interpreted them as pseudomorphs after ikaite ($CaCO_3 \cdot 6H_2O$). Within the pseudomorphs, calcite occurs as rounded "pearls" consisting of a clear subhedral calcite core surrounded by an acicular, often banded calcite rim; spaces between the "pearls" are partially filled by chalcedony and later quartz. The margin of the pseudomorph is coated with a calcite layer similar to the rims on the pearls. Some travertine mounds are composed, in part, of interbanded calcareous and siliceous layers. The siliceous layers contain abundant cigar-shaped fossil diatoms and bacteria filaments. Calcareous layers also contain both diatom and bacteria fossils, but in lower abundance; diatom fossils in particular are less abundant. Late quartz crystals and sparry calcite occur in voids in travertine mounds. Some travertines contain framboidal pyrite, usually partially or completely oxidized to iron oxide, and some are so rich in organic matter that globules of oily matter are released during dissolution of the

travertine in HCl. Fragments of ikaite pseudomorphs that were probably rafted from near the paleo-shore are also observed in the deeper levels of the CCM-1 drill core suggesting that travertine mound formation began very early in the history of the lake.

$\delta^{13}C$ and $\delta^{18}O$ values of travertines

The isotope data on travertines are summarized in Tables 7 and 8. In Figure 26 the isotopic composition of travertines obtained by microsampling (bold symbols) are compared with those obtained more than 15 years ago by analyzes of bulk samples (faded symbols). As expected, the micro sample data show a larger range of values, but in general the data sets are comparable. Figure 27 shows the data ranges for individual thin sections. $\delta^{13}C$-$\delta^{18}O$ values show a positive correlation except for one samples that shows an inverse covariance such as observed for early lacustrine carbonates. In Figure 28 the $\delta^{13}C$-$\delta^{18}O$ data for the travertines are compared with the data field for sedimentary carbonates. The cores of the "pearls" in the ikaite pseudomorphs have a large range of $\delta^{13}C$ values and a narrow range of large $\delta^{18}O$ values similar to those for the ^{18}O invariant group in the lacustrine carbonates at CCM-1 and 2. The $\delta^{13}C$-$\delta^{18}O$ values for the rims of pearls and later travertines overlap that of the lacustrine carbonates and the data set outlined by the dotted field on the upper left side of in Figure 28 defines a slope that is different from that of the early and transitional lacustrine carbonates but similar to that for most individual travertine samples (see Figure 27).

Temperatures of travertine mound deposition

The minimum temperature of carbonate deposition in travertine mounds was probably about ≤2°C as indicated by the presence of ikaite pseudomorphs (Bischoff et al., 1993, Larsen, 1994). The maximum temperature of travertine deposition can be estimated from calculations of the temperature of deposition of interlayered chalcedonic silica based on the $\delta^{18}O$ data of the silica, and an assumed $\delta^{18}O$ of the fluid from which it was deposited (Figure 29). By assuming that the parent fluids was meteoric water with an average $\delta^{18}O$ value of -15‰, the temperature of deposition of the silica can be calculated to have been 45±9°C.

The calculated temperature changes approximately 4.5° C for each 1‰ change in the assumed composition of the starting fluid. If a larger $\delta^{18}O_{H2O}$ value for the fluid is assumed, the calculated temperatures of deposition are higher. If a lower $\delta^{18}O_{H2O}$ value for the fluid is assumed, the calculated temperatures are lower. Even if we assume a value as low as -17‰ (the limiting value for meteoric water in the area) calculated temperatures of deposition are greater than 30 °C for most samples. This evidence, and that presented below, indicates that travertine deposition involved a warm-temperature meteoric water component.

The formation of thinolitic travertine mounds

The isotope data presented in Figure 30 and 31 require that travertine mound formation was a two stage process involving an ikaite and travertine components and that the ikaite component was derived from unmixed saline lake water and that the travertine component resulted from the mixture of heated meteoric water fluids and mixed lake water. The cores of "pearls" in the ikaite

pseudomorphs at Creede presumably represent carbonate that originally precipitated at ≤2°C. Ikaite becomes unstable at temperatures above about 4°C and during recystallization to calcite undergoes a significant volume reduction. We can thus argue that the later travertine forming the rims of the pearls must have precipitated (presumably at temperatures very close to 4-5°C) in the voids of the ikaite pseudomorph as the original ikaite recrystallized to form the pearls or the pearls would have dispersed into the lake. Figure 30 shows the $\delta^{13}C$-$\delta^{18}O$ data for the cores of pearls, the travertine rims of the pearly cores within the pseudomorphs, and the travertine margins for large thinolitic pseudomorphs after ikaite near Wason Ranch. Similar data have also been obtained for the thinolitic pseudomorphs northwest of Antlers Ranch (Table 8). The $\delta^{18}O$ values for the rims and margins are essentially the same and are distinctly different from those for the cores of pearls. If we assume a temperature of 2°C, the parent fluid for the cores of pearls had $\delta^{13}C_{CO2}$ values of ~ -7‰ and $\delta^{18}O_{H2O}$ values of ~ 2‰. These values are the same as those calculated for the lake fluids during the deposition of the upper part of CCM-2 (Figure 21). If we assume 5°C for the temperature of deposition of the later travertine rims and margins with the lowest $\delta^{18}O$ values in Figure 30, the parent fluids had $\delta^{13}C_{CO2}$ values of ~-7 to -10‰ and corresponding $\delta^{18}O$ values of ~-8 to -12‰. The data require that much travertine mound formation was a two-stage process. The ikaite formed in saline lake water and apparently decomposed to calcite forming the cores of the pearls when bathed in travertine fluids of different isotopic composition.

Figure 31 shows isotope data for travertine (solid symbols) and individual pearls for ikaite pseudomorphs (open symbols) from various localities including those for the Wason locality shown in Figure 30. The $\delta^{18}O$ values of the pearls are the same as those observed for thinolitic pseudomorphs from Wason but $\delta^{13}C$ values extend to lower values. As shown in Figure 31, these pearls had fluid compositions similar to those for the late lake in CCM -2. Some of these samples were collected at elevations above 9000 ft. The data on the pearls in the pseudomorphs thus extend the time period during which the lake was ^{18}O invariant for a time interval represented by deposition of the Creede Formation to levels at least 500 feet above the collar of the of the CCM-2 drill hole.

The $\delta^{13}C$ and $\delta^{18}O$ values of the boundary data set for the travertines indicated by the shaded background in Figure 31 shows a well defined positive correlation that is a continuation of the trend shown in Figure 30. These boundary data for travertine have a larger range of $\delta^{13}C$ and $\delta^{18}O$ values than can be obtained solely by either mixing of fluids of different composition or by changes in temperature of deposition. The trend for these data must be a result of the combined effect of mixing of fluids of different compositions at different temperatures. Calculated average fluid compositions are shown by the shaded bar in Figure 31. The extreme isotopic compositions of the ends of the bar are limited by both the presumed $\delta^{13}C$ and $\delta^{18}O$ values of meteoric water and atmospheric/volcanic CO_2. Temperatures of deposition associated with end member fluid compositions of the bar in Figure 31 were calculated using fluid compositions constrained by those of meteoric water and atmospheric/volcanic CO_2. These temperatures indicate that travertine deposition resulted from the mixing of warm meteoric water fluids ($\delta^{18}O \approx -15$‰) with cool, shallow (partially mixed) lake waters ($\delta^{18}O \geq -8$‰). The δD_{H2O} values of inclusion fluids

in travertines (-102 to -128‰; Table 8) are consistent with a strong meteoric water component in the travertine fluids.

The simplest interpretation of the data in Figure 30 and 31 is that ikaite formed during the winter (or a prolonged cold period) when the spring fed thermal meteoric water component to the lake was diminished and the $\delta^{18}O$ of the lake was relatively uniform. Travertine deposition occurred later, probably in the spring, when thermal spring water mixed with lake water in turn partially mixed with the shallow low $\delta^{18}O$ meteoric water that accumulated on top of the evaporative lake during the spring run-off.

This model for the deposition of travertine at Creede is somewhat different than that proposed for tufa at Mono (Bischoff et al., 1993) and Pyramid Lakes (L. Benson, personal communication, 1994) where meteoric water from Ca-rich springs mixes with CO_2-rich water along the lake margins to form ikaite. At Creede ikaite formed in saline water below the zone of mixing with shallow meteoric water. Travertine formed later by the mixing of warm meteoric water and cool shallow lake water which filled the framework created by the decomposition of ikaite. Repeated cycles of this process led to travertine mound formation. Some of the travertines at Creede are very rich in organic matter. This organic matter may have been responsible for the low $\delta^{13}C$ values in some of the travertine in Figure 31. However, these low $\delta^{13}C$ values may also have been derived from diagenetic fluids from the Creede Formation sediments.

Summary interpretation of travertine $\delta^{13}C$ and $\delta^{18}O$ data

The isotope data indicate that much travertine mound formation was a two stage process involving deposition of true travertine over ikaite which previously had decomposed to form calcite pseudomorphs composed of a porous framework of calcite pearls. The process by which the crystal shape of ikaite was retained during the conversion to a framework of unconnected calcite pearls is not understood except that the conversion was apparently accompanied or closely followed by travertine deposition as rims on the pearls and margins of the crystals as the ikaite started to decompose at temperatures above 4°C. Ikaite was probably deposited in the winter from isotopically uniform saline lake waters whose average $\delta^{18}O$ was about 2‰ or the same as that calculated for the lake during deposition of lacustrine carbonates in the upper part of CCM-2. The data on the pearls in the pseudomorphs thus extend the time period during which the lake was ^{18}O invariant an additional increment represented by moat filling to elevations 500 feet above the collar of the of the CCM-2 drill hole. Most travertine deposition probably began in the spring and involved mixing of deeply circulating, Ca-rich, warm meteoric water with a shallow layer of isotopically light meteoric water formed during the spring run-off. Interbanded silica was derived from the warm meteoric water component.

Description of vein calcites in CCM-1 and CCM-2 and pre-ore calcite in the wallrocks hosting the veins in the Creede mining district

Calcite occurs in veinlets up to several cm in aperture in both the Creede Formation and underlying Snowshoe Mountain Tuff. Some veinlets in the Snowshoe Mountain Tuff contain pyrite as well as several generations of calcite, some as coarse calcite blades up to several cm in length. Calcite veinlets in the sediments seldom exceed 1 cm in aperture and often contain analcime and

occasionally unidentified fibrous and platy zeolites as well as minor pyrite. Both prismatic and equant calcite crystals have been observed. Some veinlets appear to be syndepositional. Sparry calcite also occurs in vugs in travertines, usually overlying quartz crystals. Finally, pre-ore calcite occurs in open spaces in the wallrocks surrounding the veins in the southern part of the Creede mining district. The age of the carbonate veinlets in the Creede Formation and their relationship to the sparry calcite in the travertines and the pre-ore wallrock calcite and later pre-ore rhodochrosites in the hydrothermal veins in the southern part of the district is not known. However, it is most likely that the veinlets formed during diagenesis prior to ore deposition; the data presented below are consistent with this assumption. Also, with two exceptions, the temperatures of deposition of these different carbonates are not known due to lack of suitable fluid inclusions. However, depositional temperatures for the calcite veinlets in the Creede Formation and Snowshoe Mountain Tuff can probably be assumed to have been between 50° and 150°C. In some cases they may reflect temperatures of the geothermal gradient during diagenesis as indicated by the silicate mineralogy in the zeolitized tuffs (Finkelstein et al., 1994). The temperatures of deposition for the wallrock calcites around the Bulldog Mountain veins can probably be assumed to have been higher than those of the Creede Formation veinlets but less than the 190±30°C assumed for the later rhodochrosites.

$\delta^{13}C$ and $\delta^{18}O$ values of calcite in veinlets in drill cores and in wallrocks in the Creede mining district.

Figure 32 shows our carbon and oxygen isotope data for all vein and wallrock calcites in the district along with the data for the pre-ore rhodochrosites shown previously in Figure 8. Ilchik and Rumble (1994) report additional data for calcite veinlets in the Snowshoe Mountain Tuff. Each type of carbonate in Figure 32 has a distinct range of $\delta^{13}C$-$\delta^{18}O$ values and the group as a whole has $\delta^{13}C$-$\delta^{18}O$ values that overlap the lower values of the data field of the lacustrine carbonates. It is obvious that each of the five types of carbonates had its own unique fluid history. However, detailed interpretations of fluid history are difficult because temperatures of deposition are not known. Furthermore the paragenetic relationships of the calcite in travertine vugs, in the Creede Formation and Snowshoe Mountain veinlets, in the wallrocks hosting the veins in the mining district, and the pre-ore rhodochrosites in the hydrothermal veins are unknown, except that the wallrock calcite precedes the pre-ore rhodochrosite. The $\delta^{13}C$-$\delta^{18}O$ values of all vein and veinlet carbonates are consistent with formation at higher temperatures and/or greater meteoric water fluid involvement than the lacustrine carbonates. In Figures 32 to 35 we can use the inferred temperatures for some samples to calculate possible fluid compositions for a given type of calcite. The large range of $\delta^{13}C$ values suggests atmospheric/volcanic and organic carbon sources for aqueous carbon in the parent fluids. These sources of aqueous carbon suggest that a component of the parent fluids of all types of carbonates was ultimately related to lake water.

$\delta^{13}C_{CO2}$ and $\delta^{18}O_{H2O}$ values of fluids for carbonate veinlets in drill cores

Figure 33 shows the $\delta^{13}C$ and $\delta^{18}O$ data for veinlets in the sediments and underlying tuffs and breccias and the calculated $\delta^{13}C_{CO2}$ and $\delta^{18}O_{H2O}$ fields (faded print) for their parent fluids, assuming 50°, 100° and 150°C depositional

temperatures. The data on the veinlets are summarized in Table 9. The $\delta^{13}C$ and $\delta^{18}O$ values of carbonate veinlets fall in two clusters that have overlapping $\delta^{18}O$ values but distinctly different $\delta^{13}C$ values. Ilchik and Rumble (1994) have analyzed similar samples and obtained slightly larger $\delta^{18}O$ values for the low $\delta^{13}C$ samples. Paragenetic relationships suggest that the veinlets with the low $\delta^{13}C$ are earlier. Calculated fluid compositions are within the range observed for lake water or pore fluids in the Creede Formation. The low $\delta^{13}C$ values for the earliest calcite in the veinlets in the Snowshoe Mountain Tuff requires an organic source as the major component of aqueous carbon in the parent fluids. Ilchik and Rumble (1994) propose that the early veinlets in the Snowshoe Mountain Tuff formed soon after resurgence of the caldera. Whatever the timing, it appears that the veinlets were formed at temperatures of 50°C or higher; lower temperatures would require precipitation from fluids with unreasonably low values of $\delta^{18}O_{H2O}$. It is likely that temperatures of deposition of some veinlets were determined by the geothermal gradient (Table 9). As shown in Figure 33 fluid $\delta^{18}O_{H2O}$ values calculated using geothermal gradient temperatures range from about -3 to -14 ‰; values calculated using filling temperature measurements by Nora Foley (oral. comm., 1994) of fluid inclusions in two samples are about -17 and -10‰. The meteoric water origin of the -17‰ water is confirmed by δD values of -122 to -128‰ in inclusion fluids in the sample.

It appears that the calcite veinlet fluids had compositions ranging from that typical of meteoric water to that typical of the main stage ore fluids. These veinlet fluids were Creede Formation pore fluids. The strong meteoric water signature in the veinlet fluids is consistent with the strong contribution of meteoric water noted in the diagenetic silicate mineralogy of CCM-1 in Table 3. These meteoric water fluids replaced earlier pore fluids. The fact that the veinlet fluids had an end member composition similar to that of the main stage ore fluids may indicate that the ore fluids were derived from pore fluids of the Creede Formation rather than directly from the lake. In any event, meteoric water would be expected to replace these earlier Creede Formation pore fluids as they were recharged into the hydrothermal system to produce the pre-ore rhodochrosite and main stage ore fluids. If this was the case, these fluids then later mixed along the top of the system with more evolved lake water or pore fluids to form the pre-ore rhodochrosites in the southern part of the district (Figure 1) and later with fresh overlying ground water to form the main-stage mineralization. The aqueous carbon of the pore fluids contained a substantial contribution from the breakdown of organic matter in the Creede Formation much as did the ore fluids.

$\delta^{13}C_{CO2}$ and $\delta^{18}O_{H2O}$ values fluids for sparry calcite in travertine

The $\delta^{13}C$ and $\delta^{18}O$ values of the sparry calcites in travertines in the district are compared in Figure 34 with the values for travertines and drill core veinlet calcite shown in faded symbols. The data appear to show a weak inverse covariance and lie near the low $\delta^{13}C$ and $\delta^{18}O$ limit for the travertine data. They overlap the high $\delta^{13}C$ and $\delta^{18}O$ limit for the veinlet calcites suggesting that depositional temperatures were less than those for the drill core veinlets and similar to those for the higher temperature travertines. A similar negative covariance was noted for one of the travertine samples (e.g., Figure 27). Fluid compositions calculated from assumed temperatures of 50° and 100°C are also

shown in Figure 34. Since it is unlikely that $\delta^{13}C_{CO2}$ values for the fluids that were larger than those of atmospheric or volcanic CO_2, the upper temperature limit for some of the fluids was probably near 50°C. Furthermore, it is likely that the parent fluids had a significant meteoric water component similar to that responsible for travertine and interbanded silica deposition. The origin of the sparry calcites appears to be closely related to that of the travertines.

$\delta^{13}C_{CO2}$ and $\delta^{18}O_{H2O}$ values fluids for wallrock calcite in the Bulldog Mountain mine

Figure 35 shows the $\delta^{13}C$ and $\delta^{18}O$ values for wallrock calcites in the Bulldog Mountain mine and the field for calculated $\delta^{13}C_{CO2}$ and $\delta^{18}O_{H2O}$ values for parent fluids for most samples at assumed temperatures of 50° and 150°C. For comparison, the $\delta^{13}C$ and $\delta^{18}O$ values for later pre-ore rhodochrosites in the Bulldog Mountain deposit are shown in faded symbols while the field for the $\delta^{13}C_{CO2}$ and $\delta^{18}O_{H2O}$ values of rhodochrosite fluids is shown in the diagonal pattern. The $\delta^{13}C$ and $\delta^{18}O$ values of these carbonates show positive correlations like the rhodochrosites. The rhodochrosites have larger average $\delta^{18}O$ values than the wallrock calcites but the wallrock calcites have a greater range of both $\delta^{13}C$ and $\delta^{18}O$ values. Some limits on temperature of deposition can be determined using the data for samples that have extreme compositions and the limits of fluid composition determined by the composition of meteoric water and atmospheric/volcanic CO_2. The limiting compositions in Figure 35 show that some wallrock calcites could not have formed below about 80° C and others may not have formed above 130°C. Two of the samples (one with large $\delta^{13}C$ and one with large $\delta^{18}O$ values (beyond the tie lines in Figure 35) must have formed at rather low temperatures. The range of $\delta^{18}O$ and $\delta^{13}C$ values for the wallrock calcite fluids is too large to be due solely to temperature variations in the parent fluid and indicates that deposition involved the mixing of solutions of different $\delta^{18}O_{H2O}$ and $\delta^{13}C_{CO2}$. The possible calculated $\delta^{13}C_{CO2}$ values for the wallrock calcite fluids using assumed temperatures indicate a significant component of organic carbon in the aqueous carbon of the hydrothermal fluids consistent with derivation of the fluids from lake water or Creede Formation pore fluids. The organic aqueous carbon is consistent with the gas chemistry data on inclusion fluids in the calcites (Landis and Rye, 1989). Depending on the temperature deposition of these wallrock calcites may have involved the mixing of warm meteoric and lake water such as occurred during travertine deposition or the mixing of hydrothermal fluids with isotopically heavy lake water such as occurred during rhodochrosite deposition.

Summary interpretation of $\delta^{13}C$ and $\delta^{18}O$ data for carbonates in veins in the Creede Formation and in the Creede mining district

Each type of epigenetic calcite in the district (veinlets in the Creede Formation and Snowshoe Mountain Tuff, sparry calcite in travertine vugs, and calcite in wallrock adjacent to mineralized veins and later pre-ore rhodochrosite in the Bulldog Mountain mine) formed from fluids having a unique range of temperature and composition. However, all fluids may have had a heated meteoric water component such as dominant during travertine deposition and K feldspar formation in tuffaceous sediments. Also, all fluids appear to have had volcanic/atmospheric and organic sources for their aqueous carbon components.

This commonality suggests, but does not prove, that all veinlet and wallrock calcites in the district formed prior to ore deposition. The calcite in veinlets in the Creede Formation and Snowshoe Mountain Tuff were derived from fluids that had a more restricted range of $\delta^{13}C_{CO2}$ and $\delta^{18}O_{H2O}$ values and temperatures than the fluids for travertine and wallrock calcite in the mining district, probably because of the isotopic buffering capacity of the sediments. The veinlet fluids appear to have been mixtures of meteoric water and fluids that had the $\delta^{13}C$-$\delta^{18}O$ composition of the main stage ore fluids. These mixtures may reflect the displacement by meteoric water of pore fluids during their recharge into the hydrothermal system to form the main stage ore fluids.

CONCLUSIONS

The stable isotope geochemistry of the Creede Formation, when integrated with available geologic and geochemical data, places important constraints on the history of the lake which filled the moat of the Creede caldera prior to hydrothermal mineralization in the Creede mining district and on the relationship of the lake to ore deposition in the mining district. The large range of $\delta^{34}S$ values on both authigenic pyrite in the Creede Formation and vein pyrite in the underlying Snowshoe Mountain Tuff are best interpreted to have resulted from the bacteriogenic reduction of sulfate during diagenesis. Some sulfur may have been introduced into the system as H_2S in thermal springs. Most of this H_2S was probably removed as pyrite below travertine mounds and as veinlets in the lacustrine facies of the Creede Formation. However formed, the isotopically heavy authigenic pyrites require isotopically heavy sulfate in the Creede Formation pore fluids and likely in any end stage lake waters that may have overlain the vein system in the southern part of the district. The sulfate content of the lake was periodically recharged by eruption of volcanic tuffs. The bacteriogenic reduction of sulfate in the pore waters of the Creede Formation may have led to the depletion of organic matter in the sediments. Although much more work is needed to understand the details of the sulfur isotope geochemistry of the Creede Formation, all current sulfur isotope data are consistent with that part of the model of the Creede hydrothermal system that proposes that the deeply circulating ore fluids mixed with pore fluids or lake waters in the southern part of the district leading to the highly unusual $\delta^{34}S$ and $\delta^{18}O$ values of the hydrothermal barites.

The stable isotope data on the lacustrine carbonates are extraordinary and unlike any of which we are aware in the literature on such carbonates. The $\delta^{13}C$ and $\delta^{18}O$ data on lacustrine carbonates indicate that the combination of the various factors affecting carbonate precipitation underwent fundamental changes twice during the time interval represented by the CCM-2 core, and that the conditions between changes lasted for long periods of time. The nature of the factors controlling each stage of the lake are not yet well understood. The $\delta^{18}O$ of the meteoric water flowing into Lake Creede appears to have been relatively constant during the entire time represented by the CCM-2 core while the $\delta^{18}O$ of the evaporated water in the lake appears to have increased until reaching a fairly constant value that persisted for an interval represented by at least 500 feet in the upper part of the CCM-2 core. This condition apparently continued stratigraphically for at least another 500 feet as indicated by the isotope composition of pearls in ikaite pseudomorphs in travertine outcrops. Carbonate

deposition in the early and intermediate lake is believed to have involved the mixing of thermal water with lake water and/or the seasonal mixing of a shallow layer of warm meteoric water on the surface of the lake with deeper, more evaporated cold water. This latter mixing may have been facilitated by overturn or by changes in the relative positions of the productive zone and the thermocline. Carbonate deposition in the later lake appears to have occurred at ≤2°C from a stratified lake of nearly constant oxygen isotope composition. The nature of the factors controlling each stage of the lake could have been the result of changes in physiography or climate which changed the hydrologic balance or thermal structure of the lake or to less obvious factors such as a gradual increase in salinity of the lake.

The lake water underwent significant evaporation and its salinity can be inferred to have become significant from the evidence of brine shrimp in the lake, from the long period (several hundred thousand years) in which the $\delta^{18}O_{H2O}$ of the lake remained constant (suggesting stratification), and from the unusual δD_{H2O} and $\delta^{18}O_{H2O}$ of the later lake as indicated from isotope data of rice grains and their inclusion fluids. As inferred from studies of ore and gangue minerals from the Creede mining district, the isotopic composition and salinity of the water of ancient Lake Creede or Creede Formation pore fluids at one time may have been similar to that at present day Mono Lake, CA which occurs in a geologic and climatic setting similar in many respects to that for Lake Creede.

Travertine mound formation at the margin of the Creede moat was most likely a two stage process in which ikaite formed during the winter when the $\delta^{18}O$ of the lake was relatively uniform and the contribution of thermal ground water to the lake was diminished. Travertine deposition in and around ikaite pseudomorphs occurred later, probably in the spring, when deep thermal water of meteoric origin was able to mix with shallow low $\delta^{18}O$ meteoric water that accumulated on top of the evaporative lake during the spring run-off. The thermal meteoric water involved in travertine deposition may have also been involved in diagenesis in the Creede Formation as indicated by low $\delta^{18}O$ values of diagenetic K-feldspar and introduced carbonate in the lower part of the Creede Formation at CCM-1. These meteoric-water dominated diagenetic fluids appear to have been limited to CCM-1 where they apparently altered the $\delta^{18}O$ of the lacustrine carbonates. The isotopic composition of the lacustrine carbonates at CCM-2, however, does not appear to have been altered significantly during diagenesis

Each generation of cross cutting carbonates in the district, including calcite veinlets in drill core of the Creede Formation and Snowshoe Mountain Tuff, sparry calcite filling vugs in travertine, and wallrock calcite and pre-ore rhodochrosite in the Bulldog Mountain veins, precipitated under a unique set of conditions that may have involved mixing of fluids with meteoric water, different temperatures of deposition, different stages in the evolution of the lake and different amounts of organic carbon versus atmospheric/volcanic carbon in the parent fluids. The isotope data for the crosscutting carbonates in the district suggest a common meteoric water component and a common organic matter component for their parent fluids.

All of the isotopic data are consistent with the possibility that the lake in which the preserved portion of Creede Formation was deposited could have been the ultimate source of the main stage ore fluids, but it is not it is not

possible to relate the entrance of the fluids into the hydrothermal system to a specific period of lake history. The fluids from which the veinlets in the Creede Formation grew appear to have been mixtures of meteoric water and fluids which had the composition of main stage ore fluids, suggesting that pore waters were the source of the main stage ore fluids. These mixtures may reflect the displacement of pore fluids by meteoric water as the pore fluids entered the hydrothermal system. Whether the ore fluids were derived from lake or pore fluids it is clear that, during the evolution of the lake represented by our samples, they had not reached the extreme $\delta^{18}O$ values believed to be characteristic of an end stage lake that may have been present during pre-ore rhodochrosite deposition, approximately 1 m.y. after the deposition of the youngest Creede Formation preserved in the drill cores.

REFERENCES

--------, 1987, The Mono basin ecosystem: effects of changing lake level: National Academy Press, p. 272.

Barton, P.B., Jr., Bethke, P.M., and Roedder, E., 1977, Environment of ore deposition in the Creede mining district, San Juan Mountains, Colorado: Part III. Progress toward the interpretation of the chemistry of the ore-forming fluid for the OH vein: Econ.. Geol. v. 72, p 1-24.

Benson, L., 1994, Carbonate deposition, Pyramid Lake subbasin, Nevada: 1. Sequence of formation and elevational distribution of carbonate deposits (tufas) Palaeogeography, Palaeoclimatology, Palaeoecology, v. 109, in press

Bethke, P.M., 1995, Research drilling in the moat of the Creede caldera, San Juan Mountains, southwest Colorado: Preliminary scientific results: Proceedings VIIth International Symposium on the Observation of the Continental Crust Through Drilling, P. 9-12.

Bethke, P.M. and Rye R.O., 1979, Environment of ore deposition in the Creede mining district, San Juan Mountains, Colorado: Part IV, Source of fluids from oxygen, hydrogen, and carbon isotope studies: Econ. Geol. v. 74, p. 1832-1851.

Bethke, P.M., Campbell, W.R., Hulen, J.B., and Moses, T.H., Jr., 1994, Overview of the Creede Caldera Continental Scientific Drilling Program: U.S. Geological Survey Open-file Report 94-260-A.

Bischoff, J.L., Herbst, D.B., and Rosenbauer, R.J., 1991, Gaylussite formation at Mono Lake, California: Geochim. et Cosmochim. Acta, v. 55 p. 1743-1747.

Bischoff, J.L., Fitzpatrick, J.A., and Rosenbauer, R.J., 1993, The solubility and stabilization of ikaite ($CaCO_3.6H_2O$) for 0° to 25°C: environmental and paleoclimatic implications for thinolite tufa: Jour. Geology, v. 101, p. 21-33.

Bischoff, J.L, Stine, S., Rosenbauer, R.J, Fitzpatrick, J.A., and Stafford, T.W., 1993, Ikaite precipitation by mixing of shoreline springs and lake water, Mono Lake, California, USA: Geochim. et Cosmochim. Acta, v.57, p 3855-65.

Bodine, M.W., Jr., Hay, R.L., Madsen, B.M., and Altaner, S.P., 1988, Lacustrine volcaniclastic sediments in the Creede Formation, San Juan Mountain, CO: Geol. Society of America, Abstracts with Programs, v. 19, p. 261.

Bottinga, Y., 1968, Calculation of fractionation factors for carbon and oxygen exchange in the system calcite-carbon dioxide-water: Jour. Phys. Chemistry, v. 72, p. 800-808.

Conca, J.L., 1994, Transport in porous and fractured media of the Creede Formation, U.S. Geological Survey Open-file Report 94-260P.

Eardly, A.J., 1938, Sediments of Great Salt Lake, Utah: American Association of Petroleum Geologists Bulletin, 718, 198 p.

Finkelstein, D.B., Altaner, S.P., Hay, R.L., and Greenberg, S., 1994, Silicate diagenesis of tuffs in the Creede Formation: U.S. Geological Survey Open-file Report 94-260H.

Finkelstein, D.B., Altaner, S.P., and Hay, R.L., 1994, Diagenesis of tuffs in the Creede Formation, southwestern Colorado: Preliminary scientific results: Proceedings VIIth International Symposium on the Observation of the Continental Crust Through Drilling, P. 13-16.

Foley, N.K., 1990, Petrology and geochemistry of precious and base metal mineralization, north Amethyst veins system, Mineral County, Colorado: Unpub. Ph. D thesis, Virginia Polytechnic Institute and State University (Blacksburg), 324 p.

Foley, N.K., Bethke, P.M., and Rye, R.O., 1989, A reinterpretation of the $\_D_{H2O}$ of inclusion fluids in contemporaneous quartz and sphalerite, Creede mining district, Colorado: A generic problem for shallow orebodies? Econ. Geol. v. 84, p. 1966-77.

Gat, J.R., 1980, Hypersaline brines in evaporitic environments *in* Developments in Sedimentology # 28, *in* ed., A Nissenbaum, Developments in sedimentology 28, Hypersaline brines and evaporitic environments, Elsevier, p., 2-7.

Goldhaber, M.B. and Kaplan, I.R., 1974, The sulfur cycle. *In* The sea, V. 5 (ed. E. Goldberg), J. Wiley & Sons, p.569-655.

Hayba, D.O., 1986, District-wide fluid mixing during precious/base-metal epithermal mineralization at Creede, Colorado [abs.]: Geol. Soc. America Abstracts with Programs, v. 18, no. 6, p.632.

Hayba, D.O., 1993, Numerical hydrologic modeling of the Creede epithermal ore-forming system, Colorado: Unpub. Ph. D thesis, University of Illinois (Urbana) 186 p.

Holser, W. 1979, Trace elements and isotopes in evaporites: *In* Marine Minerals ed. R.G. Burns; Reviews in Mineralogy, Mineral Soc. Amer., p. 295-346.

Horton, D.G., 1983, Argillic alteration associated with the Amethyst vein system, Creede mining district, Colorado: Unpub. Ph.D. thesis, University of Illinois (Urbana-Champaign), 337 p.

Horton, D.G., 1985, Mixed-layer illite/smectite as a paleotemperature indicator in the Amethyst vein system, Creede district, Colorado, USA: Contr. Mineralogy Petrology, v. 91, p. 171-179.

Ilchik, R.P. and Rumble, D., III, 1993, Laser-fluorination investigation of sulfur isotopes in pyrite from the moat deposits of the Creede caldera, Colorado (abs.): Geological Society of America Program with Abstracts, v. 25, n. 6, p. A315.

Ilchik, R.P. and Rumble, D., III, 1994, Sulfur, carbon and oxygen systematics during diagenesis and fluid infiltration in the Creede caldera, Colorado: U.S. Geological Survey Open-file Report 94-260K.

Kelts, K, and Shahrabi, M., 1986, Holocene sedimentology of hypersaline Lake Urmia, northwestern Iran: Palaeogeography, Palaeoclimatology, Palaeoecology, v. 54, p 105-130.

Knauth, L.P. and Beeunas, M.A., 1986, Isotope geochemistry of fluid inclusions in Permian halite with implications for the isotopic history of ocean water and the origin of saline formation waters: Geochim. et Cosmochim. Acta, v.50, p. 419-33.

Lajoie, K.R., 1968, Late Quaternary stratigraphy and geologic history of Mono Basin. Unpub. thesis, Univ. California, Berkeley, 271 p.

Landis, G.P. and Rye, R.O., 1989, Reconnaissance gas chemistry of the Creede, Colorado, hydrothermal system: Open-file Report 89-94, p. 50.

Larsen, D., 1991, Pseudomorphs after ikaite in the Creede Formation: implications for the paleoenvironments of the Creede caldera, San Juan Mountains, CO: Geol. Society of America, Abstracts with Programs, v. 23, no. 4 p. A 40.

Larsen, D., 1994, Origin and environmental significance of calcite pseudomorphs after ikaite in the Oligocene Creede Formation, Colorado: Journal of Sedimentary Petrology, v. A64, p 593-603.

Larsen, D. and Crossey, L., 1994, Sedimentation and diagenesis in the Creede Formation; a basin-scale perspective. U.S. Geological Survey Open-file Report 94-260G.

Larsen, D. and Nelson, P.H., 1994, Stratigraphy and geophysical characteristics of the Oligocene Creede Formation in the two cored boreholes; U.S. Geological Survey Open-file Report 94-260F

Larsen, D. and Crossey, L.J., 1994, An integrated core and surface study of intracaldera sedimentation and diagenesis in the Creede Formation, CO: Preliminary scientific results: Proceedings VIIth International Symposium on the Observation of the Continental Crust Through Drilling, P. 29-32.

Leventhal, J., Daws, T., and Bostick, N., 1994, Organic geochemical studies to understand ore genesis at Creede: U.S. Geological Survey Open-file Report 94-260L.

Leventhal, J., 1994, Carbon-sulfur plots and degree of pyritization determinations to show diagenetic and epigenetic sulfidation in Creede caldera cores: U.S. Geological Survey Open-file Report 94-260M.

Love, L.G. and Amstutz, G.C., 1966, Reviews of microscopic pyrite: Fortschr. Mineral., v. 43, p. 273-309.

McKibben, M.A. and Eldridge, C.S., 1994, SHRIMP ion microprobe isotopic study of pyrite in corehole CCM-2: Evidence for multiple episodes of extreme biogenic sulfate reduction: U.S. Geological Survey Open-file Report 94-260J

McKibben, M.A., Eldridge, C.S., and Reyes, A.G., Sulfur isotopic systematics of the June 1991 Mount Pinatubo eruptions: a SHRIMP ion microprobe study: *in* Mount Pinatubo Monograph, eds. C.G. Newhall and R.S. Punongbayan, U.S. Geol. Surv. Prof. Paper (in press).

McKibben, M.A., Eldridge, C.S., Bethke, P.M., and Rye, R.O., 1993 SHRIMP study of the extreme bacteriogenic sulfur isotope enrichments in the moat sediments of the Creede caldera (abs.): Geological Society of America Program with Abstracts, v. 25, n. 6, p. A316.

O'Neil, J.R., Clayton, R.N., and Mayeda., T.K., 1969, Oxygen isotope fractionation in divalent metal carbonates: Jour Chem. Physics, v. 51, p. 5547-5558.
Plumlee, G.S., 1989, Processes controlling epithermal mineral distribution in the Creede mining district, Colorado: Unpub. Ph. D thesis, Harvard University, 378 p.
Reynolds, R.L., Rosenbaum, J.G., Sweetkind, D.S., Lanphere, M.A., Rice, C., and Tuttle, M., 1994, Rock Magnetic studies of the Oligocene Creede Formation and prospects for a polarity stratigraphy: U.S. Geological Survey Open-file Report 94-260O.
Russell, I.C., 1889, Quaternary history of Mono Valley, California. U.S. Geol. Survey 8th Annual Report for 1886-1887, p. 261-394.
Rye, R.O., Luhr, J.F., and Wasserman, M.D., 1984, sulfur and oxygen isotope systematics of the 1982 eruptions of El Chichon volcano Chiapas Mexico: Jour. of Volcanology and Geothermal Research, v. 23, p. 109-123.
Rye, R.O., Plumlee, G.S., Bethke, P.M., and Barton, P.B., 1988, Stable isotope geochemistry of the Creede, Colorado, hydrothermal system: U.S. Geological Survey Open-file Report 88-356, 40 p.
Savin, S.M. and Epstein, S., 1970a, The oxygen and hydrogen isotope geochemistry of clay minerals: Geochim. Cosmochim. Acta, v. 34, p. 25-42.
Savin, S.M. and Epstein, S., 1970b, The oxygen and hydrogen isotope geochemistry of ocean sediments and shales: Geochim. Cosmochim. Acta, v. 34, p. 43-63.
Sofer, Z. and Gat, J.R., 1975, The isotope composition of evaporating brines: effect of the isotopic activity ratio in saline solutions: Earth and Planetary Science Letters, v. 26, p. 179-186.
Stine, S, 1990, Late Holocene fluctuations of Mono Lake, eastern California: Palaeogeography, Palaeoclimatology, Palaeoecology, v. 78, p. 333-381.
Talbot, M.R., 1990, A review of the palaeohydrological interpretation of carbon and oxygen isotopic rations in primary lacustrine carbonates: Chemical Geology, v. 80 p 261-279.
Taylor, H.P., Jr., 1974, Oxygen and hydrogen isotope evidence for large-scale circulation and interaction between ground waters and igneous intrusions with particular reference to the San Juan volcanic field, Colorado: *in* Geochemical transport and kinetics eds. A.W. Hofmann, B.J. Giletti, H.S. Yoder, Jr., R.A. Yund: Carnegie Institution of Washington Publication 634, p. 299-334.
Tuttle, 1991, Petrography of iron sulfide minerals in the Green River Formation of Wyoming, Utah, and Colorado. In Geochemical, Biogeochemical and Sedimentological Studies of the Green River Formation, Wyoming, Utah, and Colorado (ed. M.L. Tuttle): USGS Bull. 1973G.
Tuttle M.L. and Goldhaber, M.B., 1991, Sulfur geochemistry and isotopy of the Green River Formation, Wyoming, Utah, and Colorado. In Geochemical, Biogeochemical and Sedimentological Studies of the Green River Formation, Wyoming, Utah, and Colorado (ed. M.L. Tuttle): USGS Bull. 1973B.
Varekamp, J., Luhr, J.F., and Prestegaard, K.L., 1984, The 1982 eruption of El Chichon volcano (Chiapas, Mexico): Character of the eruptions, ash-fall deposits, and gas phase: Jour. of Volcanology and Geothermal Research, v. 23, p. 39-68.

Vergo, N., 1984, Wallrock alteration at the Bulldog Mountain Mine, Creede mining district, Colorado: Unpub. MS. Thesis, University of Illinois (Urbana-Champaign), 87. p.
Wetlaufer, P.H., 1977, Geochemistry and mineralogy of the carbonates of the Creede mining district, Colorado: U.S. Geol. Survey Open-File Report 77-706, 134 p.

TABLE 1. $\delta^{34}S$ OF SEDIMENTARY/DIAGENETIC AND VEINLET SULFIDES

Sample Number	Depth m.	Method	Description	$\delta^{34}S‰$
1R042A-0.0	113.3	Chromic ion	Disseminated and fine bands	-9.5
1R043A-5.2	118.0	Chromic ion	Disseminated	-0.9
1R073A-8.0	198.0	Chromic ion	Disseminated in tuff	-4.8
1R083A-9.0	224.7	Chromic ion	Light 1.5 mm stratiform band	25.8
1R083A-9.1	224.7	HF	Moderate 3 mm stratiform band	-9.0
1R083A-9.2	224.7	Chromic ion	Heavy 3 mm stratiform band	34.8
1R090A-2.7	241.5	HF	Stratiform on thin parting	-4.7
1R090A-2.8	241.6	HF	Coarse 1.5 mm stratiform band	-7.8
1R090A-2.9A	241.6	Chromic ion	Disseminated	-6.0
1R090A-2.9B	241.6	Chromic ion	Disseminated fine	-2.5
1R090A-3.1	241.6	Chromic ion	Disseminated fine	3.4
1R052A-1.4	144.3	Chromic ion	Disseminated immediately above tuff	6.6
1R057A-2.2	153.2	Chromic ion	Disseminated immediately below tuff	33.2
1R066A-0.07	176.5	Chromic ion	Disseminated immediately above tuff	-16.6
1R067A-7.6	180.7	Chromic ion	Disseminated 1.5 m below tuff	11.8
1R070A-1.56	186.8	Chromic ion	Disseminated 6 cm above tuff	-20.4
1R072A-0.9	192.7	Chromic ion	Disseminated 30 cm below tuff	6.7
1R073A-3.0	196.4	Chromic ion	Disseminated 12 cm above tuff	-0.3
1R074A-5.68	198.8	Chromic ion	Disseminated 1.5 m below tuff	-1.3
1R084A-4.1	226.4	Chromic ion	Disseminated 6 cm above tuff	-0.4
1R085A-2.7	235.1	Chromic ion	Disseminated Just below tuff	-8.3
2R051A-0.2	174.3	Chromic ion	Disseminated 20 cm above tuff	-6.6
2R055A-2.1	187.2	Chromic ion	Disseminated Middle of tuff	18.5
2R057A-2.4	192.8	Chromic ion	Disseminated Immediately below tuff	8.6
2R111A-8.76	348.4	Chromic ion	Disseminated 3 cm above tuff	-19.8
2R118A-1.19	366.3	Chromic ion	Disseminated 1.5 m above tuff	-0.9
2R120A-0.2	372.1	Chromic ion	Disseminated 1 m below tuff	-0.3
2R150A-6.8	462.5	Chromic ion	Framboids	16.9
2R150A-6.8	462.5	Chromic ion	Framboids + overgrowths	17.0
2R236A-9.28	706.8	Drill	Veinlet mean "right curtain"	-3.5
2R236A-9.28	706.8	Drill	Veinlet mean "left curtain"	17.6
2R106A-1.0	332.3	Drill	Veinlet mean largest	8.0
2R106A-1.0	332.3	Drill	Veinlet mean smallest vein	4.2
2R224A-1.20	671.0	Drill	Veinlet mean small band	7.4
2R224A-1.20	671.0	Drill	Veinlet mean large band	8.0

Table 2. Comparison: Mono Lake and main stage Creede ore fluids

	Mono Lake*	Creede Ore Fluids**
δD of local meteoric water	-125‰	-110‰
δD lake/ore fluid water	-60‰	≥-50‰
$\delta^{18}O$ lake/ore fluid water	-2.7‰	≥-3‰
Salinity	~10%	~13%
Source of salts	Sierra plutons/volcanic tuffs	Fisher tuffs

* I. Friedman, unpublished (δD); L. Bensen, unpublished; ($\delta^{18}O$); Bischoff et al., 1993; **Rye et al., 1988

Table 3. δD and $\delta^{18}O$ of clay minerals and $\delta^{18}O$ of Kspar from Creede Formation and Snowshoe Mountain Tuff and calculated $\delta^{18}O_{H2O}$ for assumed temperatures

Sample	Depth (m)	Mineral	Unit	$\delta^{18}O$	δD	T°C	$\delta^{18}O_{H2O}$
1R024A-3.3	71.9	Smectite	Creede Fm	8.7	-85	85	-7.3
1R024A-3.3	71.9	Kspar	Creede Fm	6.3		85	-13.0
1R048A-6.0	133.7	Smectite	Creede Fm	6.8	-108	97	-7.9
1R071A-2.0	190.0	Smectite	Creede Fm	6.7	-84	100	-7.7
1R080A-0.0	214.3	Smectite	Creede Fm	7.1	-116	105	-6.8
1R100B-1.6	272.3	Smectite	Creede Fm	6.8	-100	112	-6.4
1R112B-3.9	305.0	Smectite	Creede Fm	5.0		115	-7.9
1R112B-3.9	305.0	Kspar	Creede Fm	4.5		115	-13.0
1R137A-9.1	374.4	Kaolinite	Snowshoe Mtn	1.9	-128	167*	-8.1
2R011A-2.3	68.3	Smectite	Creede Fm	18.6	-91	90	1.5
2R042A-1.3	150.1	Smectite	Creede Fm	18.9		100	2.3
2R056A-6.1	191.4	Smectite	Creede Fm	13.9	-104	105	-2.2
2R094A-8.5	301.1	Smectite	Creede Fm	19.8		118	5.0
2R123A-8.9	389.0	Smectite	Creede Fm	13.6	-110	128	0.3
2R156A-4.1	479.3	Smectite	Creede Fm	14.2		139	0.3
2R203A-1.0	609.9	Smectite	Creede Fm	9.5	-107	155	-2.3

*From fluid inclusion measurements in associated calcite by N.K.Foley (oral comm. 1994).
All other temperatures from estimated geothermal gradient (Finkelstein et al.,1994)

TABLE 4. $\delta^{13}C$-$\delta^{18}O$ DATA FOR LACUSTRINE CARBONATES FROM CCM-1

Sample Number	Depth (meters)	Depth (feet)	Morphology	$\delta^{13}C$‰ PDB	$\delta^{18}O$‰ SMOW
1R002-A2.0 #1	8.8	28.8	Rice grain	-4.2	27.9
1R002-A2.0 #4	8.8	28.8	Rice grain	-5.0	28.2
1R003-A7.55 #1	12.1	39.6	Pellet	-0.6	8.7
1R003-A7.55 #2	12.1	39.6	Pellet	-0.4	9.4
1R003-A7.55 #3	12.1	39.6	Pellet	-0.5	10.6
1R003-A7.55 #4	12.1	39.6	Pellet	-1.0	11.5
1R003-A7.55 #5	12.1	39.6	Pellet	-0.5	8.3
1R007-A1.25 #3	22.3	73.3	Rice grain	-0.8	18.3
1R007-A1.25 #4	22.3	73.3	Rice grain	-2.1	17.3
1R007-A1.25 #5	22.3	73.3	Rice grain	-3.3	17.7
1R007-A1.25 #6	22.3	73.3	Rice grain	-2.5	15.2
1R012-A8.2 #1	36.8	120.8	Micrite	1.0	10.7
1R012-A8.2 #2	36.8	120.8	Micrite	1.1	10.8
1R012-A8.2 #3	36.8	120.8	Micrite	1.3	10.1
1R012-A8.2 #4	36.8	120.8	Micrite	-0.4	15.4
1R012-A8.2 #5	36.8	120.8	Micrite	-3.7	16.5
1R020-A8.85 #1	61.4	201.4	Pellet	-1.3	9.6
1R020-A8.85 #2	61.4	201.4	Pellet	-0.6	8.6
1R020-A8.85 #3	61.4	201.4	Pellet	-1.6	9.1
1R020-A8.85 #4	61.4	201.4	Pellet	-2.0	10.8
1R020-A8.85 #5	61.4	201.4	Pellet	-1.9	10.0
1R020-A8.85 #6	61.4	201.4	Pellet	-0.9	9.1
1R024-A5.6 #1	72.6	238.2	Pellet	2.0	7.6
1R024-A5.6 #2	72.6	238.2	Pellet	0.8	7.7
1R024-A5.6 #3	72.6	238.2	Pellet	1.4	7.9
1R024-A5.6 #4	72.6	238.2	Pellet	1.6	7.9
1R024-A5.6 #5	72.6	238.2	Pellet	2.3	7.6
1R025-A1.44 #2	73.7	241.9	Pellet	-0.1	12.5
1R025-A1.44 #3	73.7	241.9	Pellet	0.4	12.0
1R025-A1.44 #4	73.7	241.9	Pellet	-0.8	13.6
1R025-A1.44 #5	73.7	241.9	Pellet	-2.4	17.4
1R025-A1.44 #6	73.7	241.9	Pellet	-2.1	15.4
1R025-A1.44 #7	73.7	241.9	Pellet	-0.3	13.5
1R025-A1.44 #8	73.7	241.9	Pellet	-0.7	14.2
1R031-A2.2 #1	88.3	289.7	Micrite	-5.6	4.0
1R031-A2.2 #2	88.3	289.7	Micrite	-1.2	9.0
1R031-A2.2 #3	88.3	289.7	Micrite	-2.2	9.1
1R031-A2.2 #4	88.3	289.7	Micrite	-1.2	10.0
1R031-A2.2 #5	88.3	289.7	Micrite	-2.1	10.0
1R031-A2.2 #6	88.3	289.7	Micrite	-3.7	14.6
1R031-A2.2 #7	88.3	289.7	Micrite	-1.2	9.6
1R031-A2.2 #8	88.3	289.7	Pellet	-2.3	11.3
1R031-A8.8 #2	90.3	296.3	Micrite	-4.8	12.0
1R031-A8.8 #3	90.3	296.3	Micrite	-4.7	12.7
1R031-A8.8 #4	90.3	296.3	Micrite	-4.7	13.1
1R031-A8.8 #5	90.3	296.3	Micrite	-4.9	12.6
1R031-A8.8 #6	90.3	296.3	Micrite	-2.4	6.8
1R031-A8.8 #6	90.3	296.3	Micrite	-5.2	11.9
1R031-A8.8 #7	90.3	296.3	Micrite	-2.4	7.0
1R031-A8.8 #7	90.3	296.3	Micrite	-4.8	13.2
1R031-A8.8 #8	90.3	296.3	Micrite	-4.8	13.3
1R031-A8.8 #9	90.3	296.3	Micrite	-5.5	11.5
1R031-A8.8 #1	90.3	296.3	Pellet	-2.4	12.8

TABLE 4. $\delta^{13}C$-$\delta^{18}O$ DATA FOR LACUSTRINE CARBONATES FROM CCM-1 (Continued)

Sample Number	Depth (meters)	Depth (feet)	Morphology	$\delta^{13}C$‰ PDB	$\delta^{18}O$‰ SMOW
1R031-A8.8 #2	90.3	296.3	Pellet	-0.4	7.7
1R031-A8.8 #3	90.3	296.3	Pellet	-0.1	7.1
1R031-A8.8 #3	90.3	296.3	Pellet	0.3	8.2
1R031-A8.8 #4	90.3	296.3	Pellet	-2.8	11.1
1R050-A5.6 #1	139.6	458.1	Pellet	-3.7	10.1
1R050-A5.6 #2	139.6	458.1	Pellet	-3.5	9.4
1R050-A5.6 #3	139.6	458.1	Pellet	-4.1	9.9
1R050-A5.6 #4	139.6	458.1	Pellet	-4.0	9.6
1R050-A5.6 #5	139.6	458.1	Pellet	-2.5	10.4
1R050-A5.6 #7	139.6	458.1	Pellet	-4.0	9.0
1R050-A5.6 #8	139.6	458.1	Pellet	-1.2	26.4
1R057-A3.45 #1	153.7	504.2	Pellet	-3.6	12.0
1R057-A3.45 #2	153.7	504.2	Pellet	-4.5	10.0
1R057-A3.45 #2	153.7	504.2	Pellet	-3.9	11.3
1R057-A3.45 #3	153.7	504.2	Pellet	-3.5	11.6
1R057-A3.45 #4	153.7	504.2	Pellet	-2.1	11.2
1R057-A3.45 #5	153.7	504.2	Pellet	-1.6	9.8
1R057-A3.45 #8	153.7	504.2	Pellet	-4.4	8.7
1R057-A8.4 #1	155.2	509.1	Pellet	1.4	6.7
1R057-A8.4 #10	155.2	509.1	Pellet	0.5	6.8
1R057-A8.4 #2	155.2	509.1	Pellet	-0.2	8.4
1R057-A8.4 #3	155.2	509.1	Pellet	-3.4	9.1
1R057-A8.4 #4	155.2	509.1	Pellet	-2.6	9.3
1R057-A8.4 #6	155.2	509.1	Pellet	-2.8	9.2
1R057-A8.4 #7	155.2	509.1	Pellet	-3.1	9.2
1R057-A8.4 #8	155.2	509.1	Pellet	-0.2	6.3
1R057-A8.4 #9	155.2	509.1	Pellet	-2.7	10.9

TABLE 5. $\delta^{13}C$-$\delta^{18}O$ DATA FOR LACUSTRINE CARBONATES FROM CCM-2

Sample Number	Depth (meters)	Depth (feet)	Morphology	$\delta^{13}C$‰ PDB	$\delta^{18}O$‰ SMOW
2R016 3.2/3.2	80.7	264.9	Rice grain	-8.5	36.5
2R016 3.2/3.2	80.7	264.9	Rice grain	-3.7	35.7
2R016 3.2/3.2	80.7	264.9	Rice grain	-4.8	36.6
2R016 3.2/3.2	80.7	264.9	Rice grain	-5.4	36.2
2R019-A1.82 #1	80.7	293.6	Rice grain	-3.6	36.4
2R019-A1.82 #2	89.5	293.6	Rice grain	-3.7	35.9
2R019-A1.82 #3	89.5	293.6	Rice grain	-5.4	36.5
2R019-A1.82 #4	89.5	293.6	Rice grain	-3.8	36.3
2R019-A1.82 #5	89.5	293.6	Rice grain	-3.9	36.2
2R019-A1.82 #6	89.5	293.6	Rice grain	-3.7	36.0
2R019-A1.82 #7	89.5	293.6	Rice grain	-5.5	33.7
2R020-A3.1 #1	93.0	305.2	Micrite	0.8	36.3
2R020-A3.1 #10	93.0	305.2	Micrite	2.8	36.4
2R020-A3.1 #10	93.0	305.2	Micrite	2.5	36.2
2R020-A3.1 #11	93.0	305.2	Micrite	2.2	35.3
2R020-A3.1 #12	93.0	305.2	Micrite	3.2	36.0
2R020-A3.1 #13	93.0	305.2	Micrite	3.6	36.0
2R020-A3.1 #14	93.0	305.2	Micrite	4.5	35.2
2R020-A3.1 #15	93.0	305.2	Micrite	4.5	33.9
2R020-A3.1 #16	93.0	305.2	Micrite	4.8	35.4
2R020-A3.1 #17	93.0	305.2	Micrite	5.7	36.5
2R020-A3.1 #18	93.0	305.2	Micrite	5.0	35.5
2R020-A3.1 #19	93.0	305.2	Micrite	4.3	34.9
2R020-A3.1 #2	93.0	305.2	Micrite	0.5	37.3
2R020-A3.1 #20	93.0	305.2	Micrite	3.9	34.9
2R020-A3.1 #20	93.0	305.2	Micrite	6.2	34.7
2R020-A3.1 #21	93.0	305.2	Micrite	0.8	36.6
2R020-A3.1 #22	93.0	305.2	Micrite	1.6	36.5
2R020-A3.1 #3	93.0	305.2	Micrite	0.1	36.4
2R020-A3.1 #4	93.0	305.2	Micrite	0.5	36.9
2R020-A3.1 #5	93.0	305.2	Micrite	4.1	32.8
2R020-A3.1 #6	93.0	305.2	Micrite	0.5	36.8
2R020-A3.1 #7	93.0	305.2	Micrite	0.6	35.6
2R020-A3.1 #7	93.0	305.2	Micrite	1.2	36.7
2R020-A3.1 #8	93.0	305.2	Micrite	2.4	37.2
2R020-A3.1 #9	93.0	305.2	Micrite	1.5	35.7
2R024-A4.6 #1	105.7	346.8	Micrite	5.8	34.4
2R024-A4.6 #11	105.7	346.8	Micrite	1.0	35.1
2R024-A4.6 #12	105.7	346.8	Micrite	8.1	35.0
2R024-A4.6 #2	105.7	346.8	Micrite	5.3	34.8
2R024-A4.6 #3	105.7	346.8	Micrite	3.9	35.1
2R024-A4.6 #4	105.7	346.8	Micrite	4.1	35.7
2R024-A4.6 #5	105.7	346.8	Micrite	4.1	34.8
2R024-A4.6 #6	105.7	346.8	Micrite	2.2	35.7
2R024-A4.6 #7	105.7	346.8	Micrite	2.7	36.7
2R024-A4.6 #8	105.7	346.8	Micrite	1.4	35.0
2R024-A4.6 #9	105.7	346.8	Micrite	2.9	36.0
2R024-A4.6 #10	105.7	346.8	Pellet	5.9	33.0
2R033 3.93/4.0	129.8	426.1	Rice grain	-1.7	34.1
2R033 3.93/4.0	129.8	426.1	Rice grain	-6.3	34.3
2R034-A1.5 #1	132.1	433.4	Pellet	-2.3	34.1
2R034-A1.5 #2	132.1	433.4	Rice grain	0.9	27.9
2R034-A1.5 #3	132.1	433.4	Rice grain	-7.0	33.9
2R034-A1.5 #4	132.1	433.4	Rice grain	-5.0	34.5

TABLE 5. $\delta^{13}C$-$\delta^{18}O$ DATA FOR LACUSTRINE CARBONATES FROM CCM-2
(Continued)

Sample Number	Depth (meters)	Depth (feet)	Morphology	$\delta^{13}C$‰ PDB	$\delta^{18}O$‰ SMOW
2R040-A3.5 #1	145.5	477.5	Rice grain	-3.4	34.9
2R040-A3.5 #2	145.5	477.5	Rice grain	-3.2	35.0
2R040-A3.5 #3	145.5	477.5	Rice grain	-3.2	35.5
2R040-A3.5 #4	145.5	477.5	Rice grain	-4.0	34.9
2R040-A3.5 #5	145.5	477.5	Rice grain	-3.9	35.3
2R040-A3.5 #6	145.5	477.5	Rice grain	-7.0	35.6
2R040-A3.5 #7	145.5	477.5	Rice grain	-3.6	35.0
2R040 5.07/5.17	146.0	479.3	Micrite	2.6	34.3
2R040 5.07/5.17	146.0	479.3	Micrite	-2.8	30.2
2R040 5.07/5.17	146.0	479.3	Pellet	3.8	35.0
2R040 5.07/5.17	146.0	479.3	Pellet	4.4	35.8
2R040 5.07/5.17	146.0	479.3	Rice grain	-2.6	36.1
2R040-A5.6 #11	146.2	479.7	Micrite	-1.5	32.7
2R040-A5.6 #12	146.2	479.7	Micrite	-0.4	34.2
2R040-A5.6 #1	146.2	479.7	Pellet	-4.6	33.9
2R040-A5.6 #10	146.2	479.7	Pellet	-0.4	35.1
2R040-A5.6 #2	146.2	479.7	Pellet	3.0	33.5
2R040-A5.6 #4	146.2	479.7	Pellet	-1.1	32.6
2R040-A5.6 #5	146.2	479.7	Pellet	4.2	31.9
2R040-A5.6 #6	146.2	479.7	Pellet	1.2	32.8
2R040-A5.6 #7	146.2	479.7	Pellet	0.0	33.8
2R040-A5.6 #8	146.2	479.7	Pellet	1.7	32.3
2R040-A5.6 #9	146.2	479.7	Pellet	2.3	33.5
2R040-A5.6 #13	146.2	479.7	Rice grain	-5.2	33.8
2R041-A4.05 #3	147.9	485.3	Micrite	-2.1	34.3
2R041-A4.05 #4	147.9	485.3	Micrite	-3.5	34.7
2R041-A4.05 #5	147.9	485.3	Micrite	2.4	33.6
2R041-A4.05 #6	147.9	485.3	Micrite	-2.9	35.5
2R041-A4.05 #8	147.9	485.3	Micrite	-6.1	35.2
2R041-A4.05 #2	147.9	485.3	Pellet	4.7	31.9
2R041-A4.05 #1	147.9	485.3	Rice grain	-7.9	33.8
2R041-A4.05 #8r	147.9	485.3		-6.3	34.6
2R041-A4.05 #9	147.9	485.3		-7.7	34.9
2R041-A4.25 #1	147.9	485.5	Micrite	-3.5	34.5
2R041-A4.25 #2	147.9	485.5	Micrite	-0.1	33.7
2R041-A4.25 #5	147.9	485.5	Pellet	9.6	26.4
2R041-A4.25 #6	147.9	485.5	Pellet	-2.2	33.8
2R041-A4.25 #3	147.9	485.5	Rice grain	6.8	29.4
2R041-A4.25 #4	147.9	485.5	Rice grain	4.5	30.1
2R041-A4.25 #3r	147.9	485.5		5.6	29.0
2R041-A4.25 #4r	147.9	485.5		-9.3	34.5
2R041-A4.25 #7	147.9	485.5		-1.8	34.2
2R041-A4.25 #8	147.9	485.5		-6.2	34.5
2R044 6.20/6.25	156.3	513.1	Rice grain	-6.4	36.0
2R044 6.20/6.25	156.3	513.1	Rice grain	-7.6	36.7
2R050-A2.7 #2	172.0	564.6	Pellet	0.5	15.6
2R050-A2.7 #3	172.0	564.6	Pellet	1.0	16.5
2R050-A2.7 #5	172.0	564.6	Pellet	0.2	15.3
2R050-A3.6 #1	172.0	565.5	Pellet	2.6	15.4
2R050-A3.6 #2	172.0	565.5	Pellet	2.1	18.2
2R050-A3.6 #4	172.0	565.5	Pellet	2.7	15.0
2R051 0.00/0.02	174.2	571.7	Pellet	-0.1	33.9
2R052 1.0/1.13	177.5	582.6	Pellet	2.0	34.1

TABLE 5. $\delta^{13}C$-$\delta^{18}O$ DATA FOR LACUSTRINE CARBONATES FROM CCM-2
(Continued)

Sample Number	Depth (meters)	Depth (feet)	Morphology	$\delta^{13}C$‰ PDB	$\delta^{18}O$‰ SMOW
2R052 1.0/1.13	177.5	582.6	Rice grain	1.1	35.3
2R052 1.0/1.13	177.5	582.6	Rice grain	0.5	35.1
2R057-A4.1 #2	193.2	634.1	Pellet	-0.2	33.6
2R057-A4.1 #3	193.2	634.1	Pellet	-0.4	34.1
2R057-A4.1 #4	193.2	634.1	Pellet	-0.4	33.6
2R057-A4.1 #6	193.2	634.1	Pellet	2.8	34.2
2R057-A4.1 #1	193.2	634.1	Rice grain	-0.2	35.1
2R057-A4.3 #1	193.3	634.3	Pellet	1.5	20.9
2R057-A4.3 #2	193.3	634.3	Pellet	2.7	15.1
2R057-A4.3 #3	193.3	634.3	Pellet	2.6	15.7
2R057-A4.3 #4	193.3	634.3	Pellet	2.6	18.9
2R060 8.99/8.99	202.4	664.2	Pellet	0.9	12.8
2R060 8.99/8.99	202.4	664.2	Pellet	1.4	13.1
2R060 8.99/8.99	202.4	664.2	Pellet	1.6	12.3
2R060 8.99/8.99	202.4	664.2	Pellet	1.6	12.6
2R063 8.09/8.46	211.2	693.1	Pellet	-1.2	17.8
2R063 8.09/8.46	211.2	693.1	Pellet	1.8	12.5
2R063 8.09/8.46	211.2	693.1	Pellet	2.8	11.4
2R068 5.85/5.85	224.5	736.9	Micrite	-10.8	33.1
2R071-A2.9 #1	232.8	764.1	Micrite	-1.7	15.6
2R071-A2.9 #10	232.8	764.1	Micrite	-2.7	12.1
2R071-A2.9 #11	232.8	764.1	Micrite	-3.6	14.1
2R071-A2.9 #12	232.8	764.1	Micrite	-2.8	11.5
2R071-A2.9 #13	232.8	764.1	Micrite	-4.3	16.3
2R071-A2.9 #14	232.8	764.1	Micrite	-5.2	16.3
2R071-A2.9 #15	232.8	764.1	Micrite	-4.1	15.2
2R071-A2.9 #2	232.8	764.1	Micrite	-3.3	14.0
2R071-A2.9 #3	232.8	764.1	Micrite	-2.7	12.0
2R071-A2.9 #4	232.8	764.1	Micrite	-3.6	14.2
2R071-A2.9 #5	232.8	764.1	Micrite	-2.7	12.5
2R071-A2.9 #6	232.8	764.1	Micrite	-3.3	11.8
2R071-A2.9 #7	232.8	764.1	Micrite	-2.7	12.2
2R071-A2.9 #8	232.8	764.1	Micrite	-2.9	12.9
2R071-A2.9 #9	232.8	764.1	Micrite	-3.0	11.9
2R072 6.42/6.44	236.9	777.6	Pellet	-4.0	18.8
2R073-A5.0 #1	239.3	785.3	Micrite	-2.4	21.3
2R073-A5.0 #2	239.3	785.3	Micrite	-1.4	23.3
2R073-A5.0 #10	239.3	785.3	Micrite	-2.0	17.3
2R073-A5.0 #11	239.3	785.3	Micrite	-2.2	19.8
2R073-A5.0 #12	239.3	785.3	Micrite	-2.4	20.4
2R073-A5.0 #3	239.3	785.3	Micrite	-1.7	16.2
2R073-A5.0 #4	239.3	785.3	Micrite	-1.7	22.3
2R073-A5.0 #5	239.3	785.3	Micrite	-0.8	16.3
2R073-A5.0 #6	239.3	785.3	Micrite	-1.9	20.3
2R073-A5.0 #7	239.3	785.3	Micrite	-3.0	22.6
2R073-A5.0 #8	239.3	785.3	Micrite	-2.4	18.8
2R073-A5.0 #9	239.3	785.3	Micrite	-1.7	0.2
2R075-A4.75 #1	245.4	805.3	Rice grain	-7.1	26.2
2R075-A4.75 #2	245.4	805.3	Rice grain	-9.3	30.8
2R075-A4.75 #4	245.4	805.3	Rice grain	-8.7	24.6
2R097-A6.3 #1	309.3	1015.0	Pellet	-3.1	24.4
2R097-A6.3 #2	309.3	1015.0	Pellet	-5.9	22.1
2R097-A6.3 #3	309.3	1015.0	Pellet	-3.4	26.0

TABLE 5. $\delta^{13}C$-$\delta^{18}O$ DATA FOR LACUSTRINE CARBONATES FROM CCM-2
(Continued)

Sample Number	Depth (meters)	Depth (feet)	Morphology	$\delta^{13}C$‰ PDB	$\delta^{18}O$‰ SMOW
2R097-A6.3 #4	309.3	1015.0	Pellet	-4.1	26.4
2R097-A6.3 #5	309.3	1015.0	Pellet	-3.0	25.7
2R097-A6.3 #6	309.3	1015.0	Pellet	-4.2	25.8
2R097-A7.8 #1	310.4	1018.6	Micrite	-6.1	25.1
2R097-A7.8 #10	310.4	1018.6	Micrite	-5.4	23.3
2R097-A7.8 #11	310.4	1018.6	Micrite	-6.3	26.3
2R097-A7.8 #12	310.4	1018.6	Micrite	-4.8	19.4
2R097-A7.8 #13	310.4	1018.6	Micrite	-5.8	25.8
2R097-A7.8 #14	310.4	1018.6	Micrite	-5.4	25.8
2R097-A7.8 #15	310.4	1018.6	Micrite	-4.1	18.8
2R097-A7.8 #2	310.4	1018.6	Micrite	-5.0	27.3
2R097-A7.8 #3	310.4	1018.6	Micrite	-5.7	23.9
2R097-A7.8 #4	310.4	1018.6	Micrite	-5.0	21.6
2R097-A7.8 #5	310.4	1018.6	Micrite	-5.7	24.2
2R097-A7.8 #6	310.4	1018.6	Micrite	-5.9	25.7
2R097-A7.8 #7	310.4	1018.6	Micrite	-6.1	24.7
2R097-A7.8 #8	310.4	1018.6	Micrite	-5.6	25.7
2R097-A7.8 #9	310.4	1018.6	Micrite	-5.3	22.8
2R097-A7.8 #A	310.4	1018.6	Micrite	-4.4	17.9
2R103-A2.275 #1	323.4	1061.3	Micrite	0.1	16.2
2R103-A2.275 #10	323.4	1061.3	Micrite	2.3	17.4
2R103-A2.275 #11	323.4	1061.3	Micrite	1.8	18.5
2R103-A2.275 #12	323.4	1061.3	Micrite	2.0	15.7
2R103-A2.275 #2	323.4	1061.3	Micrite	-0.6	17.2
2R103-A2.275 #3	323.4	1061.3	Micrite	1.6	17.9
2R103-A2.275 #4	323.4	1061.3	Micrite	1.7	12.1
2R103-A2.275 #5	323.4	1061.3	Micrite	2.6	12.6
2R103-A2.275 #6	323.4	1061.3	Micrite	2.6	14.0
2R103-A2.275 #7	323.4	1061.3	Micrite	3.4	11.9
2R103-A2.275 #8	323.4	1061.3	Micrite	3.0	10.4
2R103-A2.275 #9	323.4	1061.3	Micrite	4.0	11.2
2R127-A8.9 #1	396.1	1299.9	Micrite	-8.5	21.6
2R127-A8.9 #2	396.1	1299.9	Micrite	-6.5	23.7
2R127-A8.9 #3	396.1	1299.9	Micrite	-9.8	21.9
2R132 2.35/2.35	409.4	1343.7	Micrite	-3.5	24.7
2R132 2.35/2.35	409.4	1343.7	Micrite	-0.9	24.9
2R132 2.35/2.35	409.4	1343.7	Micrite	-5.3	22.6
2R146-A6.9 #1	450.2	1477.6	Micrite	-2.8	15.3
2R146-A6.9 #2	450.2	1477.6	Micrite	-2.7	16.3
2R146-A6.9 #3	450.2	1477.6	Micrite	-3.0	15.0
2R146-A6.9 #4	450.2	1477.6	Micrite	-2.0	14.1
2R146-A6.9 #5	450.2	1477.6	Micrite	-0.9	15.5
2R146-A6.9 #6	450.2	1477.6	Micrite	-2.9	14.1
2R146-A6.9 #7	450.2	1477.6	Micrite	-1.8	15.3
2R147-B1.7 #1	451.7	1482.6	Micrite	-5.2	15.7
2R147-B1.7 #2	451.7	1482.6	Micrite	-7.2	17.9
2R147-B1.7 #3	451.7	1482.6	Micrite	-6.0	17.9
2R147-B1.7 #4	451.7	1482.6	Micrite	-4.2	15.8
2R147-B1.7 #5	451.7	1482.6	Micrite	-4.4	18.2
2R147-B1.7 #6	451.7	1482.6	Micrite	-1.5	15.6
2R147-B5.0 #1	452.7	1485.9	Micrite	1.2	10.8
2R147-B5.0 #2	452.7	1485.9	Micrite	1.0	10.6
2R147-B5.0 #3	452.7	1485.9	Micrite	0.9	10.8

Table 6. $\delta^{13}C$-$\delta^{18}O$ DATA FOR LACUSTRINE CARBONATE SAMPLES FROM OUTCROP

Sample Number	Location Figure 25	Elevation (meters)	Morphology	$\delta^{13}C$‰ PDB	$\delta^{18}O$‰ SMOW
91-07-27 H #1	a	2781	Pellet	-5.7	18.6
91-07-27 H #2	a	2781	Pellet	-5.1	19.9
91-07-27 H #3	a	2781	Pellet	-5.4	18.6
91-07-27 H #4	a	2781	Pellet	-5.5	23.4
91-07-27 H #5	a	2781	Pellet	-5.3	21.6
91-07-27 H #6	a	2781	Pellet	-5.4	18.2
91-07-27 I #1	b	2781	Rice grain core A	-2.0	31.7
91-07-27 I #2	b	2748	Rice grain rim A	-5.2	15.6
91-07-27 I #3	b	2748	Rice grain cloudy	-6.3	11.2
91-07-27 I #6	b	2748	Rice grain core B	-4.5	13.0
91-07-27 I #7	b	2748	Rice grain inner rim B	-6.2	10.0
91-07-27 I #8	b	2748	Rice grain outer rim B	-5.7	10.8
91-07-27 J #1	c	2369	Rice grain.	-7.6	9.9
91-07-27 J #2	c	2369	Rice grain core-A	-6.0	12.2
91-07-27 J #3	c	2369	Rice grain rim-A	-6.3	11.8
91-07-27 J #4	c	2369	Rice grain core-B	-7.4	15.2
91-07-27 J #5	c	2369	Rice grain rim-B	-7.9	13.0
91-07-27 J #6	c	2369	Rice grain core-C	-5.6	10.7
91-07-27 J #8	c	2369	Rice grain rim-C	-6.7	12.6
91-07-27 Y2 #1	d	2664	Pellet	-2.6	16.8
91-07-27 Y2 #2	d	2664	Pellet	-2.8	15.2
91-07-27 Y2 #3	d	2664	Pellet	-2.5	16.7
91-07-27 Y2 #5	d	2664	fine-grained Micrite.	-5.1	16.3
91-07-26 R #1	e	2685	Pellet	-0.7	13.8
91-07-26 R #2	e	2685	Pellet	-0.4	13.8
91-07-26 R #4	e	2685	Pellet	-0.2	13.6
91-07-28 B2 #1	f	2684	Pellet	-2.2	12.2
91-07-28 B2 #2	f	2684	Pellet	-2.1	12.6
91-07-28 B2 #3	f	2684	Pellet	-2.2	12.3
91-07-28 B2 #4	f	2684	Pellet	-2.5	11.2
91-07-28 D #1	g	2685	Rice grain core-A	-5.7	35.7
91-07-28 D #2	g	2685	Rice grain matrix-A	-6.2	34.7
91-07-28 D #3	g	2685	Rice grain core-B	-4.2	35.7
91-07-28 D #4	g	2685	Rice grain matrix-B	-4.4	35.7
91-07-28 D #5	g	2685	Rice grain darkk	-6.2	36.5
91-07-28 D #6	g	2685	Rice grain light	-6.0	35.7
91-07-28 F #1	h	2684	Rice grain core-A	-2.1	34.8
91-07-28 F #2	h	2684	Rice grain inner rim-A	-2.4	28.7
91-07-28 F #3	h	2684	Rice grain outer rim-A	-2.3	19.2
91-07-28 F #4	h	2684	Rice grain	-4.7	34.4
91-07-28 F #5	h	2684	Rice grain core-B1	-2.1	35.1
91-07-28 F #6	h	2684	Rice grain core-B2	-2.1	32.2
91-07-28 F #7	h	2684	Rice grain matrix	-2.0	23.8
91-07-28 H #1	h	2684	Pellet	-4.5	19.4
91-07-28 H #2	h	2684	Pellet	-5.5	20.2
91-07-28 H #3	h	2684	Pellet	-5.4	23.7
91-07-28 H #4	h	2684	Pellet	-5.2	21.1
91-07-28 I #1	i	2718	Pellet	-0.3	17.7
91-07-28 I #2	i	2718	Pellet	-0.9	20.4
91-07-28 I #3	i	2718	Pellet	-0.3	17.4
91-07-28 I #4	i	2718	Pellet	-0.8	18.4
91-07-28 I #5	i	2718	Pellet	-0.6	17.4
91-07-28 I #6	i	2718	Pellet	-2.6	24.3
91-07-28 P1 #1	j	2802	Rice grain	-6.4	34.8
91-07-28 P1 #2	j	2802	Rice grain	-4.6	35.4
91-07-28 Q #1	k	2815	Rice grain core-A	-2.9	34.7
91-07-28 Q #10	k	2815	Rice grain laminated matrix	-8.7	34.7
91-07-28 Q #2	k	2815	Rice grain inner rim-A	-5.1	34.8
91-07-28 Q #3	k	2815	Rice grain outer rim-A	-4.6	34.9
91-07-28 Q #4	k	2815	Rice grain laminated matrix	-9.2	35.5

Table 6. $\delta^{13}C$-$\delta^{18}O$ DATA FOR LACUSTRINE CARBONATE SAMPLES FROM OUTCROP (Continued)

Sample Number	Location Figure 25	Elevation (meters)	Morphology	$\delta^{13}C‰$ PDB	$\delta^{18}O‰$ SMOW
91-07-28 Q #5	k	2815	Rice grain core-B	-4.8	34.1
91-07-28 Q #6	k	2815	Rice grain rim-B	-4.4	34.3
91-07-28 Q #7	k	2815	Rice grain core-C	-5.0	34.0
91-07-28 Q #9	k	2815	Rice grain laminated matrix	-8.4	34.5
91-07-28 S #1	l	2605	Individual Pellet	-6.7	33.7
91-07-28 S #2	l	2605	Individual Pellet	-6.5	34.1
91-07-28 S #3	l	2605	Individual Pellet	-7.1	32.1
91-07-28 S #4	l	2605	Individual Pellet	-6.3	34.4
91-07-28 S #5	l	2605	Individual Pellet	-6.2	34.2
91-07-28 S #6	l	2605	Individual Pellet	-6.3	33.6
91-07-28 V #1	m	2619	Laminated Micrite	-7.8	34.3
91-07-28 V #2	m	2619	Laminated Micrite	-7.1	33.4
91-07-28 V #3	m	2619	Laminated Micrite	-5.7	33.2
91-07-28 V #4	m	2619	Laminated Micrite	-4.5	29.9

TABLE 7. $\delta^{13}C$-$\delta^{18}O$ FOR BULK TRAVERTINE AND CHALCEDONIC SILICA AND δD OF INCLUSION FLUIDS

Sample Number	Location Figure 25	Sample description	Travertine $\delta^{18}O$	Travertine $\delta^{13}C$	Inclusion δD	Silica $\delta^{18}O$
1CR79A	1.	Interbanded silica & travertine	29.0	1.5		18.1
1CR79B	2.	Pseudomorphs & massive travertine	29.2	1.8		
1CR79B	2	Pseudomorphs & massive travertine	29.2	1.7		15.8
2CR79A	3	Microbial fragments, fecal pellets	30.0	-2.3		
2CR79B	4	Pseudomorphs & massive travertine	24.1	1.6		
3CR79A	5	Massive travertine	19.4	-5.8		
3CR79B	6	Cement in crystal breccia sandstone	29.3	-2.8		
4CR79	7	Massive travertine, weakly banded	20.6			16.8
5CR79	8	Massive travertine	27.8	-8.5		
6CR79A	9	Finely banded travertine	25.4	-2.6		
6CR79B	10	Travertine cement in conglomerate	24.1	-0.4		
6CR79C	11	Banded travertine in conglomerate	28.1	0.8		
6CR79D	11	Banded & massive travertine	20.1	-1.5	-116	
7CR79	12	Travertine cement in tuff	21.2	-3.8		
8CR79	13.	Pseudomorphs & massive travertine	14.5	-0.2		
9CR79	14	Pseudomorphs & banded travertine	25.3	1.5		
10CR79	15	Pseudomorphs & banded travertine	23.4	-0.4		
11CR79A	16	Pseudomorphs & botryoidal travertine	20.0	4.4		
11CR79B	17	Botryoidal travertine	17.6	2.0		16.8
12CR79A	18	Finely banded botryoidal travertine	21.3	-1.0		
12CR79B	18	Pseudomorphs	23.8	2.5	-102	14.2
14CR79	19	Fragmental travertine	28.1	1.7		
15CR79	20	Pseudomorphs & botryoidal travertine	28.0	4.2		
15CR79	20	Pseudomorphs & botryoidal travertine	27.7	4.2		
16CR79A	21	Pseudomorphs & banded travertine	29.9	2.1		
16CR79B	22	Micro-fragmental travertine	27.3	-4.1	-110	
17CR79A	22	Micro-fragmental travertine	25.3	-0.7		17.0
17CR79B	22	Banded travertine with silica	24.3	-3.4		
18CR79A	23	Micro-plumose travertine	32.7	4.3		
18CR79E	23					14.1
18CR79F	23	Massive travertine with black chert	31.5	2.1		13.8
19CR79A	24	Fragmental travertine	27.3	2.1		16.1
19CR79B	24	Fragmental cauliform travertine	25.9	0.8		
20CR79A	25	Botryoidal to pisolitic travertine	23.7	2.2		14.3
20CR79B	25	Pisolitic to reniform travertine	10.5	-0.1		
20CR79C	25	Botryoidal travertine with peloids	13.2	0.3		18.1
20CR79D	25	Finely banded tubular aggregates	15.6	1.0		17.4
20CR79E	25	Pisolitic to reniform aggregates	15.5	0.9		
20CR79F	25	Finely banded tubular aggregates	10.6	-1.2		
20CR79G	25	Fragmental and banded travertine	14.6	-1.3		
20CR79H	25	Banded and massive microbial masses	15.0	0.7		
20CR79I	25	Flaggy pisolitic to reniform travertine	20.0	-4.0		

TABLE 8. $\delta^{13}C$-$\delta^{18}O$ FOR TRAVERTINES BY MICROSAMPLING

Sample Number	Loca			SMOW
1CR79B	A	Ikaite pearl, core	2.4	32.8
1CR79B	A	Ikaite pearl, coarse rim	-2.6	11.7
1CR79B	A	Ikaite pearl, rim	-3.8	11.6
1CR79B	A	Ikaite pearl, core	4.9	37.1
1CR79B	B	Ikaite pearl, core	-8.0	34.0
1CR79B	B	Ikaite pearl, cloudy rim	-4.0	27.8
1CR79B	B	Ikaite pearl, clear outer rim	-6.9	31.4
1CR79B	B	Ikaite pearl, cloudy rim	-4.1	22.2
1CR79B	B	Ikaite pearl, clear outer rim	-2.3	16.4
1CR79B	B	Ikaite pearl, core	-8.4	34.4
1CR79B	B	Ikaite pearl, cloudy rim	-5.5	23.3
8CR79B	C	Ikaite pearl, core	3.7	34.6
8CR79B	C	Ikaite pearl, rim	1.4	12.4
8CR79B	C	Ikaite pearl, core	2.1	30.8
8CR79B	C	Ikaite pearl, rim	-4.4	7.4
8CR79B	C	Rim	-1.2	11.1
18CR79B	D	Core	3.0	33.4
18CR79B	D	White floret w/darker core	5.2	34.2
18CR79B	D	Structureless core	3.5	31.7
18CR79B	D	Bulbous core	1.4	28.7
18CR79B	D	Rim	2.0	29.6
18CR79B	D	Rim	-2.2	25.6
1CR92*	E	Core 1	5.3	35.3
1CR92	E	Core 2	5.1	33.9
1CR92	E	Core 3	4.6	34.6
1CR92	E	Rim 1	5.2	25.2
1CR92	E	Rim 2	5.7	24.2
1CR92	E	Rim 3	1.2	20.6
1CR92	E	Margin oldest	3.1	20.2
1CR92	E	Margin	4.3	22.0
1CR92	E	Margin	4.4	22.3
1CR92	E	Margin	5.2	24.7
1CR92	E	Margin	4.4	23.4
1CR92	E	Margin youngest	5.2	25.0
2CR92†	F	Core 1	2.4	32.8
2CR92	F	Rim 1 inner	-2.6	11.7
2CR92	F	Rim 1 outer	-3.8	11.6
2CR92	F	Core 2	4.9	37.1
2CR92	F	Rim 2	-3.8	10.3

* δD of fluid inclusions in bulk sample 1CF92 = -118‰

† δD of fluid inclusions in bulk sample 2CF92 = -129‰

TABLE 9. $\delta^{13}C$-$\delta^{18}O$ of Creede Formation (CFm) and Snowshoe Mountain Tuff (SsMT) veinlets and δD of inclusion fluids

Sample	Host	$\delta^{13}C$	$\delta^{18}O$	T°C	δD_{incl}	Age
1R77 4.7/4.7	CFm	-6.3	12.4	104		
1R095 0.0/0.0 -1	CFm	-5.3	5.3	110		oldest
-2	CFm	-5.5	6.9			
-3	CFm	-3.7	5.7			
-4	CFm	-4.4	3.8			
-5	CFm	-6.8	3.2			youngest
1R118 2.5/2.5	CFm	-3.8	9.5	120		
	ColBx	-5.7	1.5	165±2'		
1R138 9.7/9.8	ColBx	-6.1	0.6	125		
2R137 5.5/5.58	CFm	-4.7	11.0	100		
2R201 6.4/6.4-1	CFm	-4.5	7.1	117		oldest
-2	CFm	-6.5	11.5			youngest
2R218 3.2/3.4 -1	CFm	-5.7	10.5	120		oldest
-2	CFm	-5.8	10.1			
-3	CFm	-5.5	9.9			
-4	CFm	-6.8	8.4			
-5	CFm	-7.1	9.3			
-6	CFm	-7.5	4.3			
-7	CFm	-5.8	9.7			
-8	CFm	-6.9	5.8			
-9	CFm	-6.1	6.4			
-10	CFm	-6.9	8.6			
-11	CFm	-6.0	10.7			youngest
2R233 1.35/1.5-1	SsMT			125	-127	oldest
2R233 1.35/1.5-1	SsMT	-6.9	4.1			
-2	SsMT	-7.0	3.0	70-98*		
-3	SsMT	-6.9	3.9		-121	
-4	SsMT	-7.1	5.4			youngest
2R236 3.5/3.5-1	SsMT	-11.1	9.4	125		
-2	SsMT	-13.7	8.4			
2R236 9.1/9.28-1	SsMT	-10.5	8.4			oldest
-2	SsMT	-12.1	10.6	125		
-3	SsMT	-11.3	11.2			
-4	SsMT	-10.7	11.0			
-5	SsMT	-11.4	4.5			
-6	SsMT	-11.3	8.0			youngest

T°C Temperature based on geothermal gradient from Finkelstein et al. (1994)
*Filling temperature of fluid inclusions (N.A. Foley, written communication, 1994)

CONCEPTUAL MODEL OF CREEDE MINERALIZATION

Showing Stable Isotope Constraints

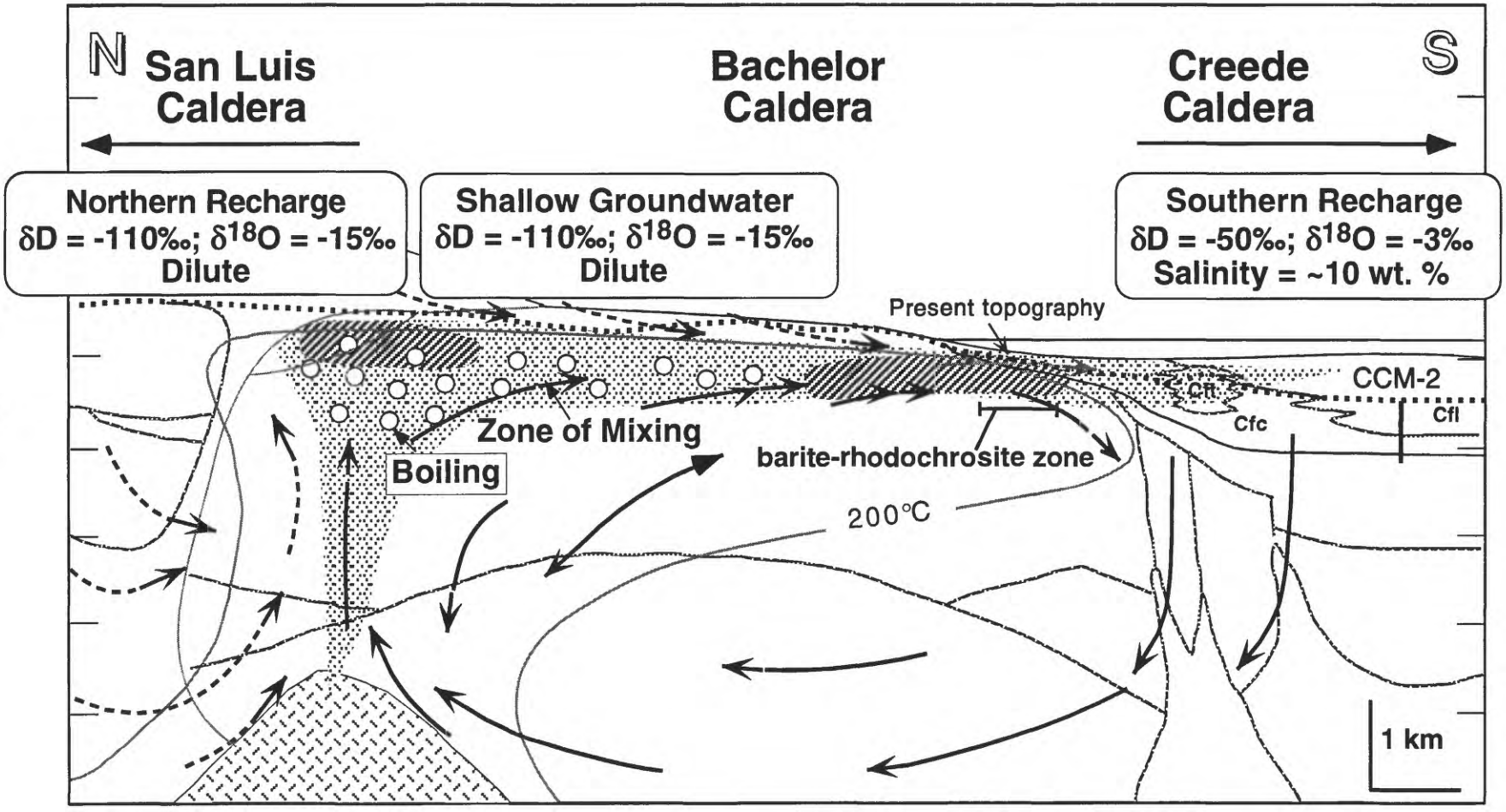

Facies of Creede Formation (Creede caldera moat fill)

Cfc = clastic, lake margin facies; Cfl = lacustrine facies; Cft = travertine

Volcanic units undifferentiated; zones of major mineralization hachured

Figure 1

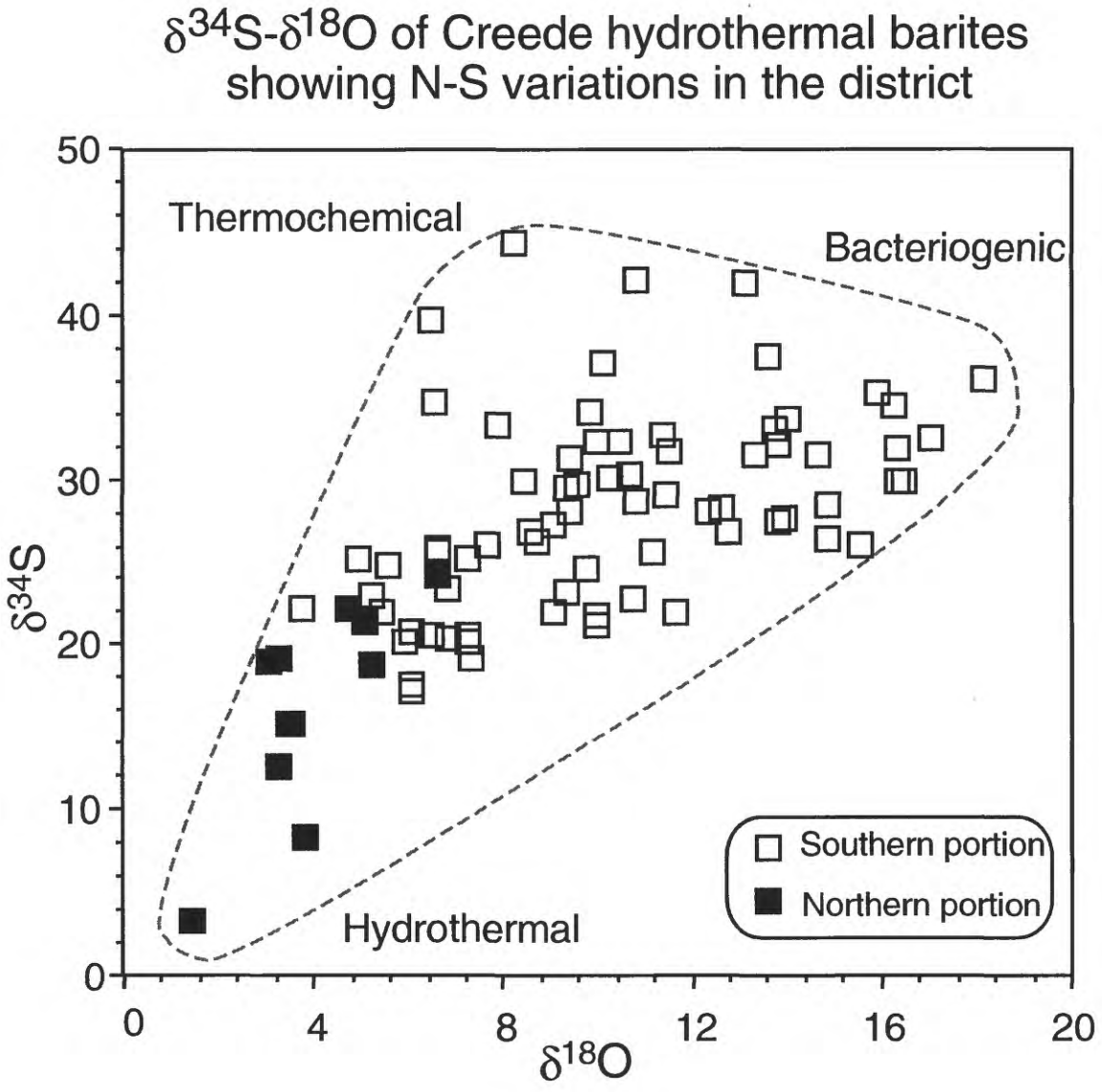
δ34S-δ18O of Creede hydrothermal barites
showing N-S variations in the district
Thermochemical
Bacteriogenic
Hydrothermal
Southern portion
Northern portion
δ34S
δ18O
0
10
20
30
40
50
0
4
8
12
16
20

Figure 2

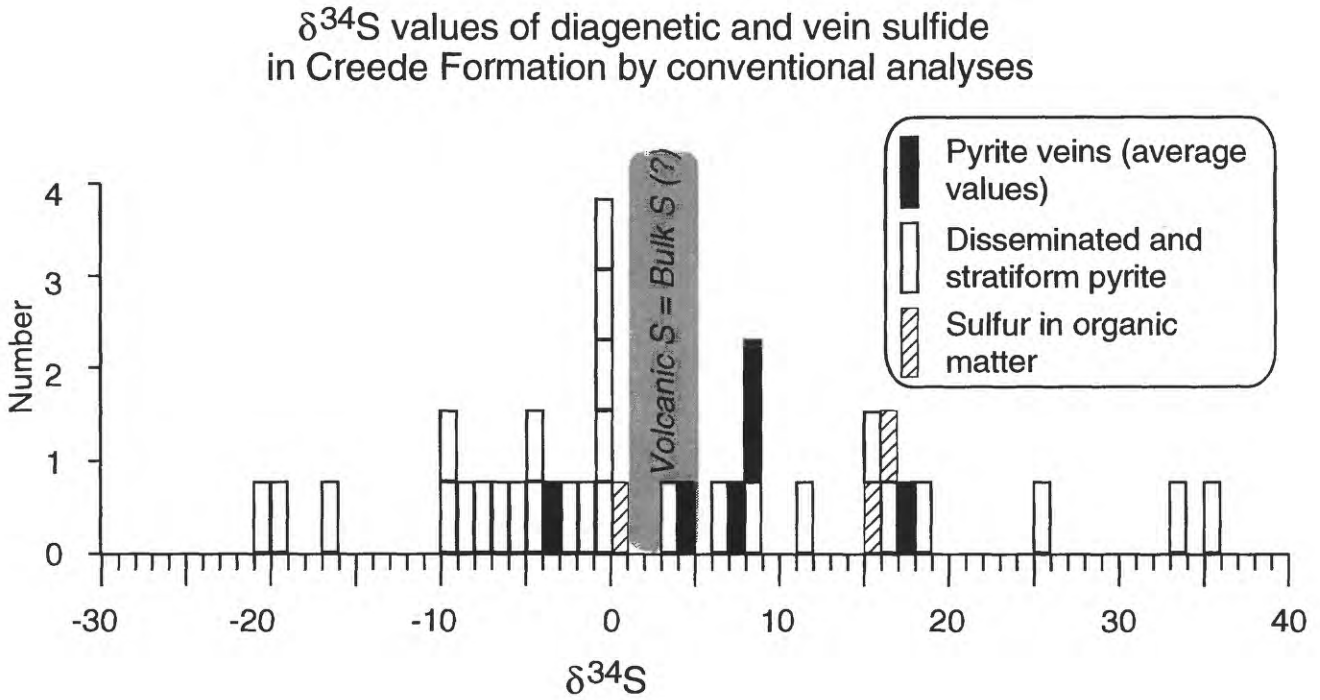
δ34S values of diagenetic and vein sulfide
in Creede Formation by conventional analyses
Pyrite veins (average values)
Disseminated and stratiform pyrite
Sulfur in organic matter
Volcanic S = Bulk S (?)
Number
0
1
2
3
4
-30
-20
-10
0
10
20
30
40
δ34S

Figure 3

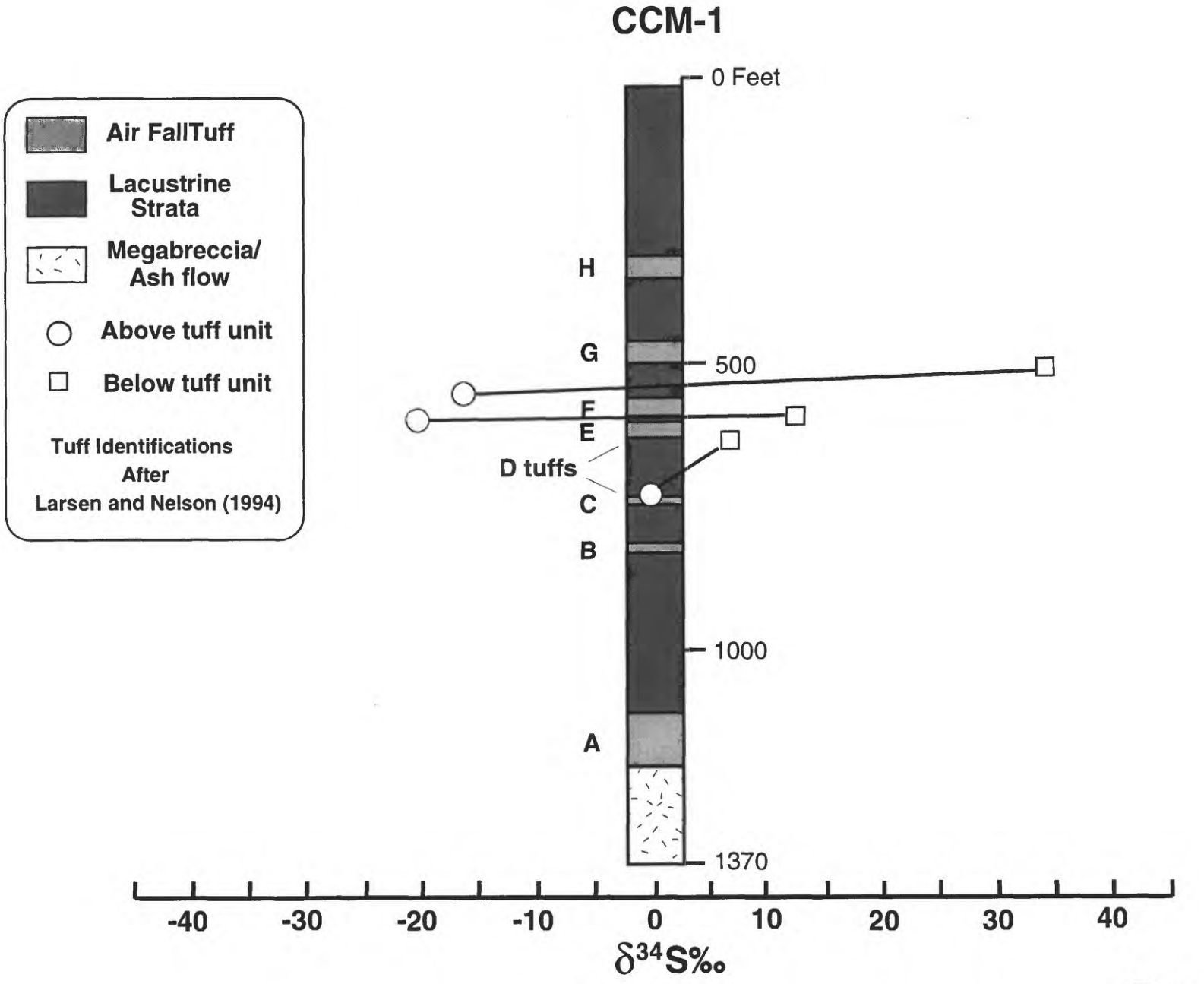
CCM-1
Air FallTuff
Lacustrine Strata
Megabreccia/ Ash flow
Above tuff unit
Below tuff unit
Tuff Identifications After Larsen and Nelson (1994)
0 Feet
500
1000
1370
H
G
F
E
D tuffs
C
B
A
-40
-30
-20
-10
0
10
20
30
40
δ34S‰

Figure 4

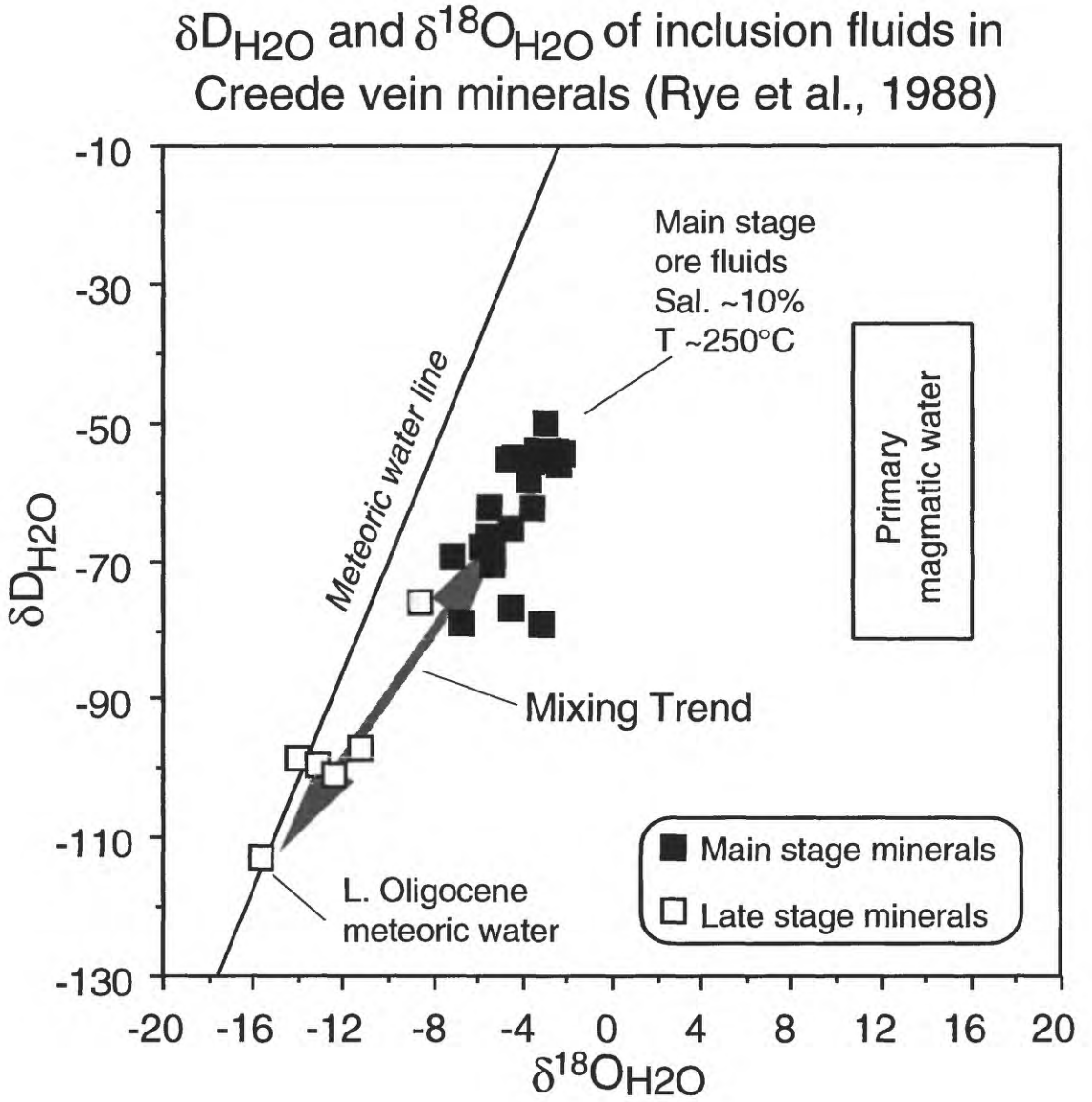
δD$_{H2O}$ and δ^{18}O$_{H2O}$ of inclusion fluids in Creede vein minerals (Rye et al., 1988)
Main stage ore fluids Sal. ~10% T ~250°C
Meteoric water line
Primary magmatic water
Mixing Trend
L. Oligocene meteoric water
Main stage minerals
Late stage minerals
δD$_{H2O}$
δ^{18}O$_{H2O}$
-10
-30
-50
-70
-90
-110
-130
-20
-16
-12
-8
-4
0
4
8
12
16
20

Figure 5

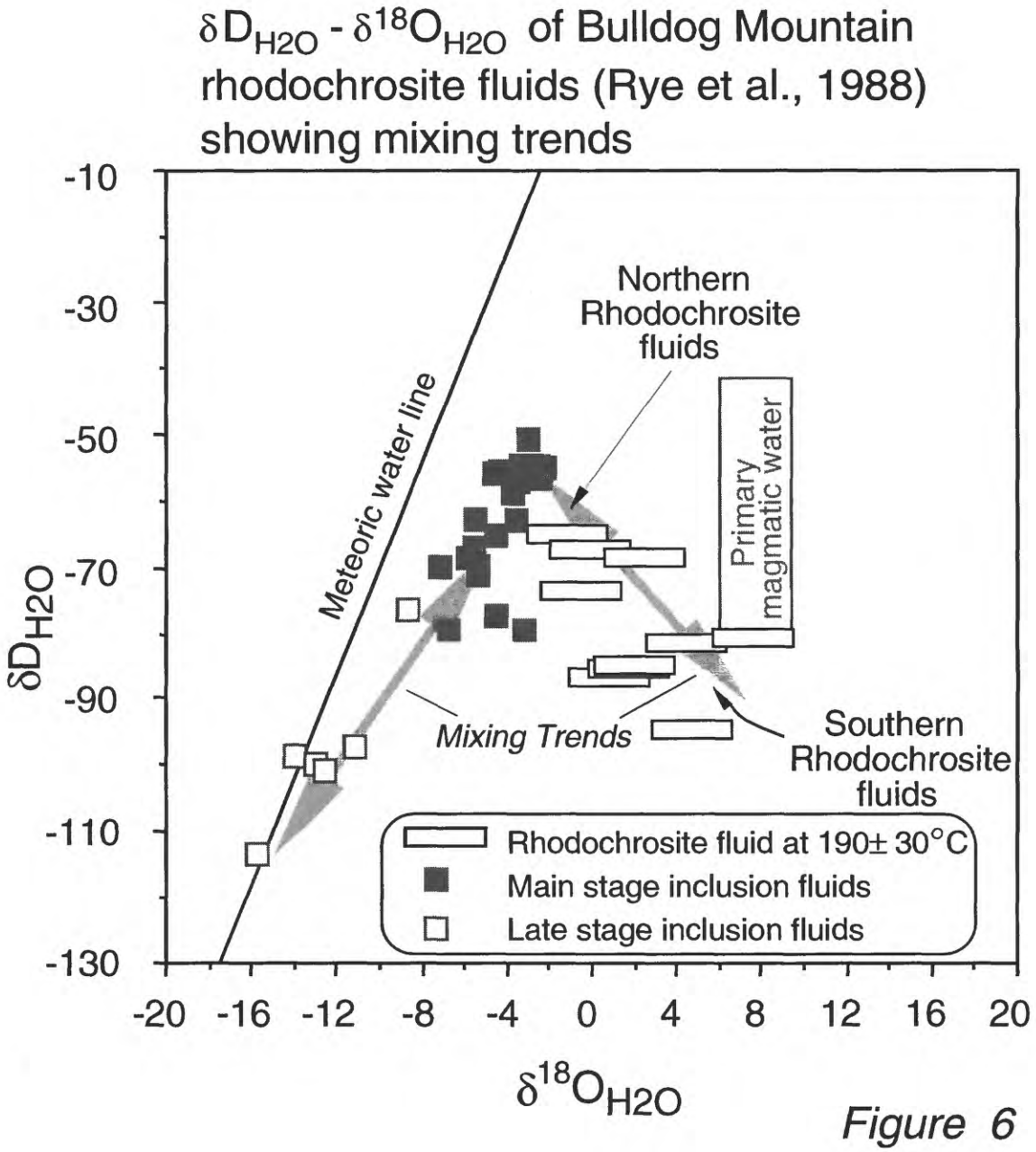
δD$_{H2O}$ - δ^{18}O$_{H2O}$ of Bulldog Mountain rhodochrosite fluids (Rye et al., 1988) showing mixing trends
-10
-30
-50
-70
-90
-110
-130
δD$_{H2O}$
-20
-16
-12
-8
-4
0
4
8
12
16
20
δ^{18}O$_{H2O}$
Meteoric water line
Northern Rhodochrosite fluids
Primary magmatic water
Mixing Trends
Southern Rhodochrosite fluids
Rhodochrosite fluid at 190± 30°C
Main stage inclusion fluids
Late stage inclusion fluids

Figure 6

δD-$\delta^{18}O$ of hydrothermal illite/smectite in Creede mining district and calculated δD_{H2O}-$\delta^{18}O_{H2O}$ of fluids

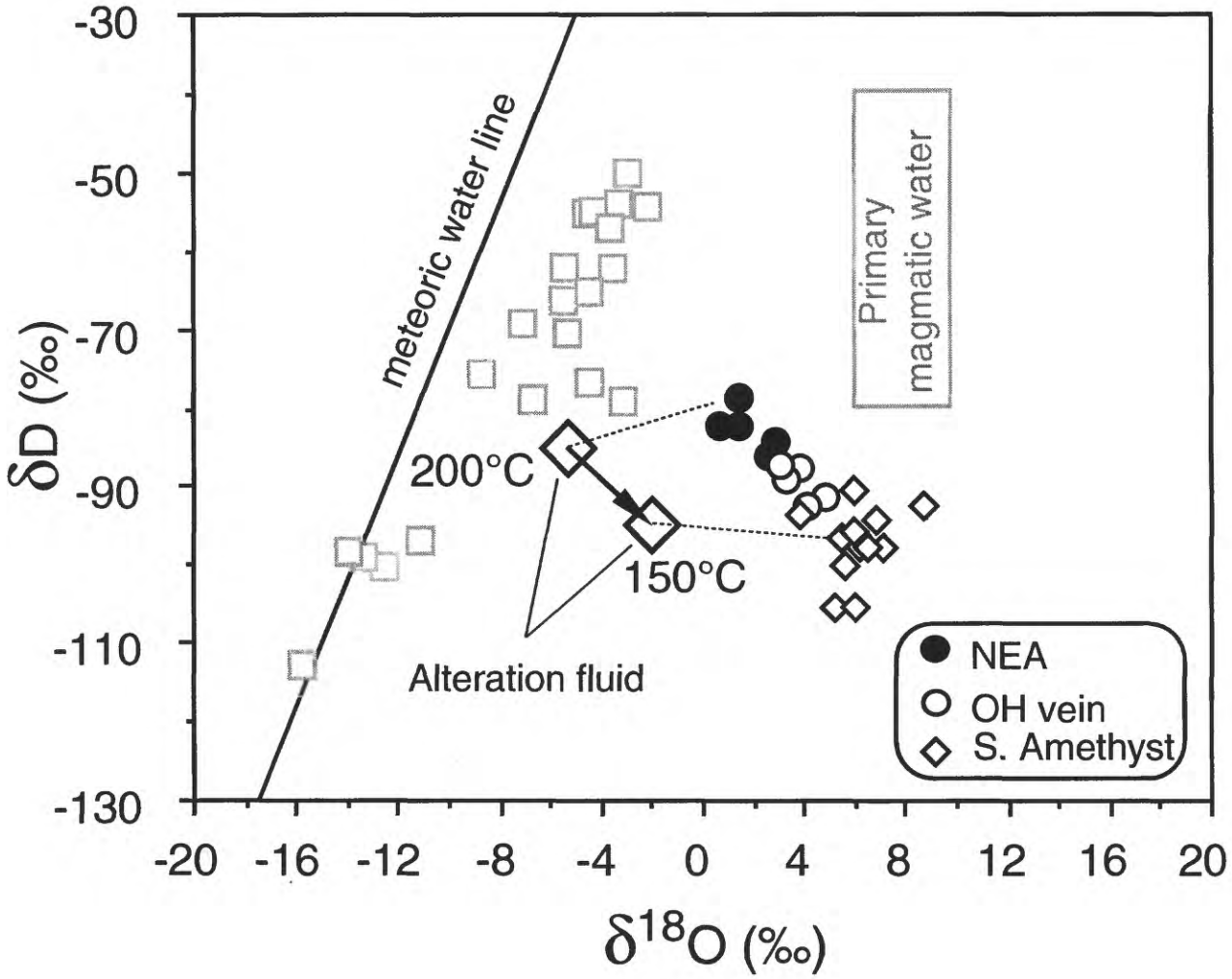

Figure 7

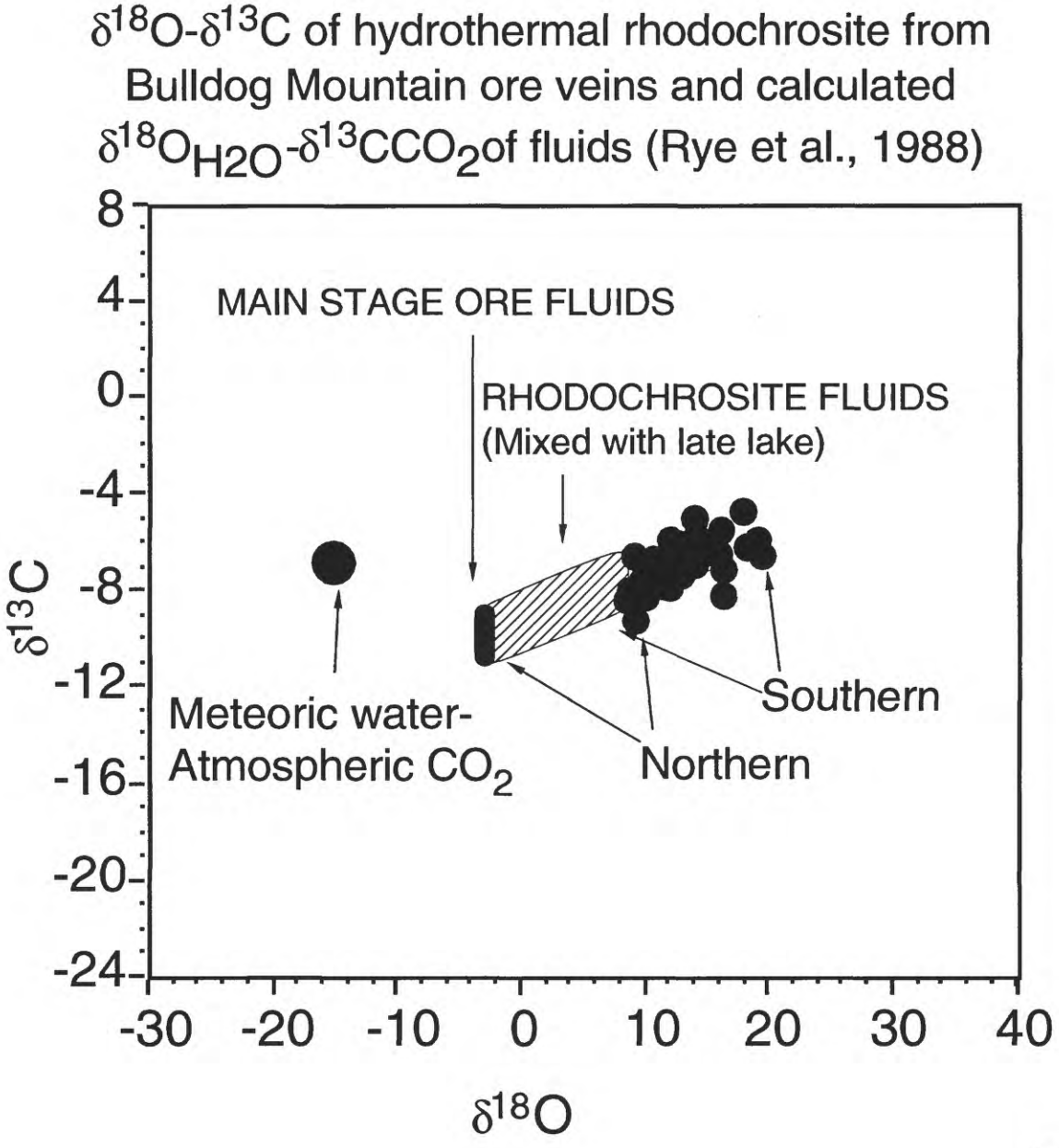
δ18O-δ13C of hydrothermal rhodochrosite from Bulldog Mountain ore veins and calculated δ18OH2O-δ13CCO2of fluids (Rye et al., 1988)
MAIN STAGE ORE FLUIDS
RHODOCHROSITE FLUIDS
(Mixed with late lake)
Meteoric water-
Atmospheric CO2
Southern
Northern
δ13C
δ18O
8
4
0
-4
-8
-12
-16
-20
-24
-30
-20
-10
0
10
20
30
40

Figure 8

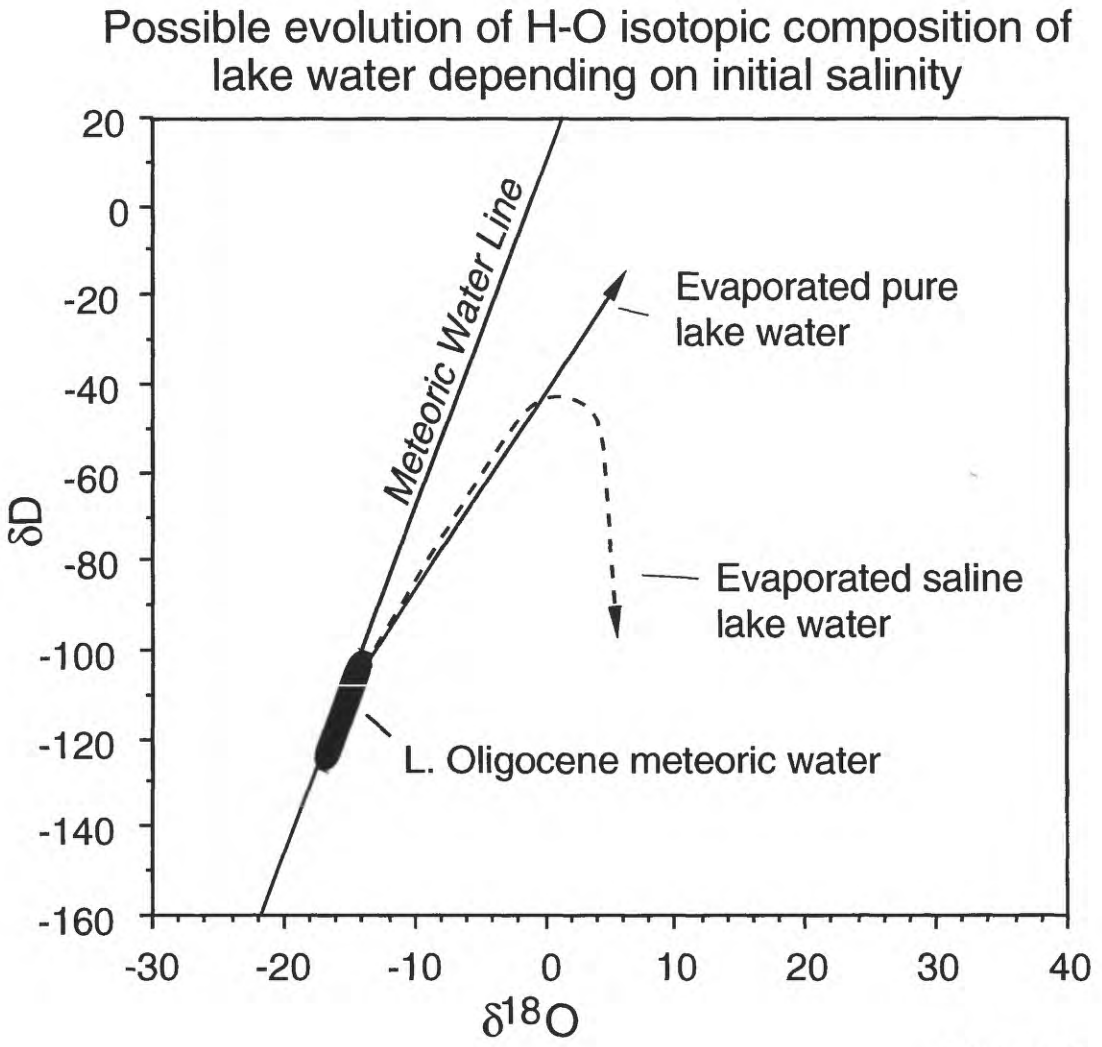
Possible evolution of H-O isotopic composition of lake water depending on initial salinity
20
0
-20
-40
-60
-80
-100
-120
-140
-160
δD
-30
-20
-10
0
10
20
30
40
δ18O
Meteoric Water Line
Evaporated pure lake water
Evaporated saline lake water
L. Oligocene meteoric water

Figure 9

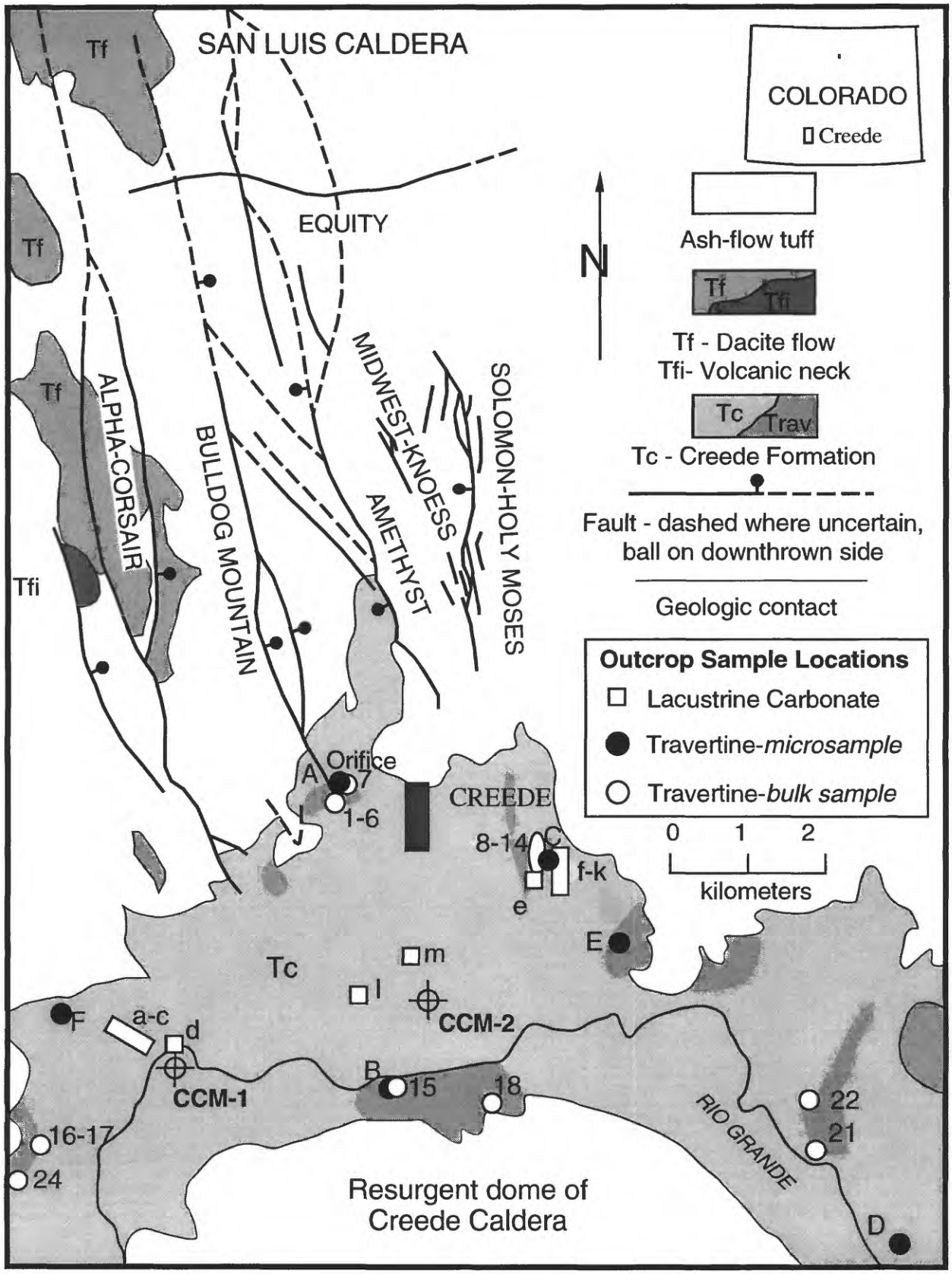
SAN LUIS CALDERA
Tf
Tf
Tf
Tfi
EQUITY
ALPHA-CORSAIR
BULLDOG MOUNTAIN
MIDWEST-KNOESS
AMETHYST
SOLOMON-HOLY MOSES
Orifice
A
7
1-6
CREEDE
8-14
C
f-k
e
E
Tc
m
l
CCM-2
F
a-c
d
CCM-1
B
15
18
16-17
24
22
21
RIO GRANDE
D
Resurgent dome of
Creede Caldera
COLORADO
Creede
N
Ash-flow tuff
Tf
Tfi
Tf - Dacite flow
Tfi- Volcanic neck
Tc
Trav
Tc - Creede Formation
Fault - dashed where uncertain,
ball on downthrown side
Geologic contact
Outcrop Sample Locations
Lacustrine Carbonate
Travertine-microsample
Travertine-bulk sample
0 1 2
kilometers

Figure 10

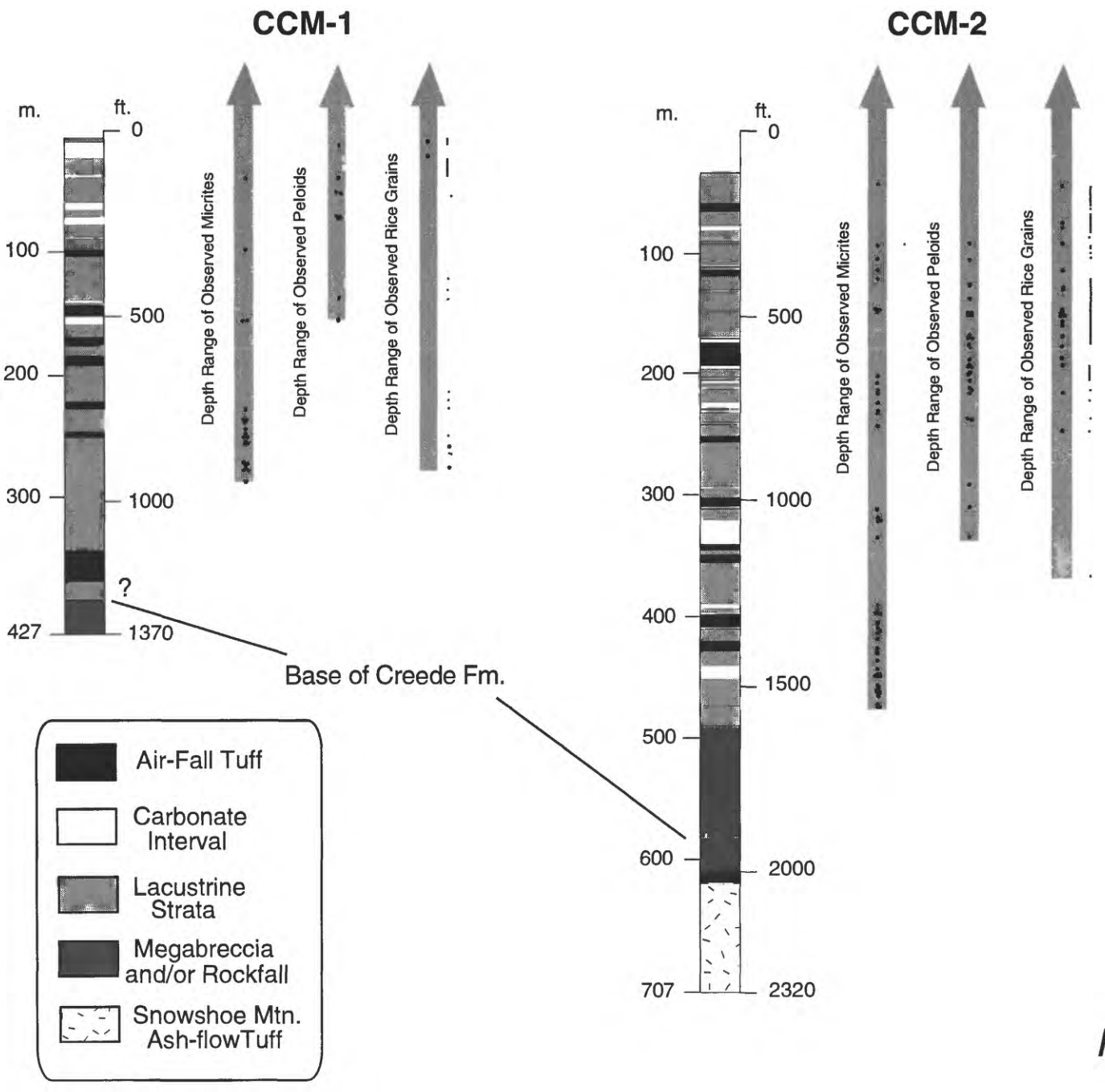
CCM-1
m.
ft.
0
100
500
200
300
1000
?
427
1370
Depth Range of Observed Micrites
Depth Range of Observed Peloids
Depth Range of Observed Rice Grains
Base of Creede Fm.
CCM-2
m.
ft.
0
100
500
200
300
1000
400
1500
500
600
2000
707
2320
Depth Range of Observed Micrites
Depth Range of Observed Peloids
Depth Range of Observed Rice Grains
Air-Fall Tuff
Carbonate Interval
Lacustrine Strata
Megabreccia and/or Rockfall
Snowshoe Mtn. Ash-flowTuff

Figure 11

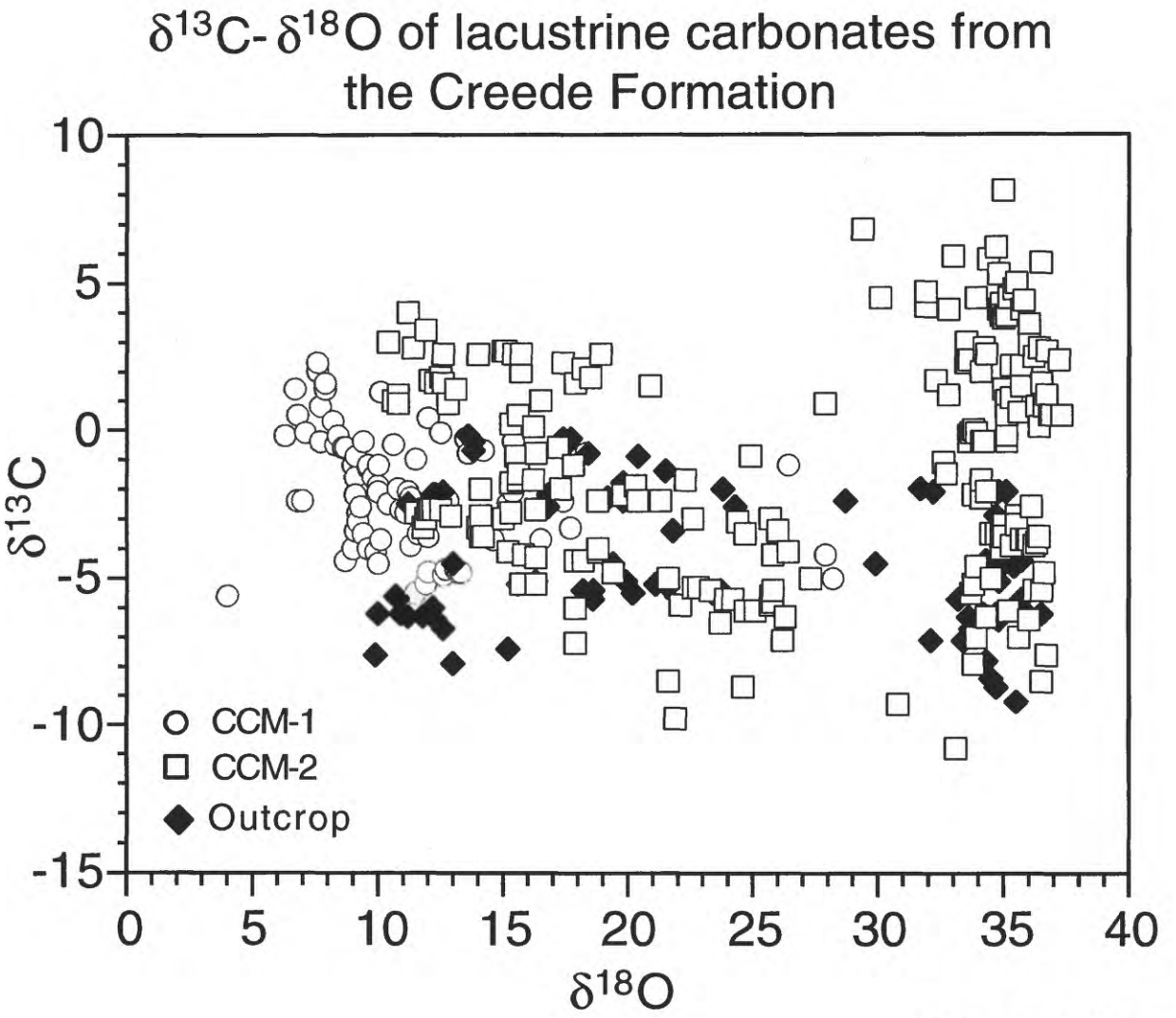
δ13C- δ18O of lacustrine carbonates from the Creede Formation
10
5
0
-5
-10
-15
δ13C
0
5
10
15
20
25
30
35
40
δ18O
CCM-1
CCM-2
Outcrop

Figure 12

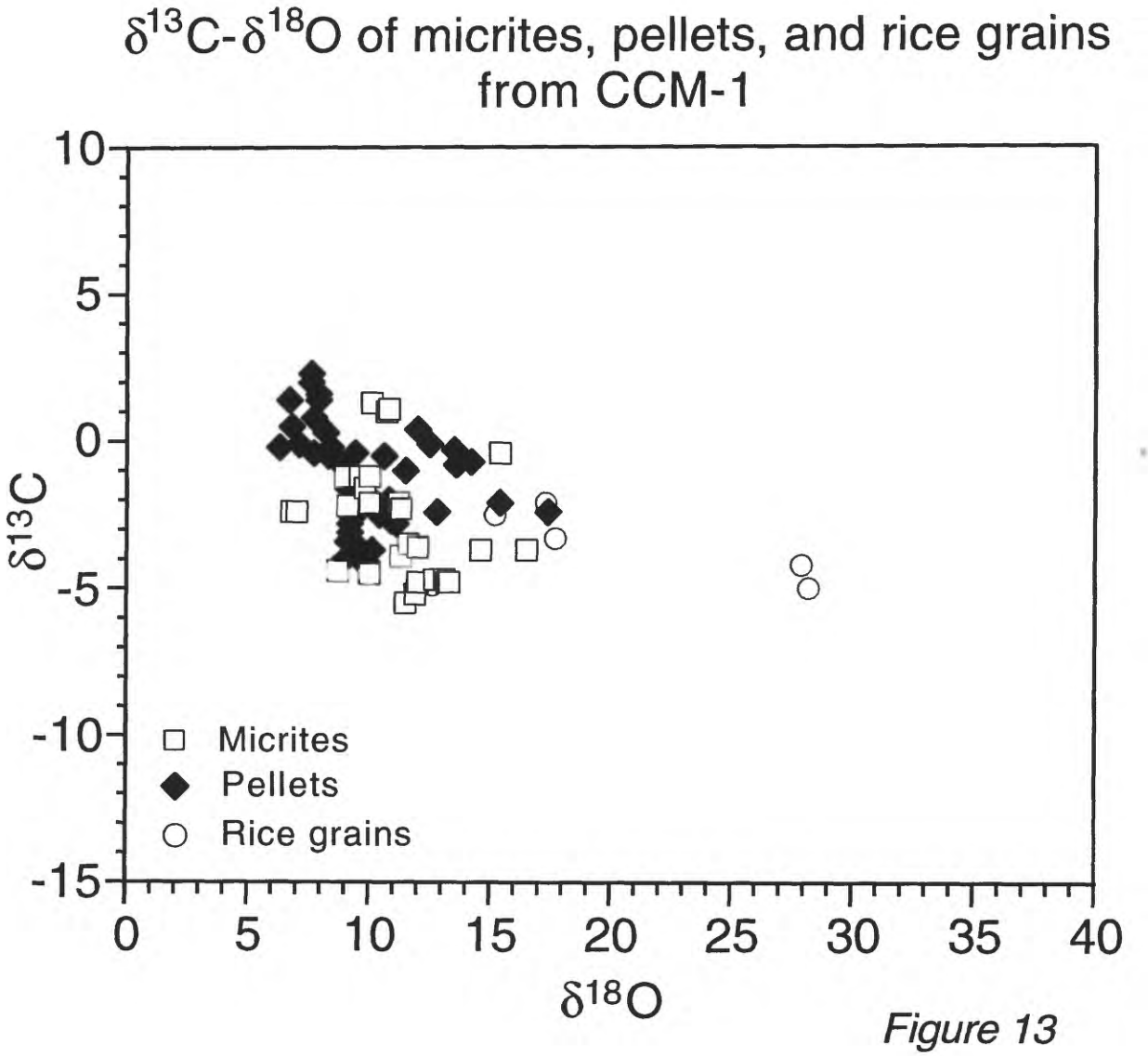
δ13C-δ18O of micrites, pellets, and rice grains from CCM-1
10
5
0
-5
-10
-15
δ13C
0
5
10
15
20
25
30
35
40
δ18O
Micrites
Pellets
Rice grains

Figure 13

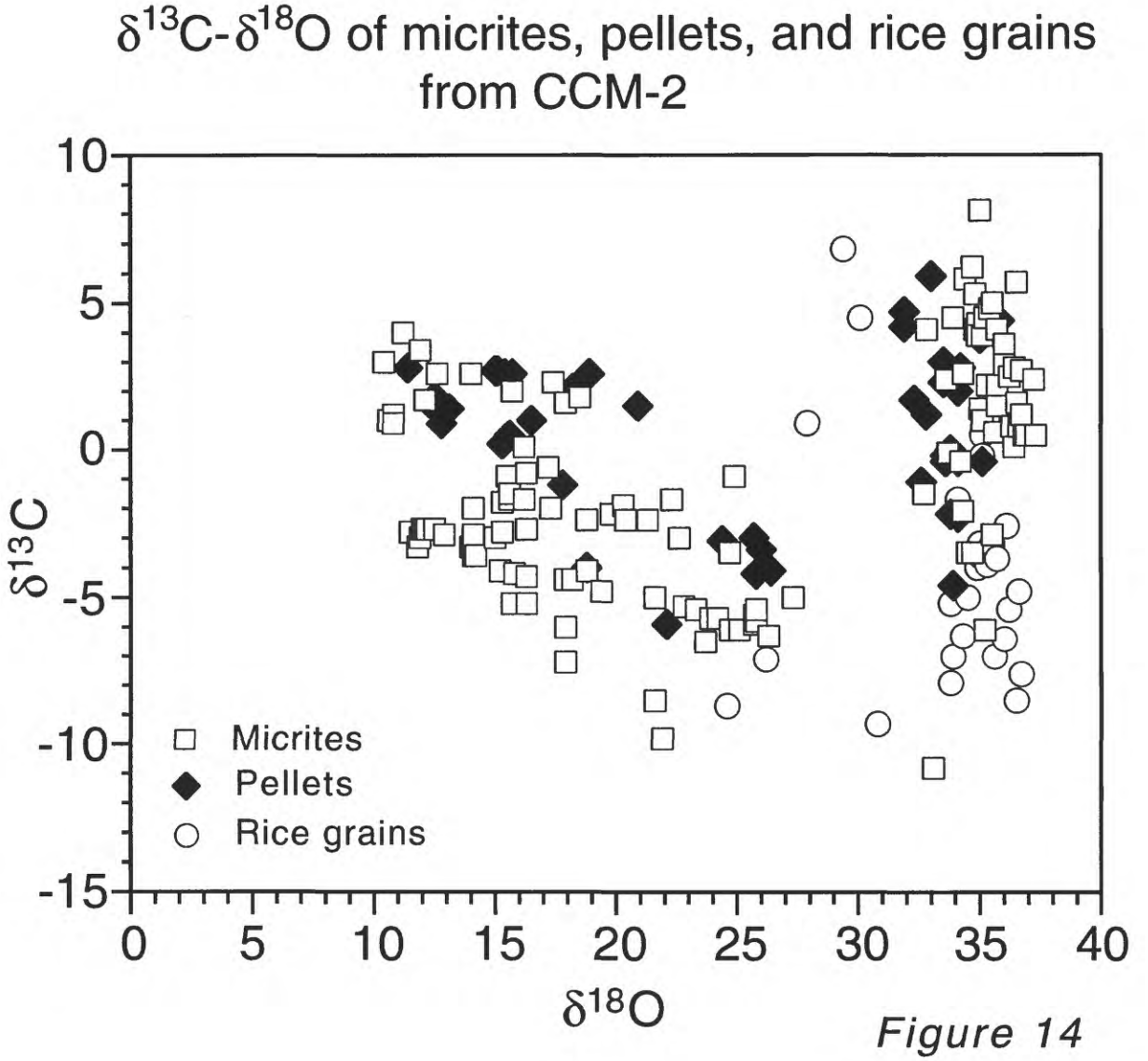
δ13C-δ18O of micrites, pellets, and rice grains from CCM-2
10
5
0
-5
-10
-15
δ13C
0
5
10
15
20
25
30
35
40
δ18O
Micrites
Pellets
Rice grains

Figure 14

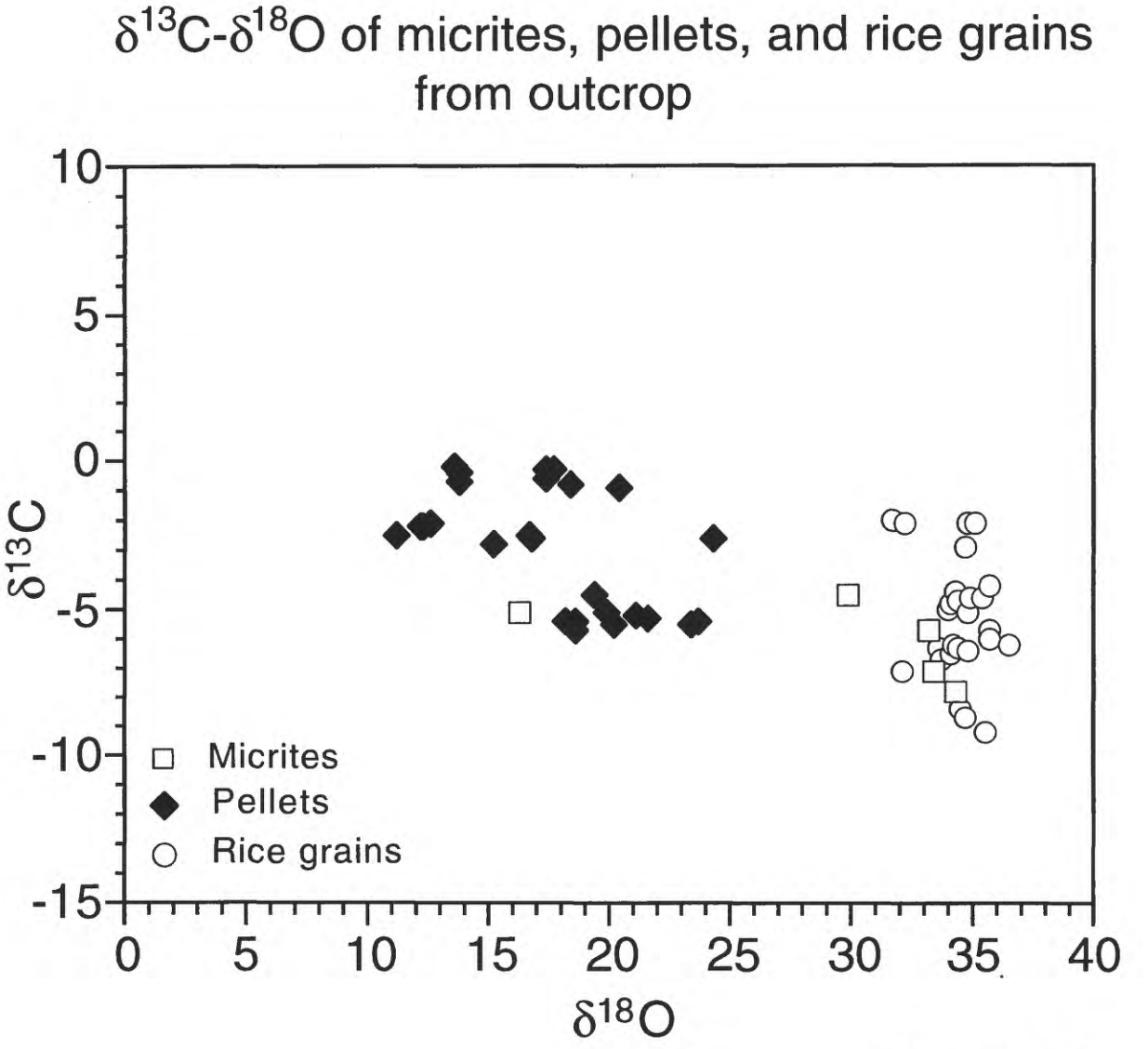
δ13C-δ18O of micrites, pellets, and rice grains from outcrop
10
5
0
-5
-10
-15
δ13C
0
5
10
15
20
25
30
35
40
δ18O
Micrites
Pellets
Rice grains

Figure 15

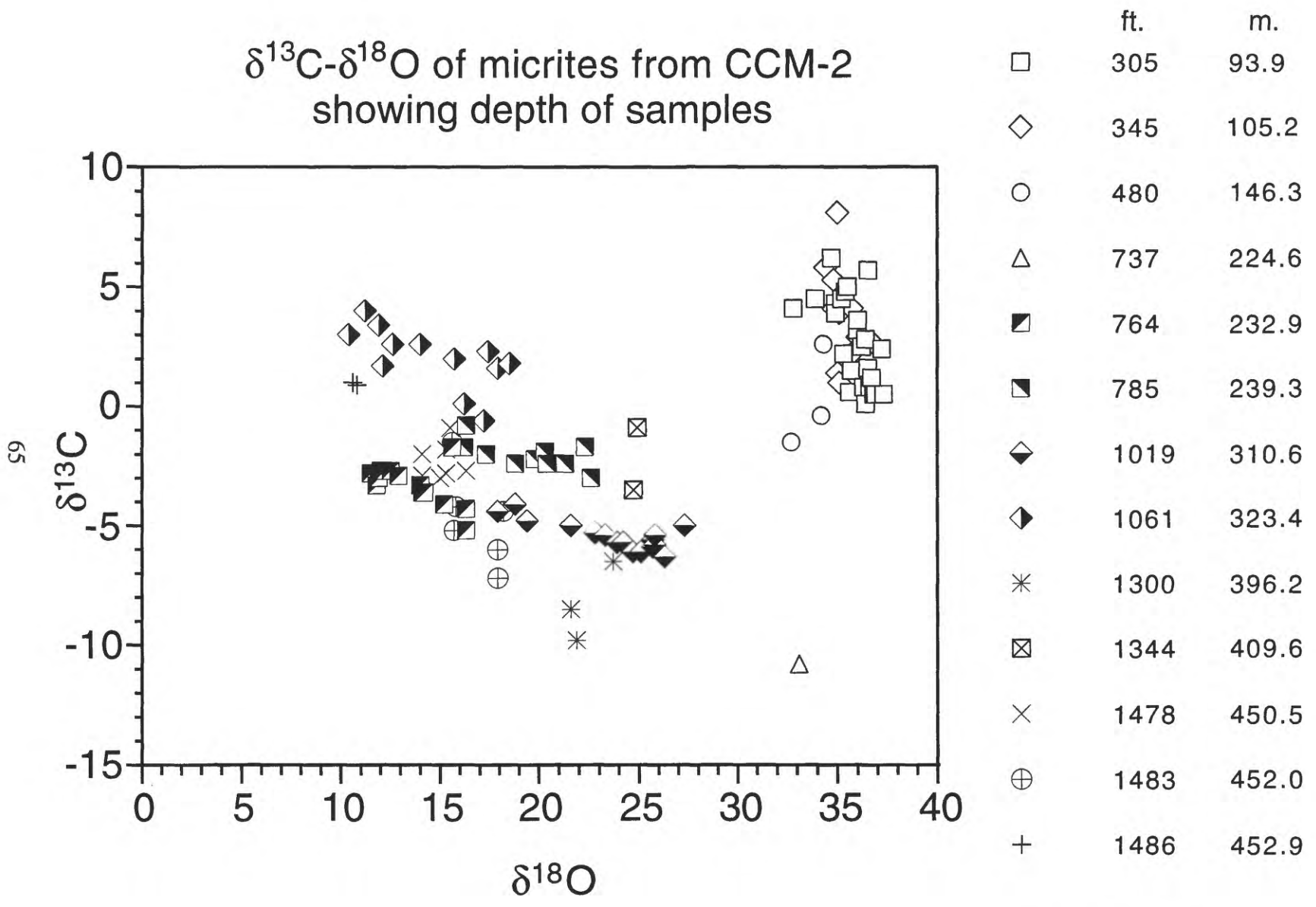
δ13C-δ18O of micrites from CCM-2
showing depth of samples
δ13C
δ18O
10
5
0
-5
-10
-15
0
5
10
15
20
25
30
35
40
ft.
m.
305 93.9
345 105.2
480 146.3
737 224.6
764 232.9
785 239.3
1019 310.6
1061 323.4
1300 396.2
1344 409.6
1478 450.5
1483 452.0
1486 452.9

Figure 16

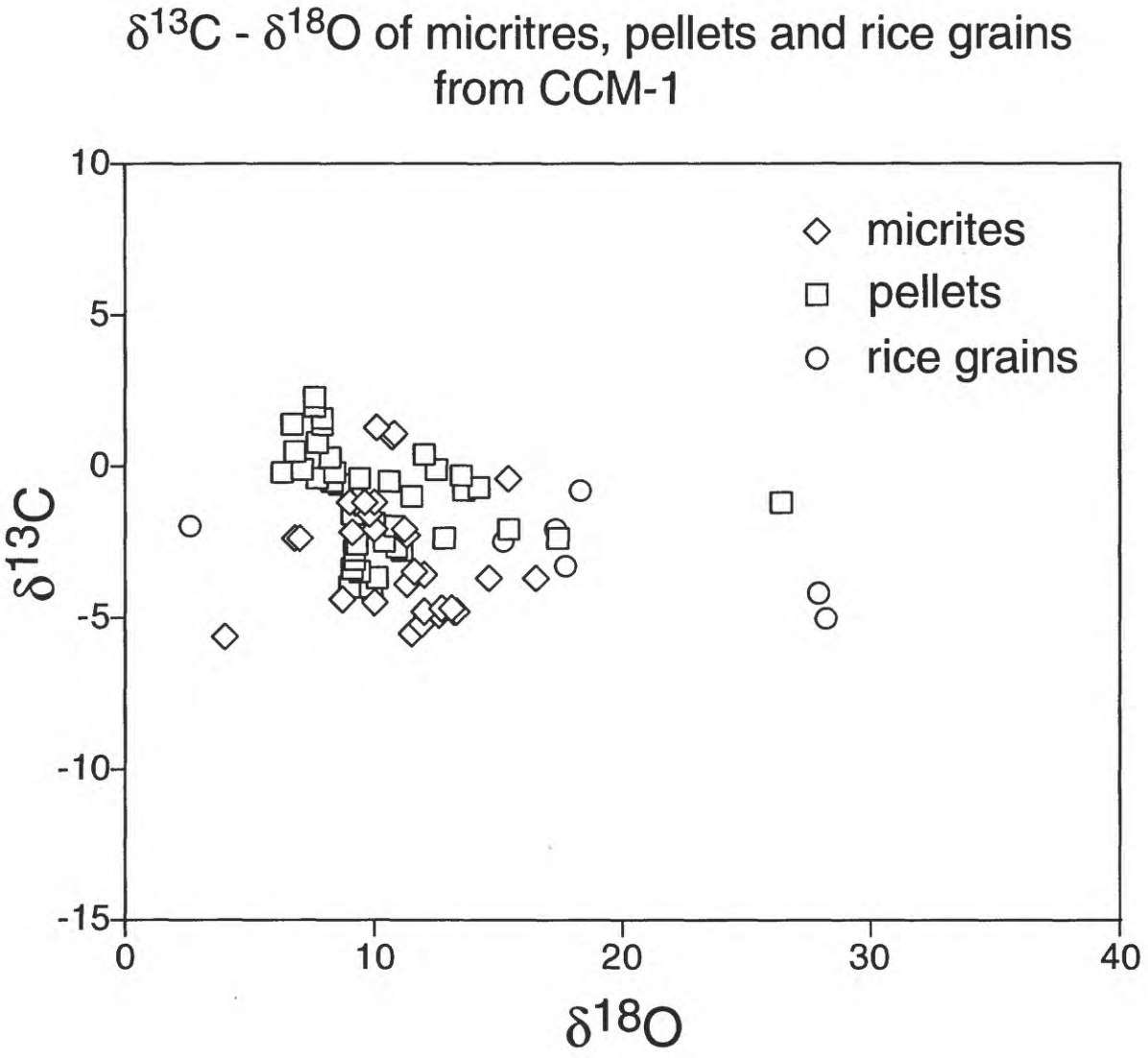
δ13C - δ18O of micritres, pellets and rice grains from CCM-1
micrites
pellets
rice grains
δ13C
δ18O
10
5
0
-5
-10
-15
0
10
20
30
40

Figure 17

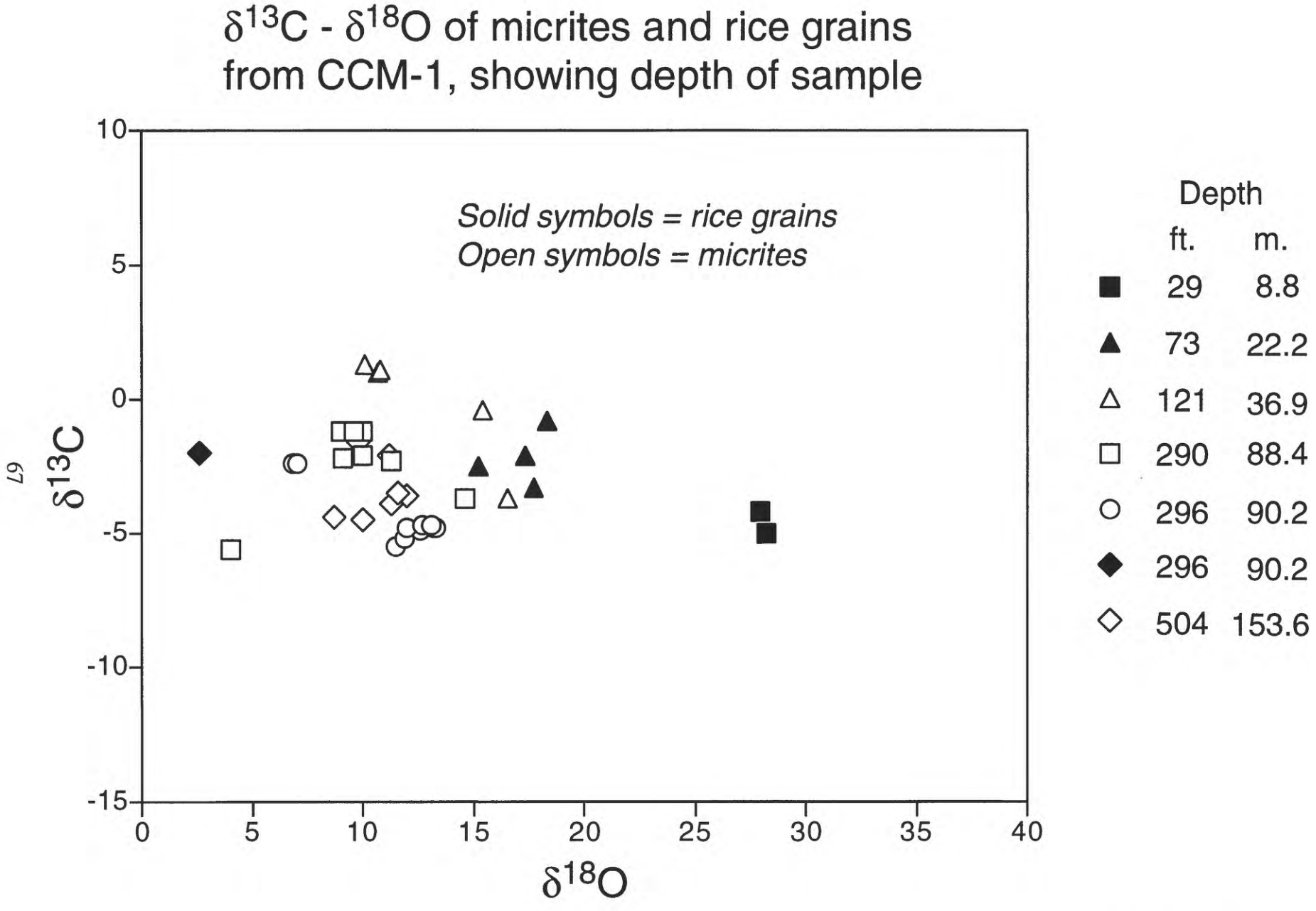
δ13C - δ18O of micrites and rice grains
from CCM-1, showing depth of sample
Solid symbols = rice grains
Open symbols = micrites
δ13C
δ18O
10
5
0
-5
-10
-15
0
5
10
15
20
25
30
35
40
Depth
ft. m.
29 8.8
73 22.2
121 36.9
290 88.4
296 90.2
296 90.2
504 153.6

Figure 18

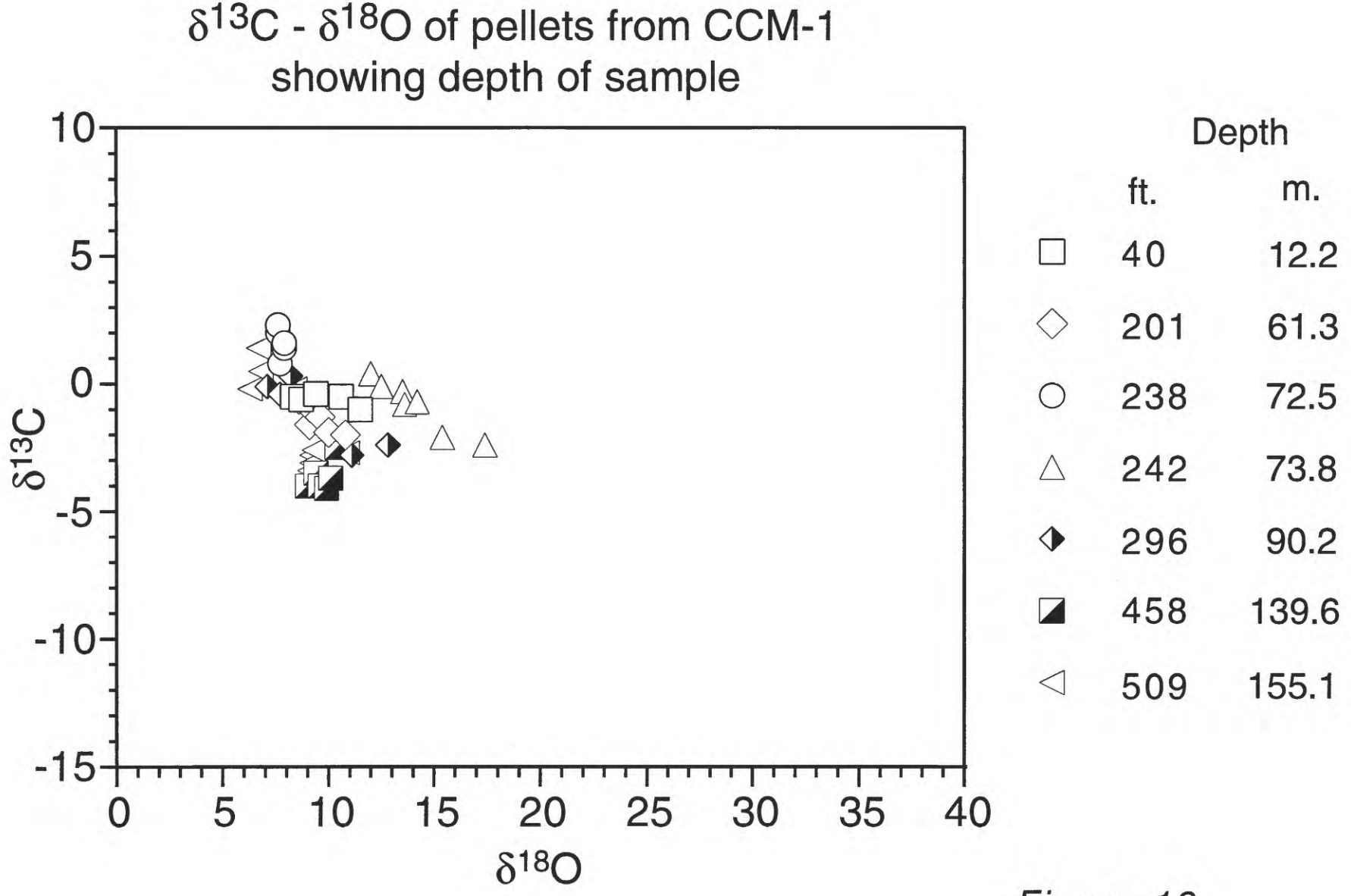
δ13C - δ18O of pellets from CCM-1
showing depth of sample
δ13C
δ18O
10
5
0
-5
-10
-15
0
5
10
15
20
25
30
35
40
Depth
ft.
m.
40
12.2
201
61.3
238
72.5
242
73.8
296
90.2
458
139.6
509
155.1

Figure 19

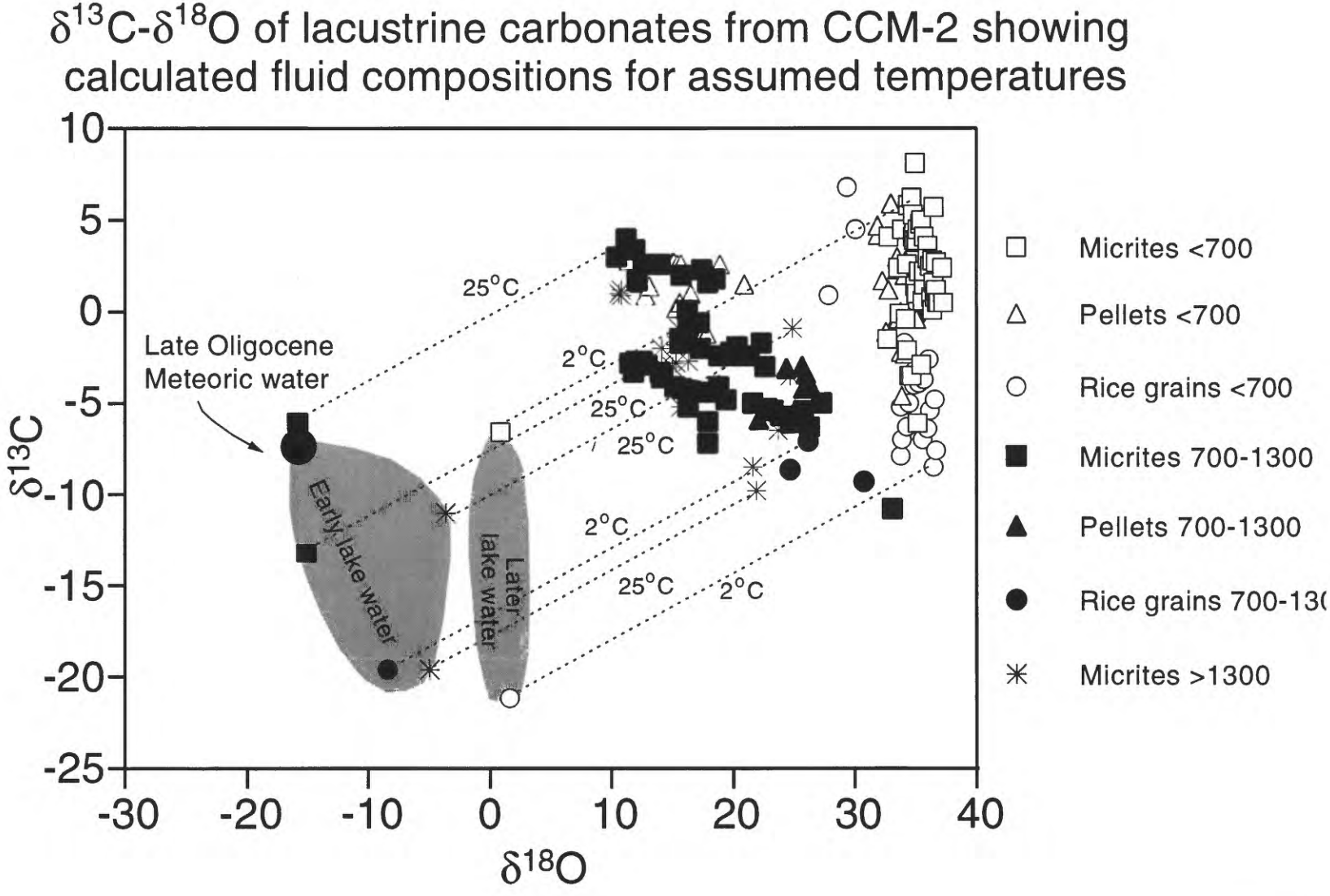
δ13C-δ18O of lacustrine carbonates from CCM-2 showing calculated fluid compositions for assumed temperatures
δ13C
δ18O
10
5
0
-5
-10
-15
-20
-25
-30
-20
-10
0
10
20
30
40
Late Oligocene Meteoric water
Early lake water
Later lake water
25°C
2°C
25°C
25°C
2°C
25°C
2°C
Micrites <700
Pellets <700
Rice grains <700
Micrites 700-1300
Pellets 700-1300
Rice grains 700-13(
Micrites >1300

Fiaure 20

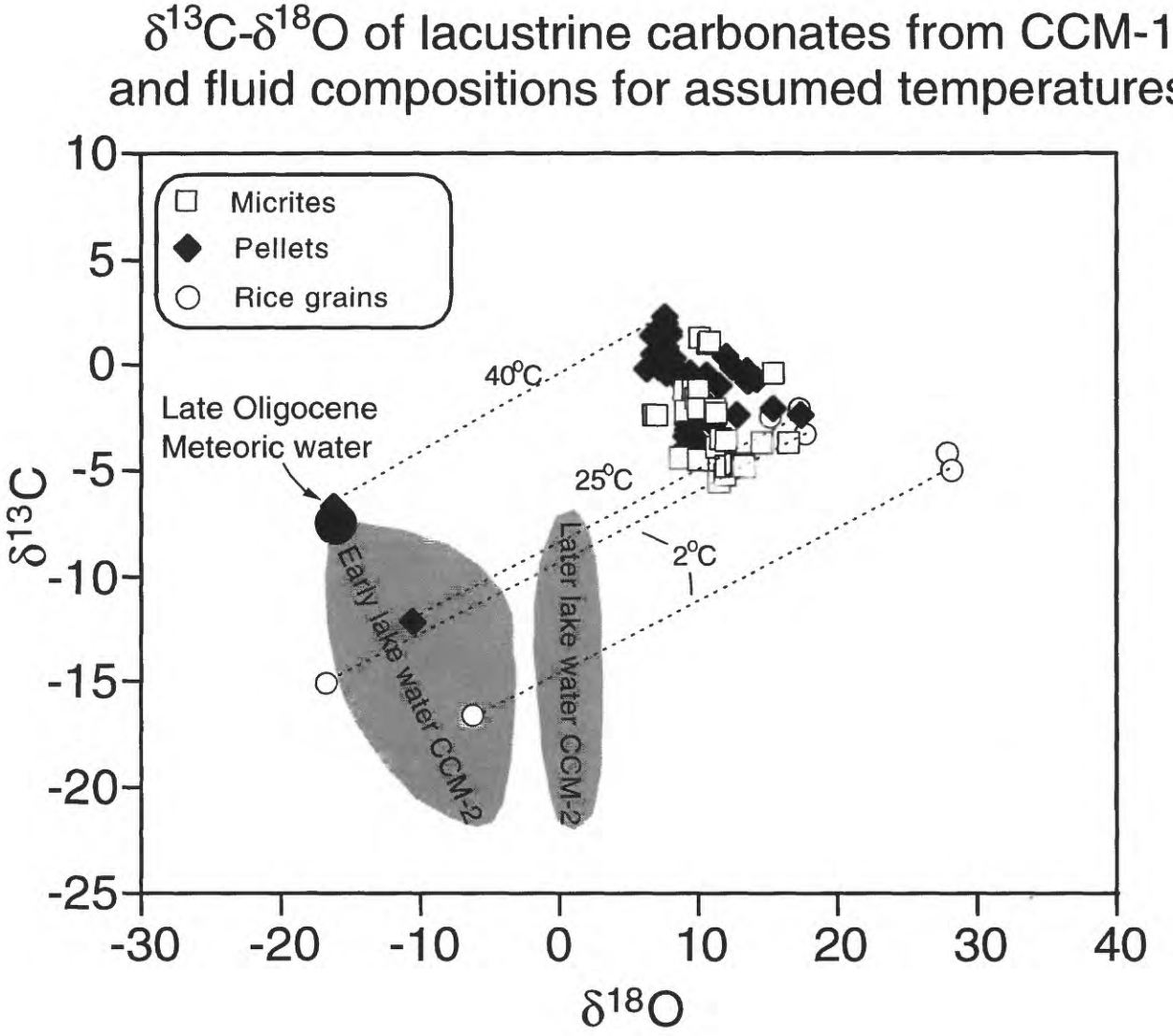
δ13C-δ18O of lacustrine carbonates from CCM-1
and fluid compositions for assumed temperatures
Micrites
Pellets
Rice grains
40°C
25°C
2°C
Late Oligocene
Meteoric water
Early lake water CCM-2
Later lake water CCM-2
δ13C
δ18O
10
5
0
-5
-10
-15
-20
-25
-30
-20
-10
0
10
20
30
40

Figure 21

$\delta^{13}C$ and $\delta^{18}O$ values versus depth for lacustrine carbonates from CCM-2 by microsampling of individual lamellae or rice grains

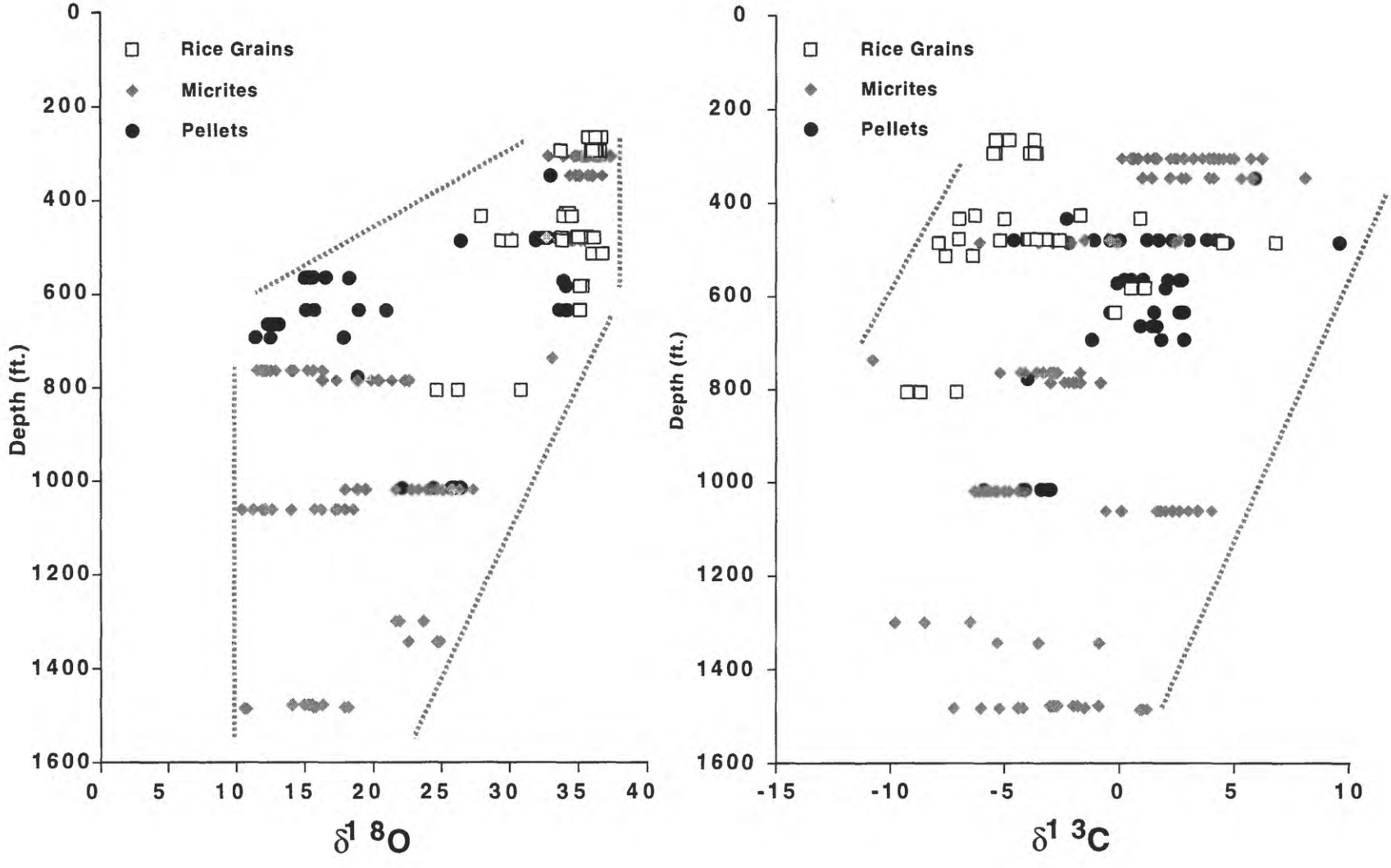

Figure 22

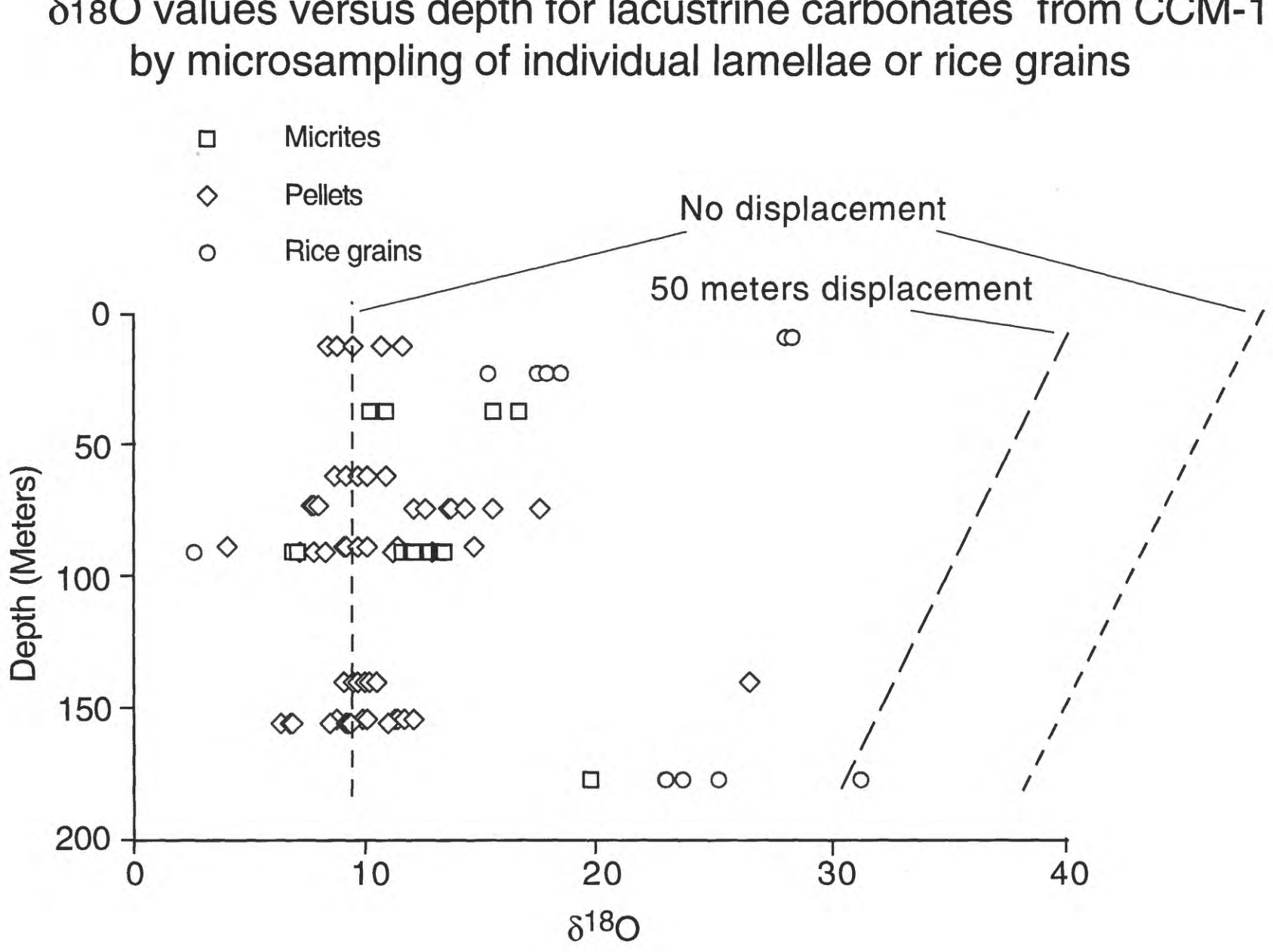
δ18O values versus depth for lacustrine carbonates from CCM-1
by microsampling of individual lamellae or rice grains
Micrites
Pellets
Rice grains
No displacement
50 meters displacement
Depth (Meters)
0
50
100
150
200
0
10
20
30
40
δ18O

Figure 23

$\delta^{13}C$-$\delta^{18}O$ of Bulldog Mountain rhodochrosite and calculated $\delta^{13}C$ and $\delta^{18}O$ of fluids compared to those for lake waters

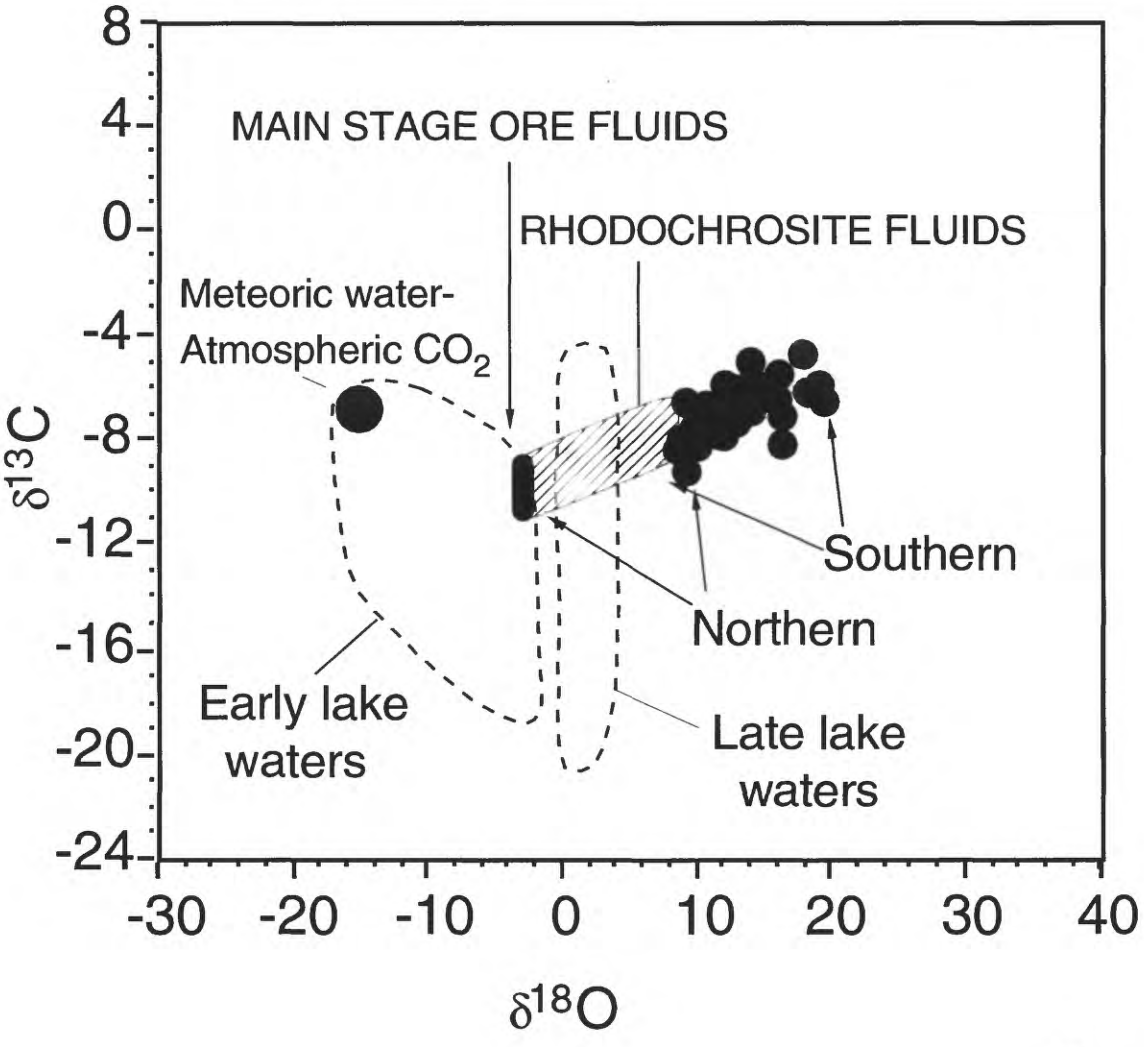

Figure 24

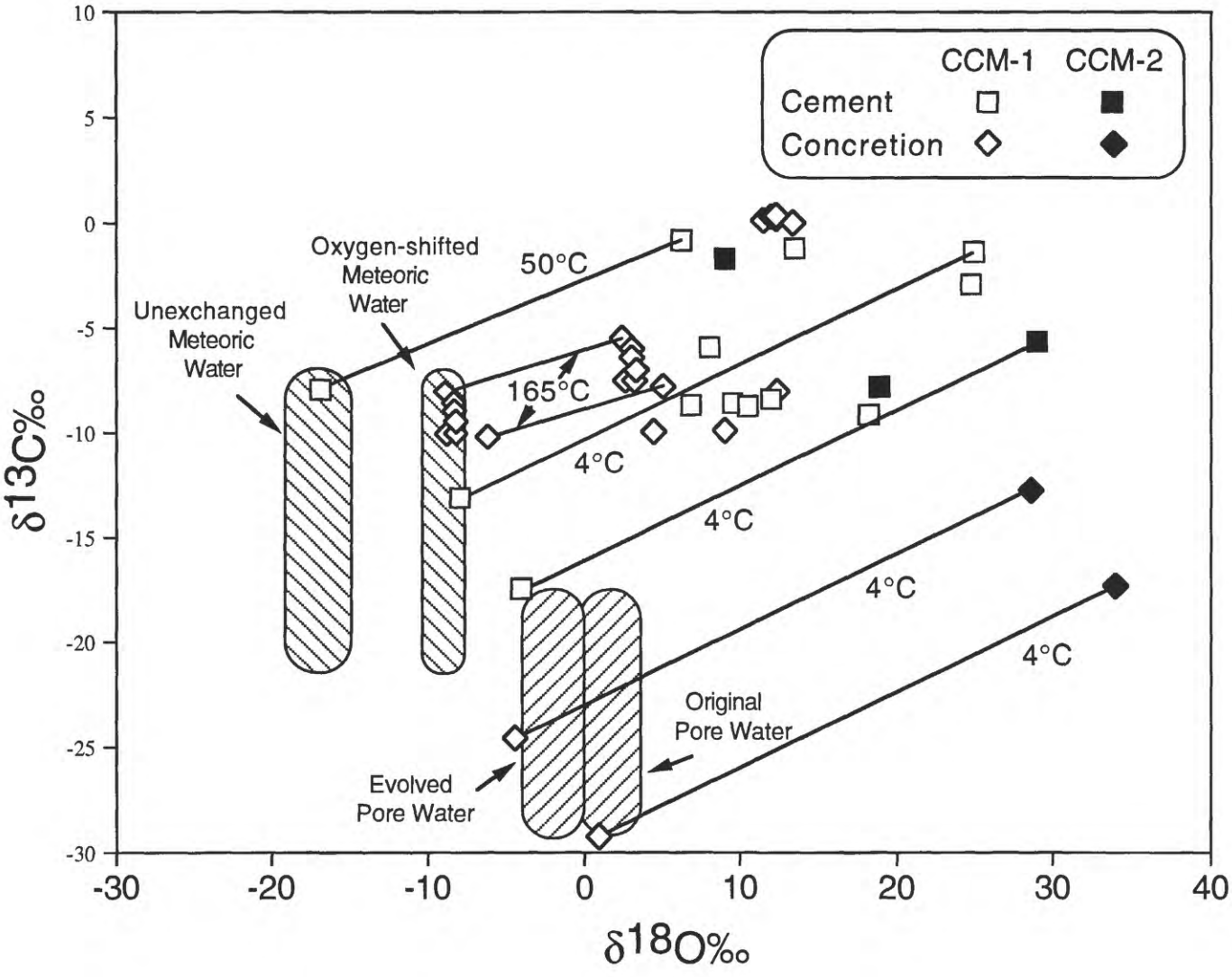
CCM-1
CCM-2
Cement
Concretion
Oxygen-shifted
Meteoric
Water
Unexchanged
Meteoric
Water
50°C
165°C
4°C
4°C
4°C
4°C
Original
Pore Water
Evolved
Pore Water
δ13C‰
δ18O‰
10
5
0
-5
-10
-15
-20
-25
-30
-30
-20
-10
0
10
20
30
40

Figure 25

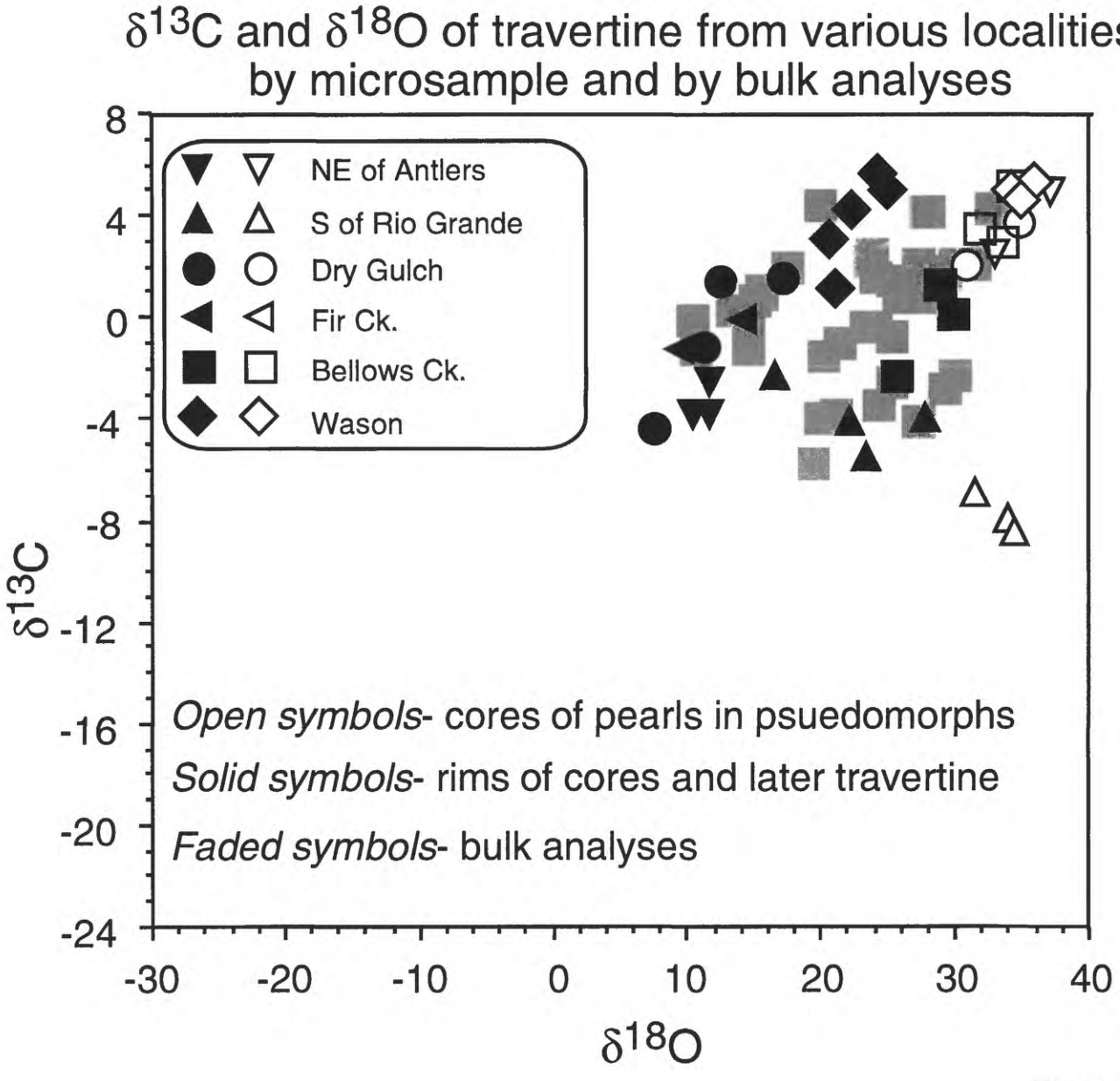
δ13C and δ18O of travertine from various localities
by microsample and by bulk analyses
NE of Antlers
S of Rio Grande
Dry Gulch
Fir Ck.
Bellows Ck.
Wason
Open symbols- cores of pearls in psuedomorphs
Solid symbols- rims of cores and later travertine
Faded symbols- bulk analyses
δ13C
δ18O
8
4
0
-4
-8
-12
-16
-20
-24
-30
-20
-10
0
10
20
30
40

Figure 26

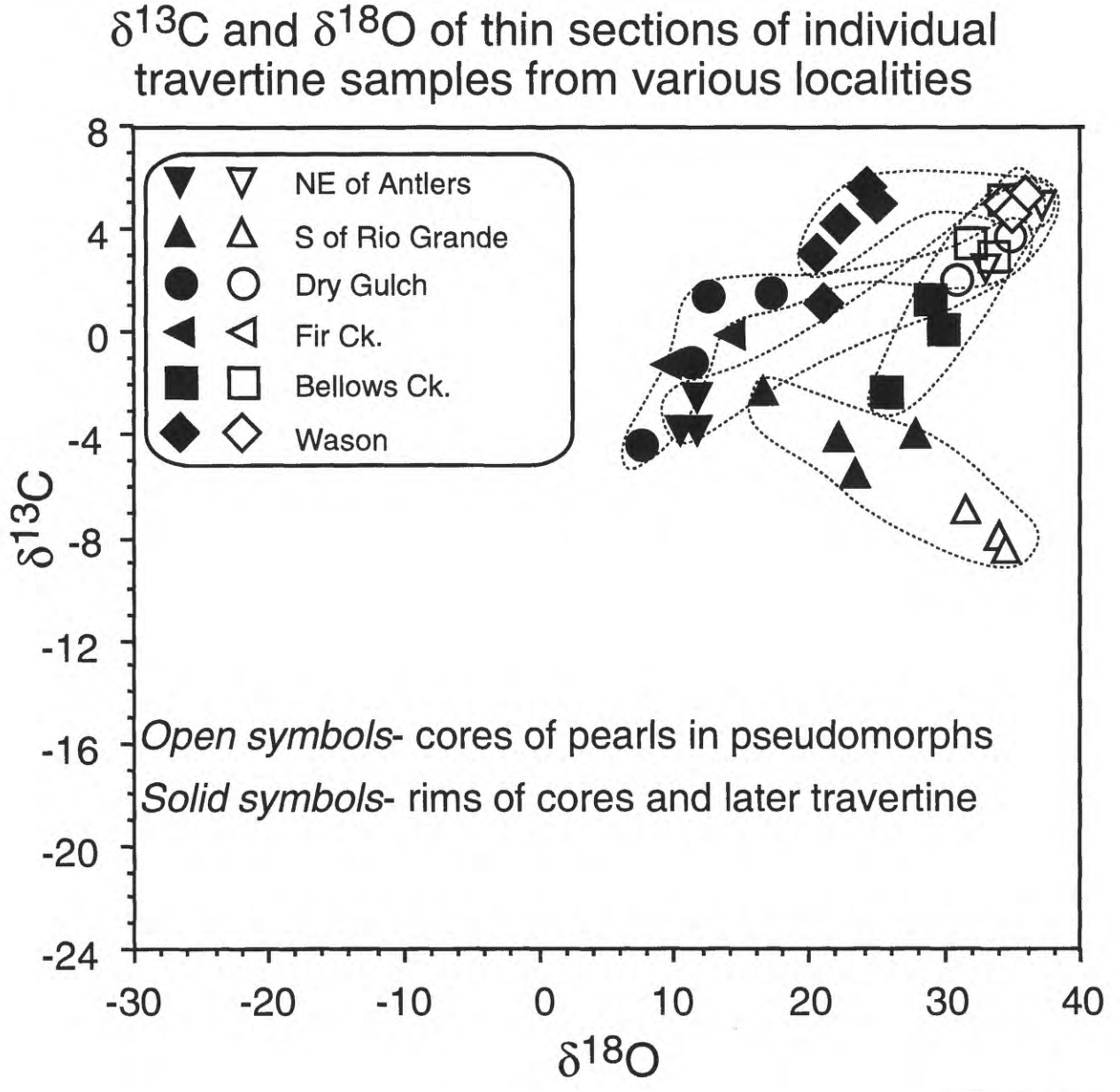
δ13C and δ18O of thin sections of individual travertine samples from various localities
NE of Antlers
S of Rio Grande
Dry Gulch
Fir Ck.
Bellows Ck.
Wason
Open symbols- cores of pearls in pseudomorphs
Solid symbols- rims of cores and later travertine
δ13C
δ18O
8
4
0
-4
-8
-12
-16
-20
-24
-30
-20
-10
0
10
20
30
40

Figure 27

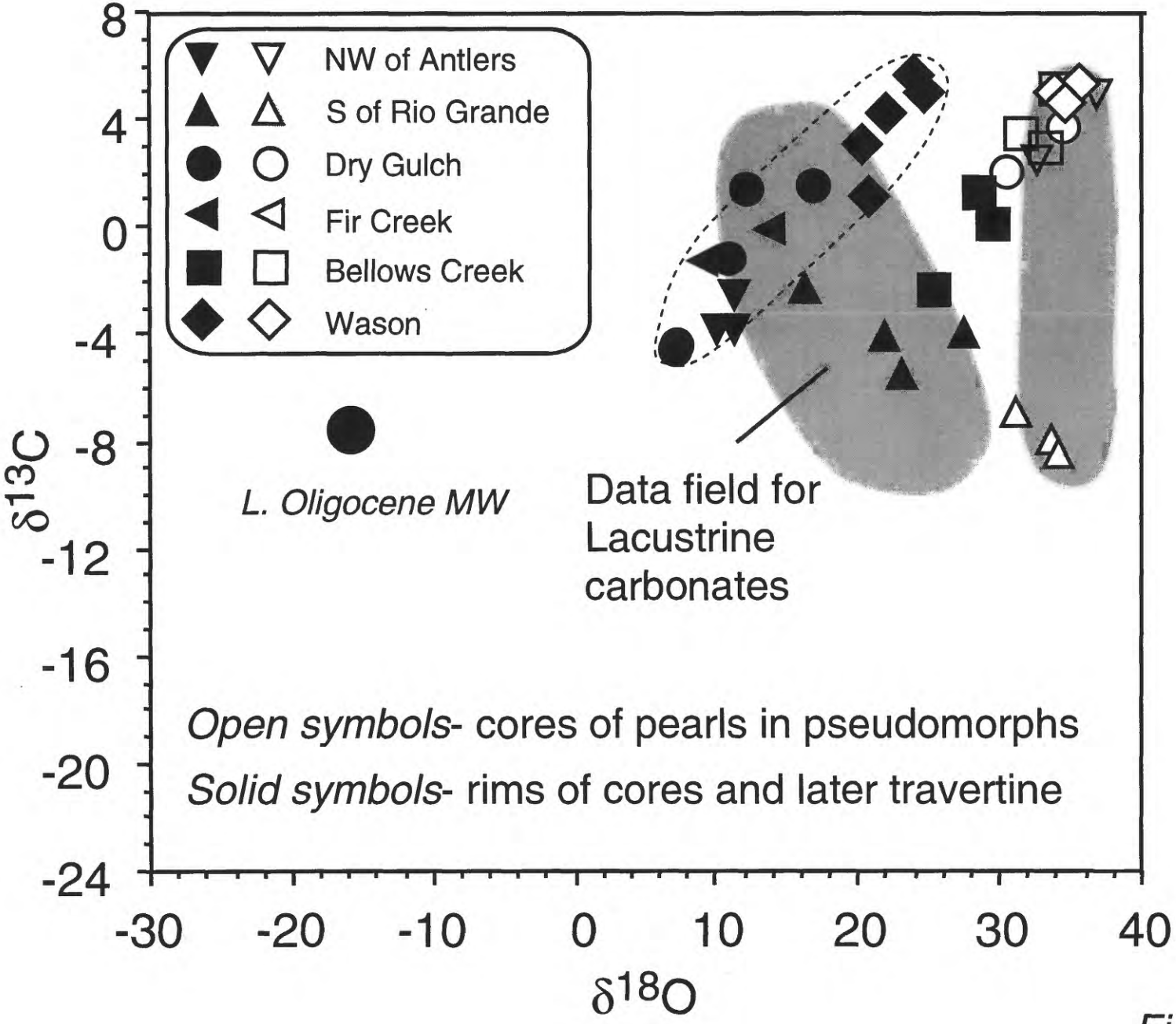
NW of Antlers
S of Rio Grande
Dry Gulch
Fir Creek
Bellows Creek
Wason
L. Oligocene MW
Data field for Lacustrine carbonates
Open symbols- cores of pearls in pseudomorphs
Solid symbols- rims of cores and later travertine
δ13C
δ18O
8
4
0
-4
-8
-12
-16
-20
-24
-30
-20
-10
0
10
20
30
40

Figure 28

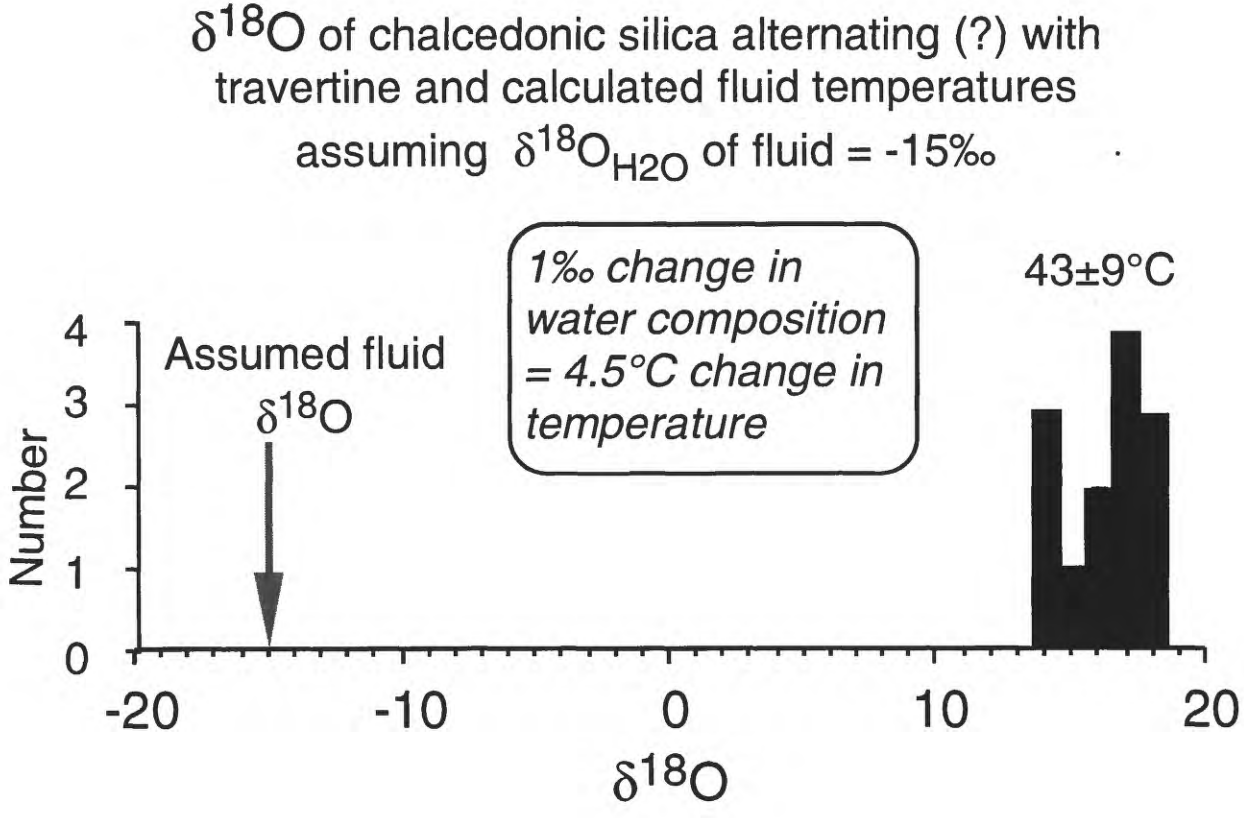
δ18O of chalcedonic silica alternating (?) with travertine and calculated fluid temperatures assuming δ18OH2O of fluid = -15‰
1‰ change in water composition = 4.5°C change in temperature
43±9°C
Assumed fluid δ18O
Number
0
1
2
3
4
-20
-10
0
10
20
δ18O

Figure 29

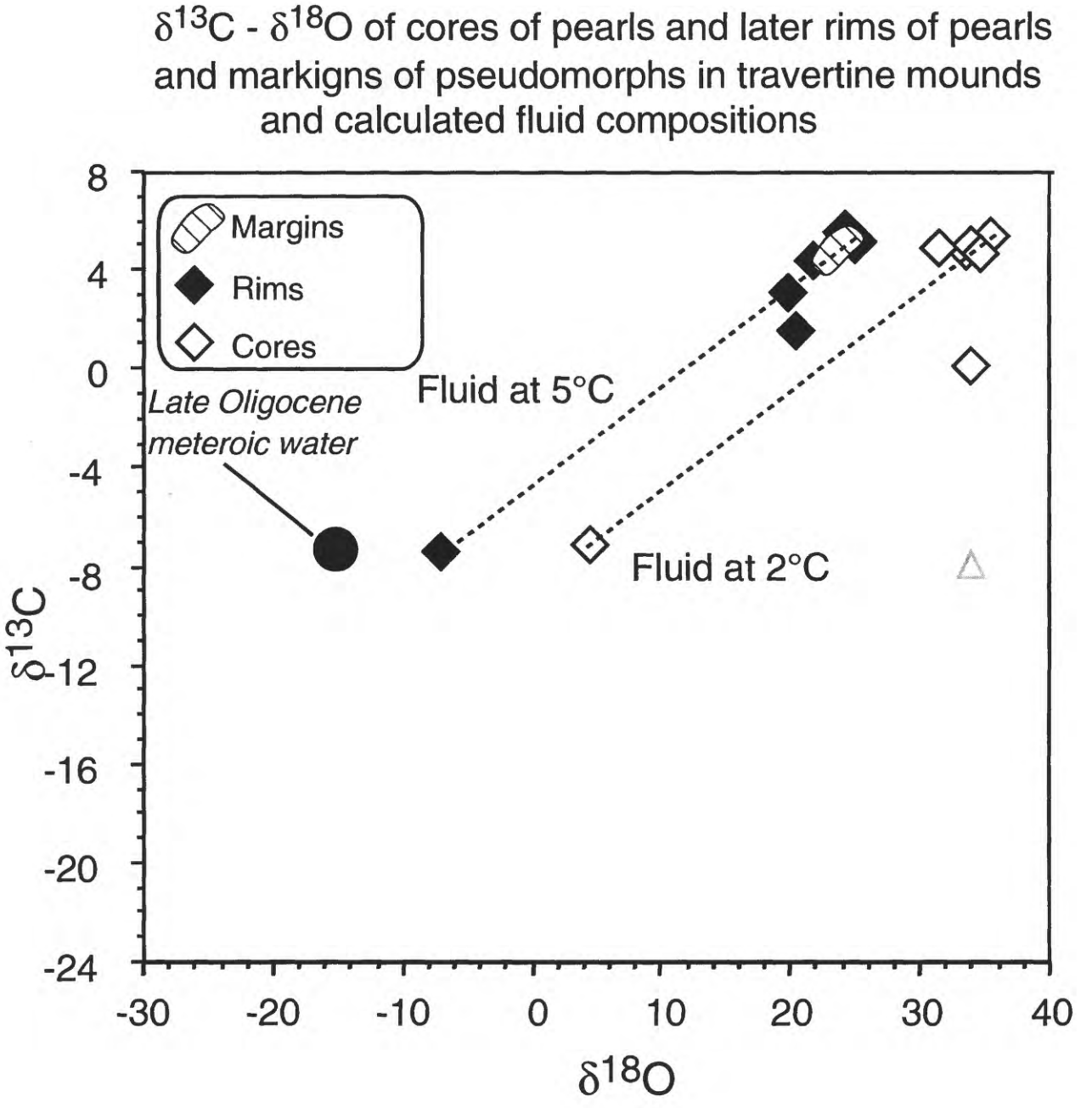
δ13C - δ18O of cores of pearls and later rims of pearls and markigns of pseudomorphs in travertine mounds and calculated fluid compositions
Margins
Rims
Cores
Late Oligocene meteroic water
Fluid at 5°C
Fluid at 2°C
δ13C
δ18O
8
4
0
-4
-8
-12
-16
-20
-24
-30
-20
-10
0
10
20
30
40

Figure 30

$\delta^{13}C$-$\delta 1^{8}O$ of pearls (dark symbnols) and rims and margins (open symbols) in pseudomorphs in travertine from various localities showing possible waters from which mounds formed.

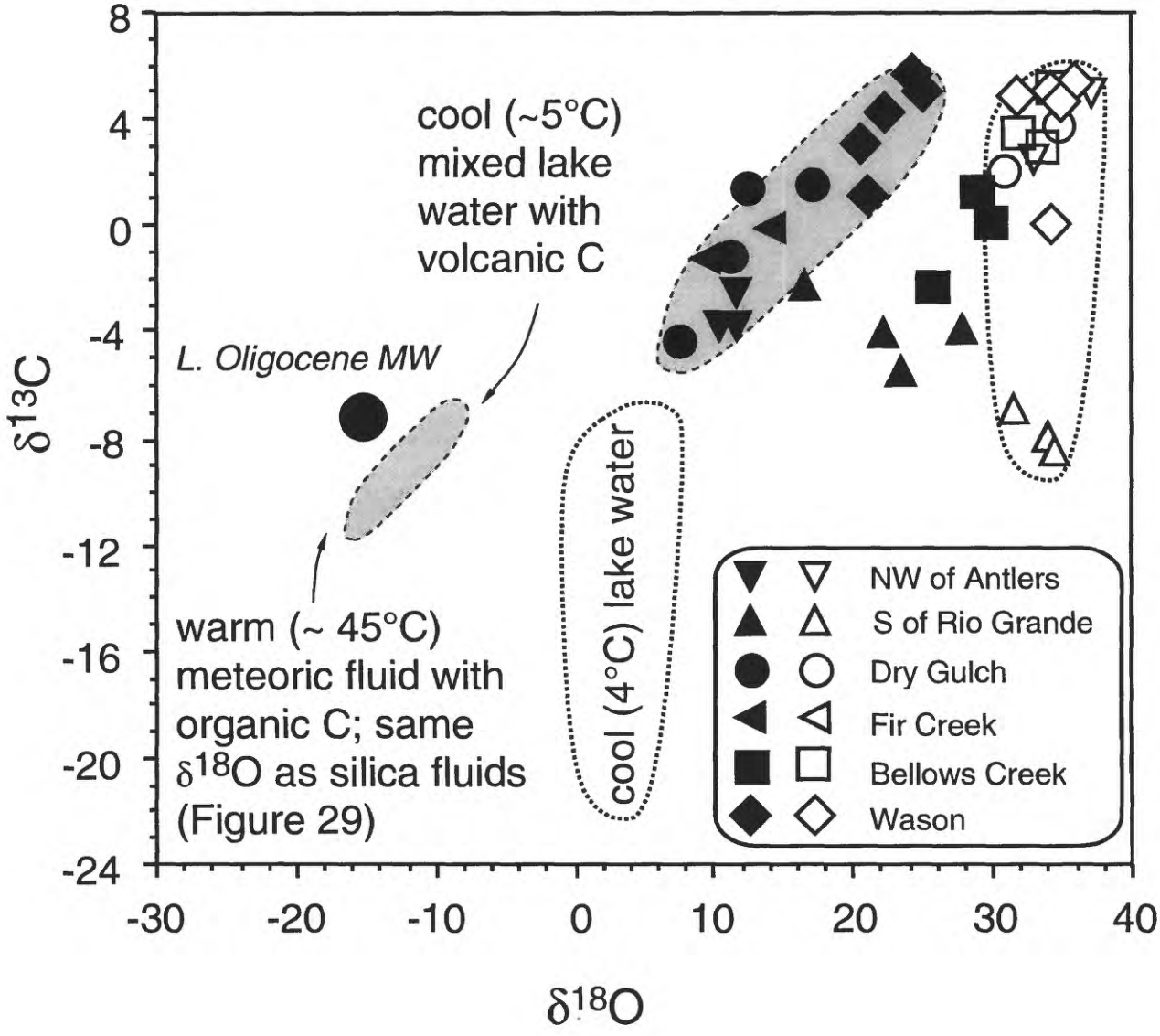

Figure 31

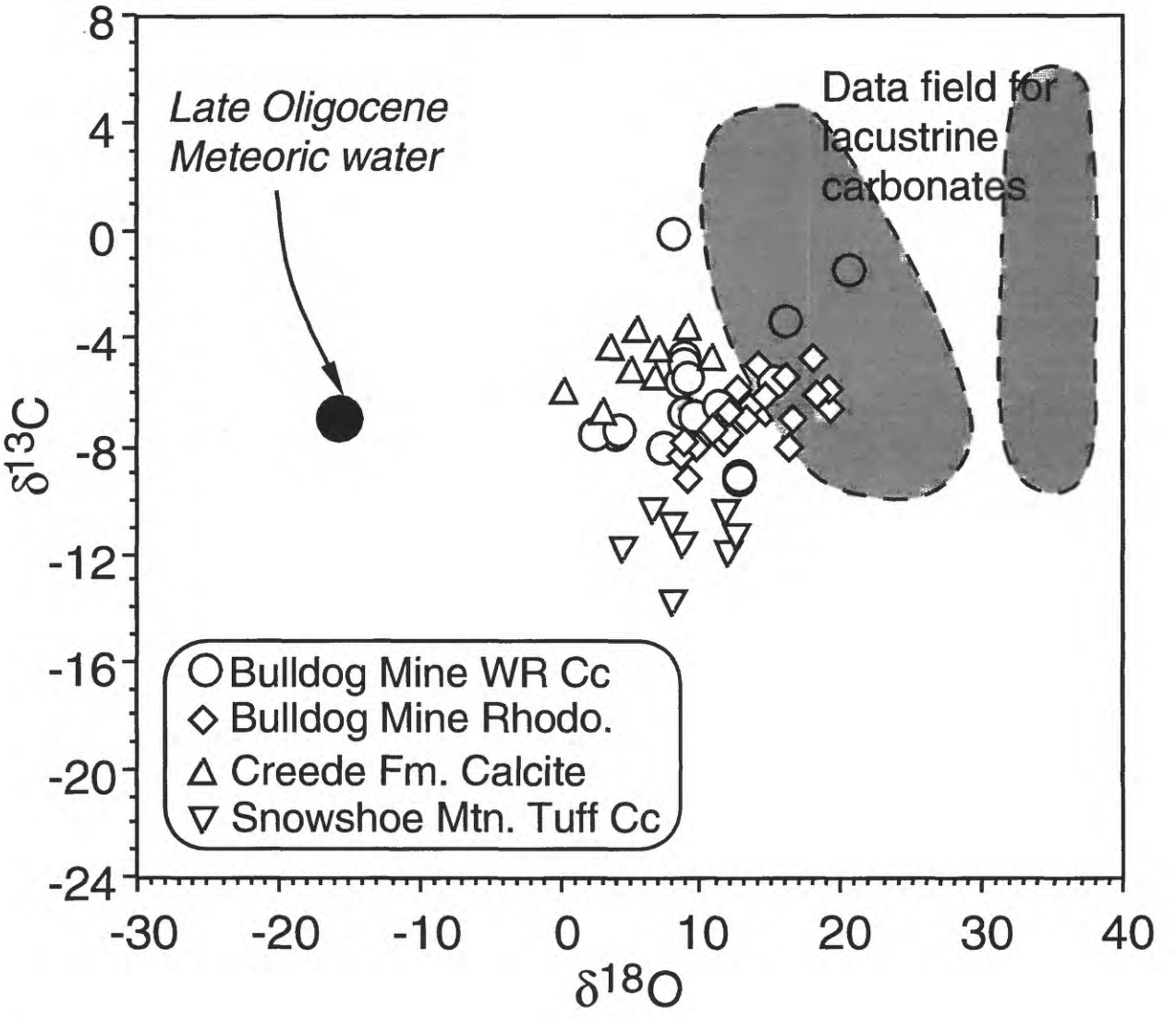
Late Oligocene
Meteoric water
Data field for
lacustrine
carbonates
Bulldog Mine WR Cc
Bulldog Mine Rhodo.
Creede Fm. Calcite
Snowshoe Mtn. Tuff Cc
δ13C
δ18O
8
4
0
-4
-8
-12
-16
-20
-24
-30
-20
-10
0
10
20
30
40

Figure 32

$\delta^{13}C$ and $\delta^{18}O$ of calcite veinlets in Creede Formation and Snowshoe Mountain Tuff and calculated fluid compositions for fluid inclusion and geothermal gradient temperatures of deposition

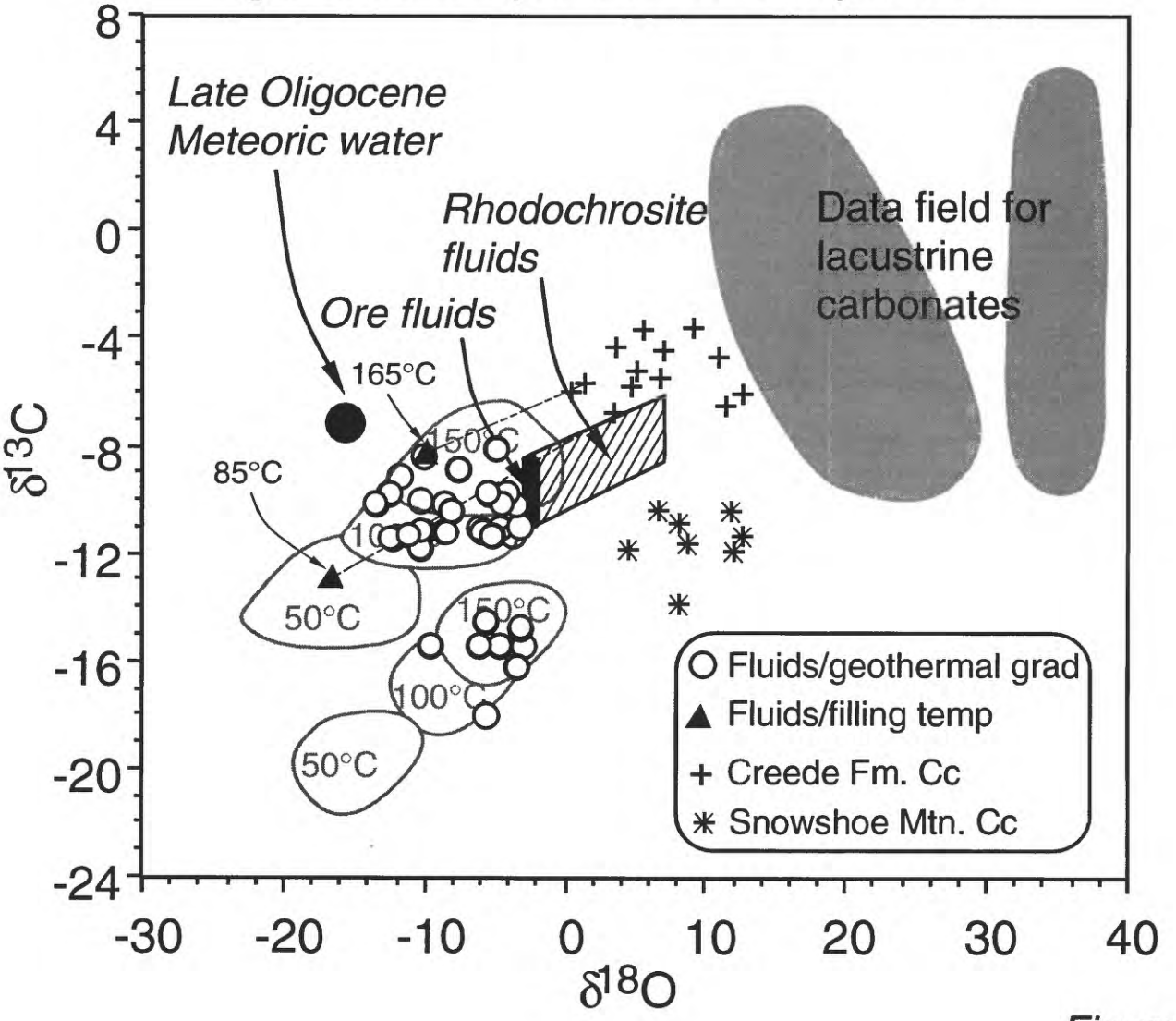

Figure 33

$\delta^{13}C$ and $\delta^{18}O$ of late sparry calcite in travertine and calculated fluid compositions for assumed temperatures

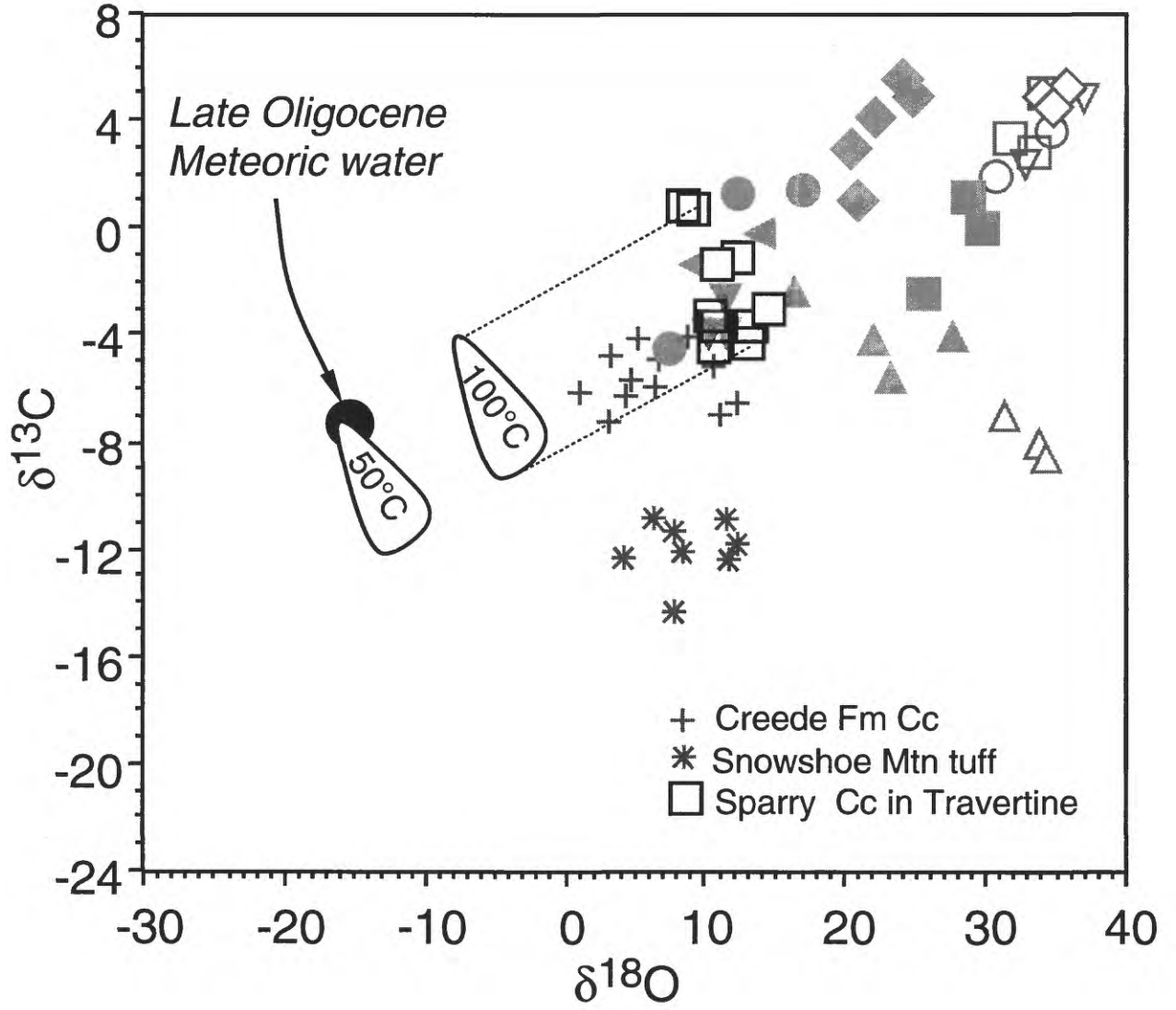

Figure 34

$\delta^{13}C$ and $\delta^{18}O$ of pre-ore wall rock calcite in ore zones and calculated fluid compositions for assumed 50° and 150°C temperatures of deposition showing relationship to ore and pre-ore rhodochrosite fluid compositions. Data for rhodochrosite, veinlets, and travertine in faded symbols. Possible temperatures and fluid compositions for wall rock calcites are limited by the late Oligocene meteoric water reference.

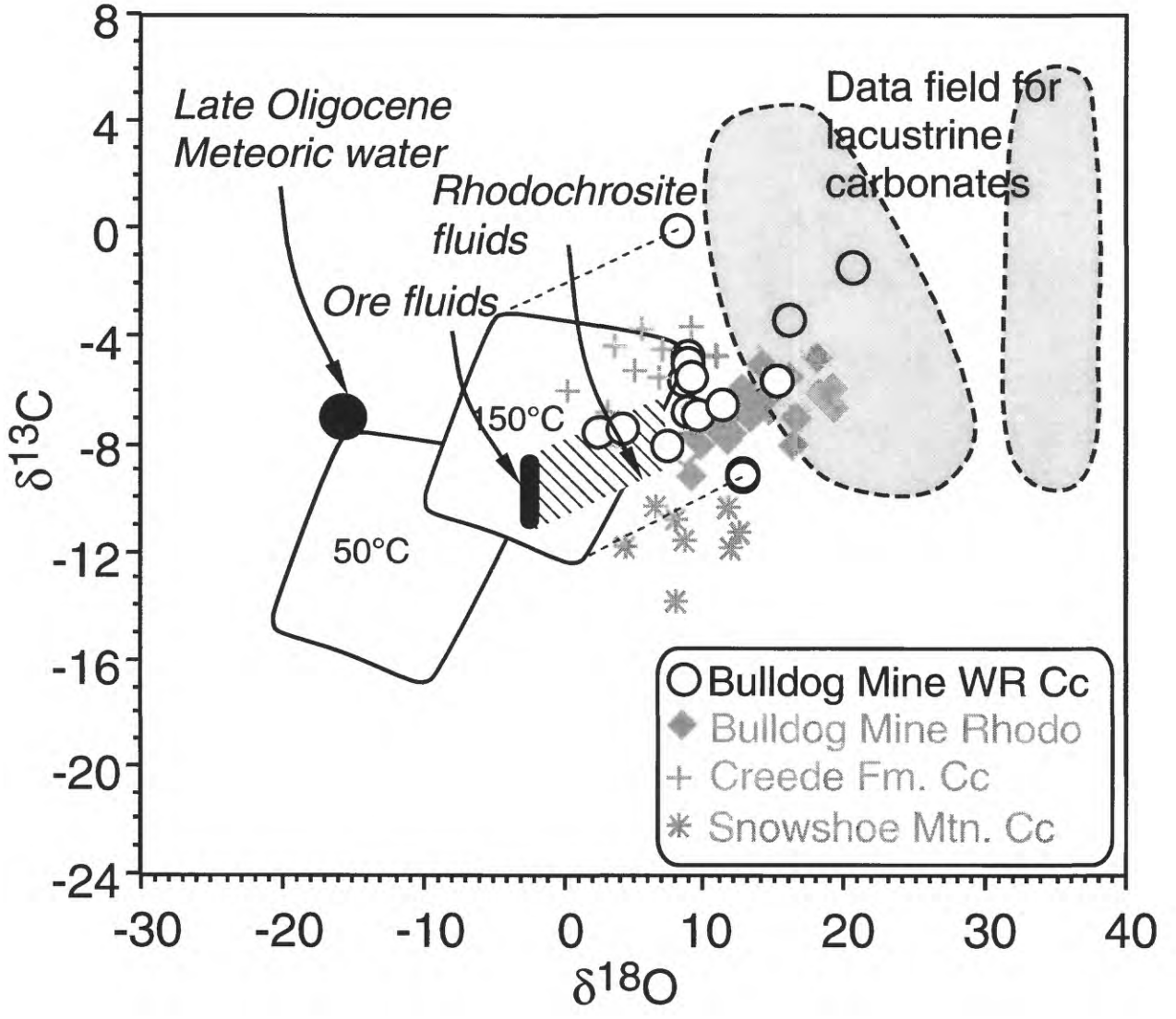

Figure 35